A mineralogical and geochemical review of Cycles V and VI of the Upper Zone of the Bushveld Complex.

By

Tawnee Lee Britt

29125732

MSc in Geology

2015

UNIVERSITEIT VAN PRETORIA
UNIVERSITY OF PRETORIA
YUNIBESITHI YA PRETORIA
Faculty of Natural and Agricultural Sciences

Declaration of Originality

University of Pretoria

Full names of student: **Tawnee Lee Britt**

Declaration

1. I understand what plagiarism is and am aware of the University's policy in this regard
2. I declare that this thesis is my own original work. Where other people's work has been used (either from a printed source, Internet or any other source), this has been properly acknowledged and referenced in accordance with departmental requirements
3. I have not used work previously produced by another student or any other person to hand in as my own.
4. I have not allowed, and will not allow, anyone to copy my work with the intention of passing it off as his or her own work.

Signature......................................

Date..

Abstract

The Upper Zone is situated at the top of the Rustenburg Layered Suite and according to Kruger *et al*. (1987) represents the final stages of magma recharge. The Upper Zone, which is comprised of gabbro, anorthosite layers and magnetite layers, shows a number of mineralogical and geochemical reversals. Previous studies by Tegner *et al.* (2006) identified nine cycles (I-IX) that makes up the Upper Zone. Two of the most prominent cycles: Cycle V and Cycle VI were studied to gain a greater understanding of the changes occurring within as well as in between two cycles. The data collected included petrological and electron microprobe data from plagioclase, olivine, pyroxene, apatite, biotite and secondary amphibole. Although the current data showed some similarities to Tegner *et al.* (2006), this study has provided a number of additional features to the two cycles. Firstly, the cycles vary in terms of lithology. Secondly, the An% and Mg# from Cycle V shows greater fluctuations than previously identified. Lastly, the An% and Mg# trends within each cycle are not as similar as previously thought. The data clearly shows that the two cycles are different and therefore the conditions responsible for the formation of each cycle are different. Using this data, a new position of the boundary between the two cycles is suggested. The genesis of the Upper Zone has been proposed in a number of models however, this study has shown that the model responsible for the formation of the Upper Zone is yet to be established. Despite the theory from Kruger *et al*. (1987), the possibility of the Upper Zone having formed from more than one magma injection needs to be reconsidered.

Acknowledgments

I would like to thank my supervisor Dr James Roberts for all the time and support provided throughout this study. I would like to thank Dr Bernard Charlier for the thin sections and his input as one of my co-supervisors. I would also like to thank Dr Gelu Costin for his time and help as co-supervisor. A special thanks all the help with the use of the microprobe. Thank you to Dr Roger Dixon for his guidance and advice throughout the writing up of this dissertation and for all the helpful literature. Thank you to David Dixon for drafting some of the figures. Thank you to Professor R.K.W. Merkle for the Upper Zone XRF data.

Lastly, I would also like to thank my family for all their support and understanding throughout my research.

Table of Contents

List of Figures

List of Tables

Chapter 1 – Introduction

The study of layered intrusions provides important information regarding the cooling, crystallisation and solidification processes of magmas in plutonic environments. The cumulate mineralogy and the geochemistry of the minerals are the primary sources of information about such processes, and thus detailed petrographic and mineralogical studies are required to improve our understanding of processes active during cumulate formation.

The purpose of this study is to document the mineralogy and geochemistry of cycles V and VI of the Upper Zone of the mafic Rustenburg Layered Suite, part of the Bushveld Complex in northern South Africa. The data collected may provide insight into the genesis of the Upper Zone, and include petrological studies of the mineralogy and electron microprobe analyses of the silicate minerals.

The 2.1 km thick Upper Zone is characterised by a number of features. The lithology transitions from gabbronorite and ferro-gabbronorite to ferro-diorite, and contains a number of anorthosite and magnetitite layers. In addition to these layers, previous studies have found the geochemistry to be cyclic. The cyclic nature of the Upper Zone was first documented by Tegner *et al*. (2006), who defined cycles based on geochemical reversals in the An content ([Ca/(Ca+Na+K) x 100]) of plagioclase and in the Mg# of olivine and pyroxene. The study identified nine cycles, (I to IX), with Cycles V and VI being the most obvious. The two cycles are located within the top third of the Upper Zone lithology and feature the most prominent reversals in An% and Mg#. Cycles V and VI are found in what is known as subzone UZc, the topmost section of the Upper Zone, which is characterised by the first appearance of cumulus apatite (Wager & Brown 1968).

The identification of these subzones and cycles originates from studies conducted on three boreholes drilled through the Upper Zone of the Western Limb of the Rustenburg Layered Suite. The boreholes, known as the Bierkraal cores (BK1, BK2 and BK3), extend from the top portion of the Main Zone, through the Upper Zone and into an overlying section of the younger Lebowa Granite Suite (Walraven & Wolmarans, 1979). The samples examined in this study came from BK1 that intersected the UZc.

Key aspects involved in petrological studies are mineral identification, mineral proportion estimation and measured grain size distribution. Textural relationships between cumulus and intercumulus minerals as well as the variations in the proportions and grain sizes will provide added insight into the formation of the Upper Zone.

Electron Microprobe Analysis (EMPA) of the cumulus and intercumulus minerals provide the necessary insight into the nature and origin of the geochemical variations. Geochemical breaks and fluctuations in the An % (plagioclase) and Mg # (olivine and pyroxene) have previously been used to identify the cyclicity of the Upper Zone. The increased sampling density in this study will allow for a more detailed examination of the trends within a cycle.

Examination of the trends identified within the An% and Mg# provides a great deal of insight into the possible conditions that potentially affected the crystallisation of an intrusions. Fractional crystallisation within an intrusion is characterised by gradual decreases in the An% and Mg#. Irregularities in the trends such as jumps back to higher An% and/or Mg# are most commonly interpreted as additions of new, more primitive magma.

Hypotheses regarding the genesis of the Upper Zone will be tested using the data collected. The results may shed additional light onto the conditions prevailing during the crystallisation of a single pulse of magma, with changes in pressure and/or temperature resulting in petrological and geochemical variations. On the other hand, the variations may point towards multiple injections of magma under a specific set of conditions.

Chapter 2 – Geological Background

The Bushveld Complex is a large igneous intrusion formed during the Palaeoproterozoic and is located in the northern part of South Africa. The complex consists of a number of intrusions all variable in morphology, chemistry and age. The best-known component of the Bushveld Complex is the ultramafic-mafic intrusion known as the Rustenburg Layered Suite, which has a generally accepted age of ~2.06 Ga (Buick *et al*., 2001; Zeh *et al.*, 2015).

The remainder of the intrusions include the Lebowa Granite Suite, the Rashoop Granophyre Suite and the Rooiberg volcanics. Isotopic studies (mainly Rb-Sr data) show that the formation of the Rooiberg volcanics predates the intrusive formations (Lenhardt & Eriksson, 2012). Subsequent to crystallisation, the Rooiberg felsites formed the roof rock of the Rustenburg Layered Suite and, following the emplacement of the Rustenburg Layered Suite, the Lebowa Granite Suite intruded. The Rashoop Granophyre Suite formed at the contacts between the Lebowa Granite Suite and the Rustenburg Layered Suite.

The areal extent of the complex is estimated at ~65000 km^2 (Eales & Cawthorn, 1996) with the surface expression of the Bushveld Complex is illustrated in Figure 1. The Rustenburg Layered Suite outcrops as a series of discrete limbs: Eastern Limb, Western Limb, Northern/Potgietersrus Limb and the poorly exposed South-eastern/Bethal Limb (Eales & Cawthorn, 1996). The lithology between the Eastern and Western Limb has been described as continuous, which led to the theory that the two limbs are connected at depth (Eales & Cawthorn, 1996; Cawthorn & Webb, 2001; Webb *et al.*, 2010).

The relationship between the stratigraphy of the Northern Limb with the Eastern and Western Limbs is much less apparent, as the mafic rocks of the Northern Limb are in contact with progressively older stratigraphy extending from the south to the north of the limb (Kinnaird *et al.*, 2005). Certain sections have also been noted as being absent, such as the upper portion of the Main Zone, or as unique to the Northern Limb, such as the Platreef (Ashwal *et al.*, 2005).

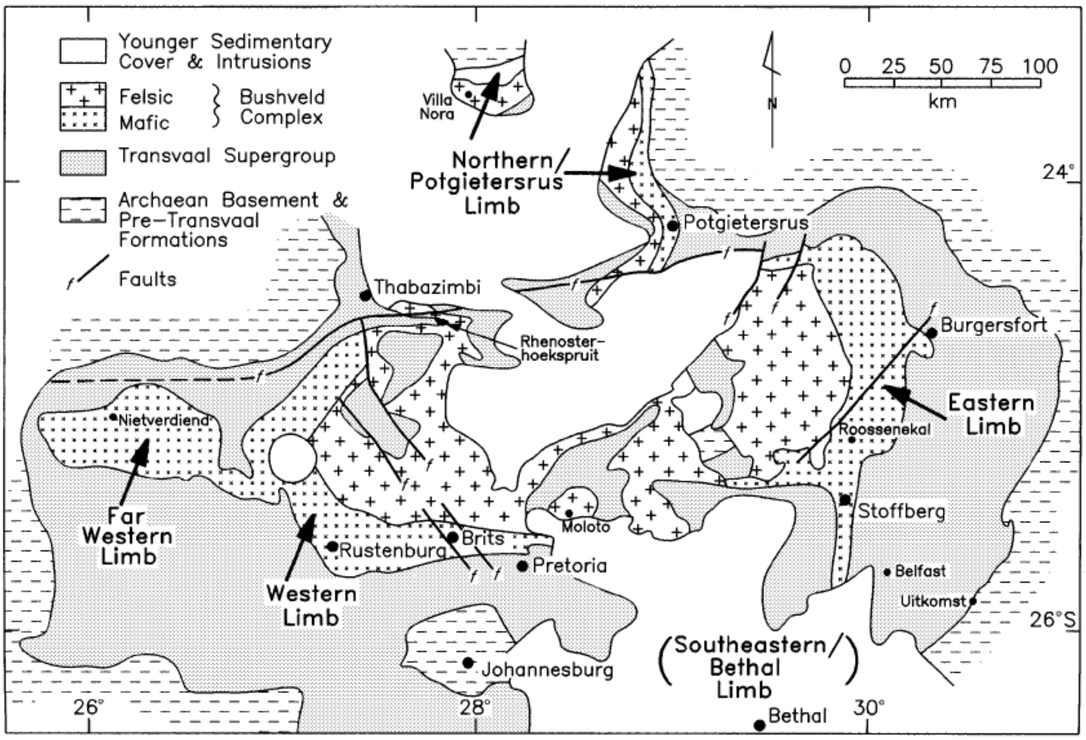

Figure 2. A geological map illustrating the extent of the Rustenburg Layered Suite (Eastern, Western, Northern and South-Eastern (Bethal) Limbs) relative to the Bushveld Complex (Cawthorn & Walraven, 1998).

The formation of the Bushveld Complex remains speculative owing to the complex relationships between the various intrusions and extrusions, and the lack of outcrop. Despite this, a number of models have been proposed, which generally involve mechanisms that require the generation of large volumes of magma over a short period.

The most popular model involves the impingement of a plume beneath the Kaapvaal Craton (Hatton & Schweitzer, 1995). A second theory, proposed by Hatton (1988), has the Bushveld Complex forming due to the melting of detrital material at a subducting plate margin near the edge of the Kaapvaal Craton. The third and most radical hypothesis is that of Rhodes (1975 & references therein) who proposed multiple meteorite impacts responsible for the generation of magma, as well as the subsequent shape of the Bushveld Complex.

The Bushveld Complex was emplaced as a series of magmas within the clastic and chemical sedimentary rocks of the Pretoria Group of the much larger Transvaal Supergroup (Cawthorn & Walraven, 1998). According to Cawthorn & Walraven (1998) the emplacement of the Bushveld Complex occurred as a series of magma injections with each pulse occurring within short succession of the previous pulse. Recent studies using U–Pb titanite ages, the emplacement of the Bushveld Complex into the Transvaal Basin took place over a period of less than 1 Ma (Buick *et al.*, 2001).

After the emplacement of the Bushveld Complex, the density of the magma resulted in the central portion of the complex sagging, creating strata gently dipping towards the centre of the complex. This sagging was accompanied by a number of faults all trending N-S with the stratigraphy dipping approximately 15-20 degrees towards the centre (Webb *et al.*, 2011).

The Rustenburg Layered Suite comprises a large portion of the Bushveld Complex. This massive layered intrusion formed due to multiple pulses of ultramafic to mafic magma (Eales & Cawthorn, 1996). The injection of compositionally variable magma into the crystallising crystal mush resulted in the formation of various zones distinguishable by their characteristic geochemistry. The subdivision of the Rustenburg Layered Suite into different zones is based on mineralogical, geochemical and isotopic variation (Eales & Cawthorn, 1996). The subdivisions of the layered intrusion are the Lower Zone, Critical Zone, Main Zone and The Upper Zone (Figure 2). The Upper Zone represents the area of interest for this study.

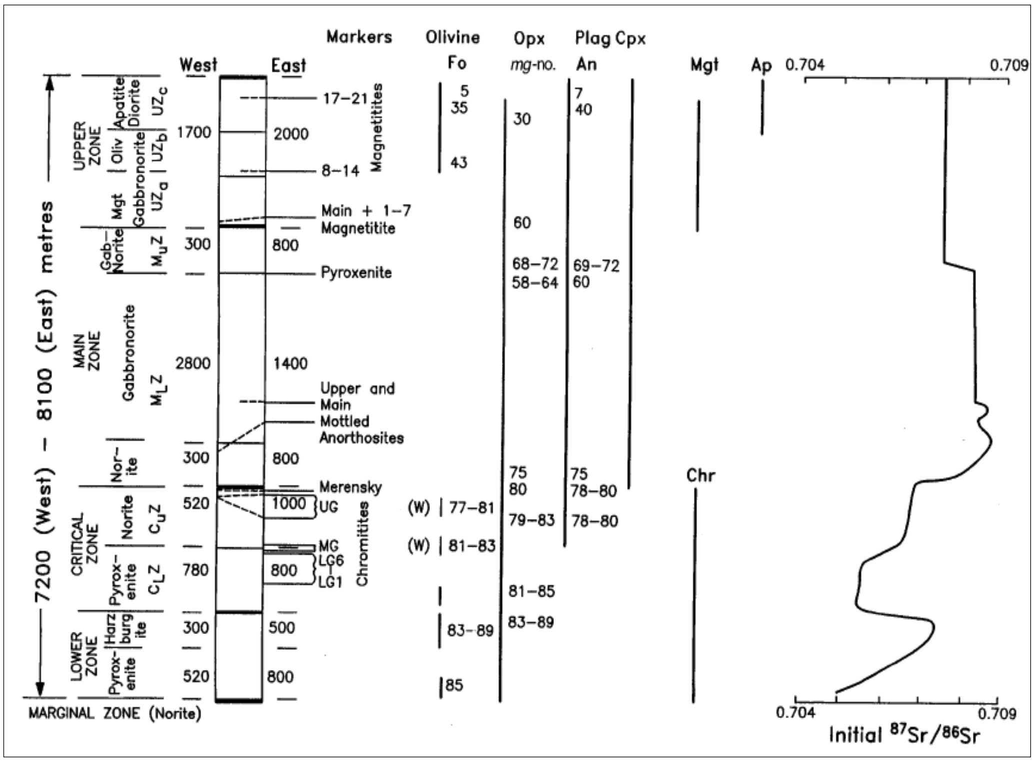

Figure 2. **A stratigraphic section of the Rustenburg Layered Suite illustrating the mineralogical variation throughout the suite (Cawthorn & Walraven, 1998).**

Stratigraphy of the Rustenburg Layered Suite

There is a distinct contrast between the more evolved Upper Zone and the more ultramafic to mafic underlying zones. The Marginal Zone is not always present but is inferred to be limited to the base of the intrusion (Eales & Cawthorn, 1996). Where present, the thickness of the Marginal Zone varies between 150-800m with the rock types varying between pyroxenite and norite (Eales & Cawthorn, 1996).

The Lower Zone is variable in thickness between the Western and Eastern Limbs (~1050m). The overall rock types alternate with dunites grading into harzburgites and then into orthopyroxenites, with layers varying in thickness from 1m to hundreds of metres. Nine cycles have been identified using the oscillatory change in Mg# that has been attributed to smaller pulses of magma being injected from the same, yet evolving magma chamber hence the increasing initial $^{87}Sr/^{86}Sr$ ratio illustrated in Figure 2 (Eales & Cawthorn, 1996).

The Critical Zone, which overlies the Lower Zone, contains the largest chromite ore reserve in the world (Eales & Cawthorn, 1996). Layers of chromitite are found throughout the stratigraphy, inter-layered with norite, orthopyroxenite and anorthosite, with minor dunite and harzburgites. The variation in isotopic ratio shown in Figure 2 implies that the Critical Zone, and the subsequent chromitite layers, formed due to multiple pulses of magma (Eales & Cawthorn, 1996). In order to form chromitite layers, injections of a primitive, chromite-rich magma into a fractionally crystallised residual magma will result in the supersaturation of chromite. The formation of the monomineralic layers forms by cooling and crystallisation of chromite followed by the accumulation at the base of the intrusion (Mondal & Mathez, 2007).

The Main Zone represents the thickest section of the mafic suite and has an average thickness of ~3km. The stratigraphy is a relatively continuous succession of norite and gabbro-norite with minor anorthosite and pyroxenite layers. The Pyroxenite Marker, a homogenous layer of orthopyroxenite, is found at ~2.4 km above the base of the Main Zone, and represents the final magma recharge event of the Rustenburg Layered Suite (Kruger *et al.*, 1987). The final pulse of magma mixed and rapidly homogenised with the residual melt of the crystallising Main Zone resulting in a magma with a constant Sr value of 0.7073 (Tegner *et al.*, 2006). Magnetite appears as a minor phase towards the top of the Main Zone but it is at the first appearance of cumulus magnetite that the upper boundary of the Main Zone is drawn.

Based on the study by von Gruenewaldt (1973) the Main Zone is subdivided into three subzones using the Ca-poor pyroxenes, subzones A, B and C. The bottom subzone A contains Ca-poor orthopyroxene throughout norite, anorthosite and gabbronorite. Subzone B is made up of relatively homogenous gabbronorite that once contained pigeonite but has inverted to orthopyroxene. This subzone consists of both original orthopyroxene and inverted orthopyroxene. The Pyroxenite Marker represents the base of subzone C. Orthopyroxene is the only Ca-poor pyroxene present throughout this zone. Above the Pyroxenite Marker, the remainder of subzone C consists of orthopyroxene with a reversal in both Mg# and Cr content. More recent studies of the Western Limb by Nex *et al.* (1998) incorporated the works of von Gruenewaldt (1973) but outlined five subzones, A to E.

Upper Zone

The 2.1 km thick Upper Zone represents the final stages of crystallisation of the Rustenburg Layered Suite (Kruger *et al.*, 1987). The Upper Zone is commonly believed to have formed from a single and final pulse of magma injected in at the Pyroxenite Marker (Kruger *et al.*, 1987). The crystallisation of this final pulse of magma formed the most felsic and differentiated compositions found throughout the Rustenburg Layered Suite.

The lithology of this zone is predominantly ferro-gabbronorite to ferro-diorite with a highly differentiated mineralogy (Figure 3). The first appearance of cumulus magnetite represents the lower boundary of the Upper Zone (SACS, 1980), and occurs 200-300 m above the Pyroxenite Marker (von Gruenewaldt, 1973; Kruger *et al.*, 1987; Cawthorn *et al.*, 1991). A number of magnetitite and anorthosite layers occur throughout the Upper Zone.

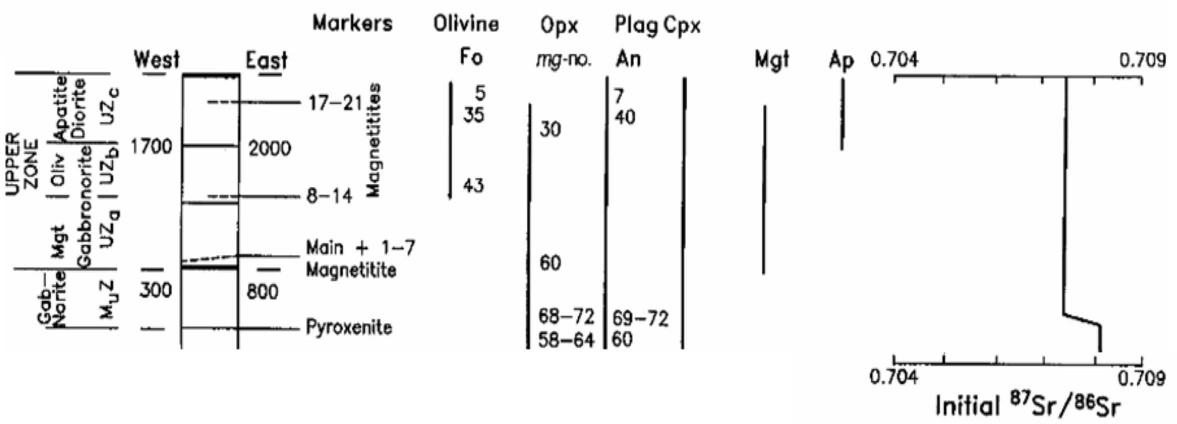

Figure 3. **A stratigraphic column of the Upper Zone showing the position of the Pyroxenite Marker, the compositional variation in the mineralogy, the position of the various magnetitite layers, and the relatively homogenous Sr initial ratios (Cawthorn & Walraven, 1998).**

Figure 3 shows the general changes in the cumulus minerals. The Upper Zone minerals include plagioclase, olivine, orthopyroxene, clinopyroxene, magnetite and apatite. The silicates range from primitive compositions at the bottom to increasingly more evolved compositions further up, with the appearance of apatite towards the top of the Upper Zone supporting extensive differentiation and crystallisation of more evolved mineral phases (Eales & Cawthorn, 1996).

Subdivisions of the Upper Zone

Kruger *et al.* (1987) proposed that the Upper Zone experienced no magma recharge and was therefore crystallised from a single isotopically homogenous magma, based on the measurement of consistent $^{87}Sr/^{86}Sr$ ratios of 0.7073 from the Pyroxenite Marker up through the Upper Zone. Crystallisation and differentiation from the Pyroxenite Marker up into the Upper Zone would thus drive the mineralogical evolution of the Upper Zone lithology (Kruger *et al.*, 1987).

Wager and Brown (1968) identified three subdivisions of the Upper Zone; UZ_a, UZ_b and UZ_c. The appearance of unique cumulus minerals at particular depths led to the delineation of three subunits. The first appearance of cumulus magnetite (UZ_a) is followed by the first appearance of cumulus olivine (UZ_b) and finally the first appearance of apatite (UZ_c).

Numerous authors have presented additional subdivisions, but the majority are based on those of Wager & Brown (1968). Table 1 below summarises the three most commonly accepted divisions. The subdivisions of Wager & Brown are used in this study.

Table 2. Comparison of stratigraphic subdivisions of the Upper Zone (after Scoon & Mitchell, 2012)

Authors	**Scoon & Mitchell (2012)**	**Von Gruenewaldt (1973)**	**Wagner & Brown (1968)**
Study area	Roossenekal	Roossenekal	Eastern Limb
Subzones	**Subzone E**	**Subzone D**	**Subzone C**
	Upper contact of Upper magnetite layer 21 (height of 1968m)	Appearance of cumulus apatite	Appearance of cumulus apatite
	Subzone D		
	Appearance of cumulus apatite (height of 1300m)		
	Subzone C	**Subzone C**	**Subzone B**
	Appearance of cumulus olivine (height of 705m)	Appearance of cumulus olivine	Appearance of cumulus olivine
	Subzone B	**Subzone B**	**Subzone A**
	Geochemical transition approximately 80m below the MML (height of 200m)	Lower contact of Main magnetitite layer (MML)	Lower contact of Lower magnetitite layer 1
	Subzone A	**Subzone A**	
	Appearance of cumulus Ti-magnetite (67m below Lower magnetitite layer 1)	Appearance of cumulus Ti-magnetite	

The mineralogy of the Upper Zone reveals a number of cyclic geochemical reversals. Tegner *et al.* (2006) showed distinct changes in composition with depth. These geochemical changes were identified after examining the An% of plagioclase and the Mg# of olivine and pyroxene, with some cycles are more distinct than others (Figure 4).

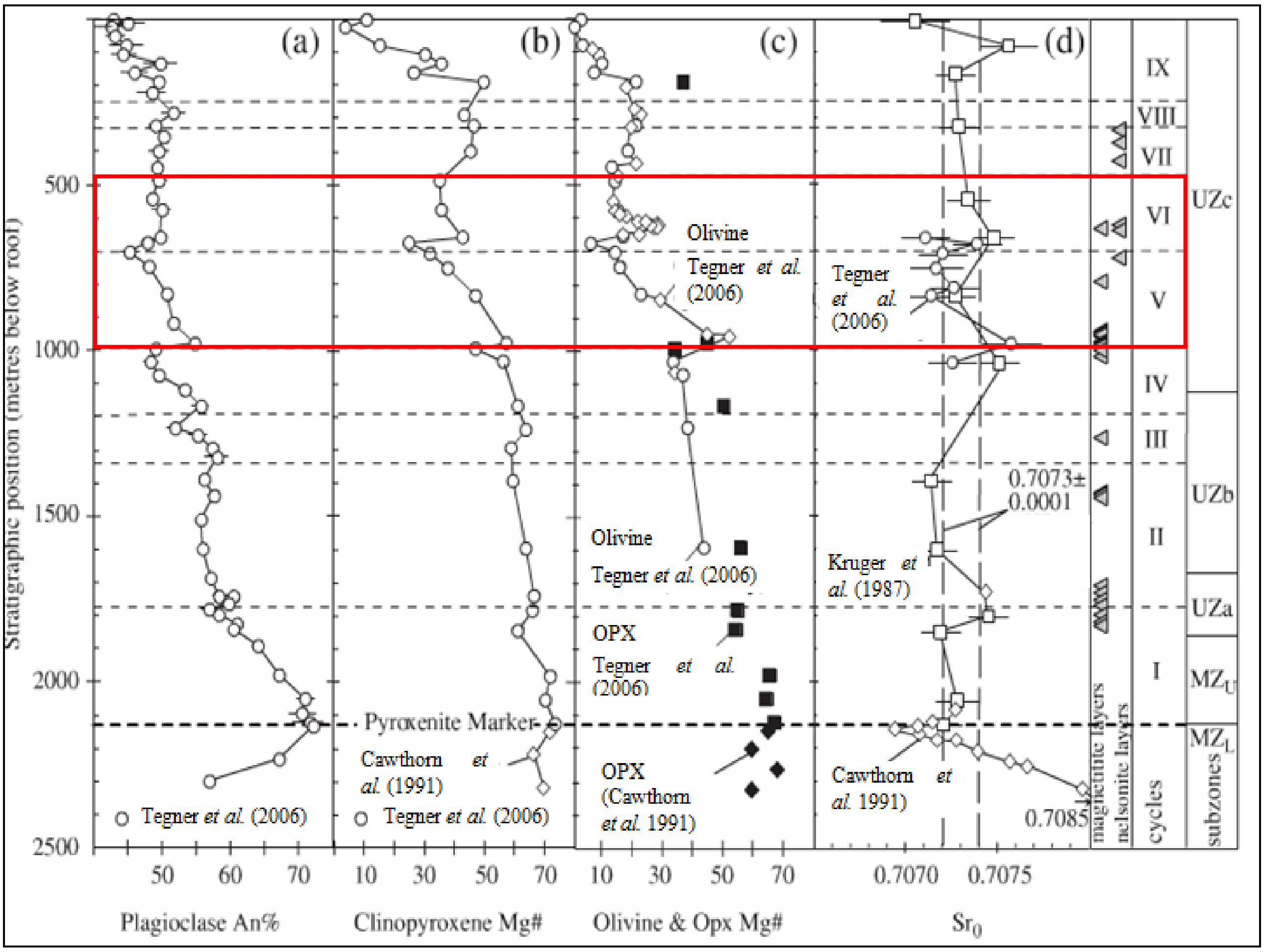

Figure 4. **The nine cycles identified within the Upper Zone based on the variation in plagioclase content and the Mg # (Tegner *et al.*, 2006) using the subdivisions of Wager & Brown (1968). Inserted red block to show the position of Cycle V and Cycle VI.**

Emplacement of the Upper Zone

The crystallisation of the Upper Zone from a single pulse of magma is the most readily accepted theory regarding the Upper Zone emplacement. Numerous studies presenting additional $^{87}Sr/^{86}Sr$ analyses agree with the study of Kruger *et al.* (1987). One such study is that of Tegner *et al.* (2006) where, after the analysis of an additional 24 samples, they confirmed the $^{87}Sr/^{86}Sr$ ratio of 0.7073 ± 0.0001.

Despite the strong support for Kruger *et al.* (1987), recent studies have proposed that the emplacement of the Upper Zone may have involved multiple injections of magma. Scoon & Mitchell (2012) hypothesise that the Upper Zone did indeed experience multiple injections of magma but from a basaltic, isotopically homogenous magma chamber. Using whole rock data and cumulate textural variation based on samples collected from boreholes in the Roossenekal area in the Eastern Limb, the authors suggest multiple injections are responsible for the lack of a complete differentiation trend throughout the Upper Zone, until the topmost sections where the final pulse of magma was injected and continuous differentiation took place.

Vantongeren & Mathez (2013) discussed a similar model whereby multiple recharge events took place at the Pyroxenite Marker. These multiple pulses were of a small volume and took place with large enough intervals to allow enough time for the magma to homogenise. Thermodynamic examination of the plagioclase grains below, within and above the Pyroxenite Marker show that no drastic temperature changes occurred, such as might be associated with a single large pulse of magma (Cawthorn *et al.*, 1991).

Eruption of the Upper Zone

The lack of a silica-rich end member to the Upper Zone crystallisation sequence led to the idea that eruption had occurred during the crystallisation of the Upper Zone (Cawthorn & Walraven, 1998). According to this hypothesis, the eruption of the Upper Zone took place as a series of periodic eruptions. Owing to the overall low estimates of Zr concentrations for a parental magma for the Main and Upper Zone, the authors argued that the remainder of the Zr had been lost due to eruption. Using Zr and K concentrations, Cawthorn & Walraven (1998) estimated the volume of erupted material to be in the order of 40% of the total volume of magma. K data collected by Von Gruenewaldt (1970) indicated similar results. Erosion is held to have subsequently removed all evidence of these eruptives.

Vantongeren *et al.* (2010) calculated a possible parent magma composition for the Upper Zone. Using this theoretical parental magma, the volume of the material lost from the Upper Zone was estimated to be between 15 and 25 %. According to this model, the Upper Zone evolved towards a felsic end member, erupting to form part of the Rooiberg rhyolites.

Initially, according to Huppert & Sparks (1984), the increased densification of an iron-rich magma due to differentiation would substantially reduce the probability of an eruption. The density contrast between the host country rock and the increasingly more dense magma would reduce the effect of pressure-induced eruption. However, according to Namur *et al.* (2012) the density of a Fe-Ti-rich residual magma would increase through fractional crystallisation. Following the liquid line of decent, Fe-Ti oxides would arrive on the liquidus and upon crystallisation would lead to significant decrease in the density of the now Fe-Ti poor liquid. Namur *et al.* (2012) showed that the density of felsic magmas is therefore less than mafic magmas. The effect of this on previously published eruption volumes by

Cawthorn & Walraven (1998) and Vantongeren et al. (2010) are in sharp contrast to the estimated eruption volumes for modern basaltic volcanoes (White et al., 2006; Crisp, 1984), which are generally much less than 10%.

Background to the Bierkraal Boreholes

The Upper Zone of the Rustenburg Layered Suite originated from a drill core taken through the Western Limb, just a few kilometres NE of Rustenburg. The Council for Geosciences, formerly known as the Geological Survey of South Africa, drilled three boreholes in 1974 in order to obtain the full stratigraphy of the Upper Zone (Walraven & Wolmarans, 1979). The boreholes, known as BK1, BK2 and BK3, were drilled on the farm Bierkraal just NE of Rustenburg in the Western Limb of the Rustenburg Layered Suite (Figure 5).

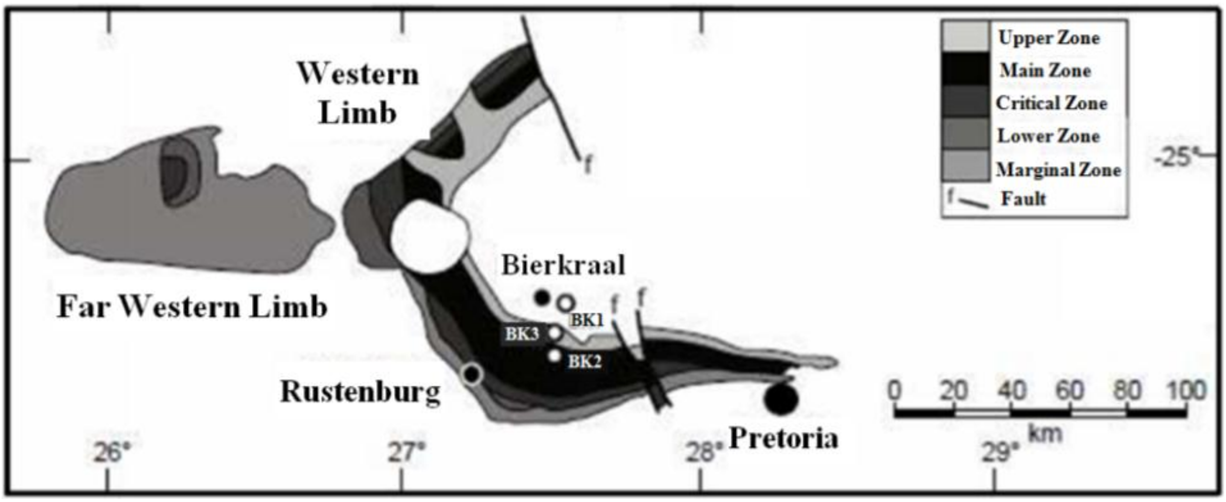

Figure 5. **Map showing the locations of the BK1, BK2 and BK3 boreholes through the Upper Zone of the Rustenburg Layered Suite just NE of Rustenburg.**

Previous work (Walraven & Wolmarans 1979; Kruger *et al.*, 1987) provided correlations between the boreholes using the appearance of apatite and the V_2O_5 content in magnetite. Figure 6 illustrates the correlation between these boreholes with the depths corrected to surface. These boreholes have previously been utilised by Cawthorn & McCarthy (1985), Reynolds (1985*a*, 1985*b*), Merkle & von Gruenewaldt (1986), Kruger *et al.* (1987), Cawthorn & Walsh (1988), von Gruenewaldt (1993), Tegner *et al.* (2006).

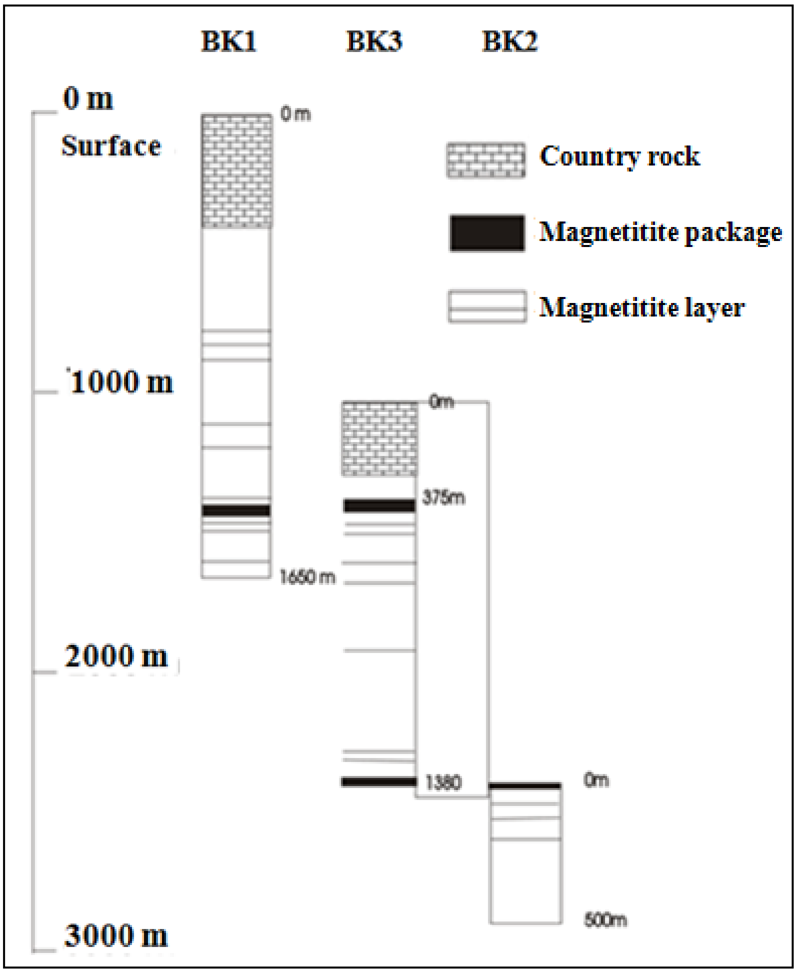

Figure 6. **Illustration of the correlation of the BK1, BK2 and BK3 boreholes using previously existing data.**

BK1 starts in the Lebowa Granite Suite and reaches a depth of approximately 1600 m where it intersects a relatively thick magnetitite layer. BK2 extends from the Main Magnetitite layer through to the Main Zone until the intersection of the Pyroxenite Marker. Drilling of the third borehole, BK3, covered the gap between the base of BK1 and the top of BK2.

Models of anorthosite layer formation

A number of anorthosite layers occur throughout the ultramafic-mafic sequence of the Rustenburg Layered Suite. The anorthosite layers found in the Upper Critical Zone are considerably different to the anorthosite layers located in the Main and Upper Zones. Some of the most significant anorthosite layering occurs in the Upper Zone, with some layers measuring tens of metres in thickness. The genesis of these particular layers has engendered some debate and several models regarding the Upper Zone anorthosite layers have been proposed.

Field mapping of the Skaergaard Intrusion by Wager & Brown (1968) led to the description of the layering of the intrusion being almost sedimentary in appearance. It was proposed that differential setting between the dense mafic minerals and the lesser dense plagioclase led to the formation of the modal layers, especially the anorthosite layers. The multiple layers formed were attributed to pulses of crystallisation followed by a period of more static conditions were crystal settling was allowed to take place, resulting in the sharp contact at the base of the layer with a gradational decrease in darker, mafic minerals and increasing amounts in the modal proportions of plagioclase.

The formation of anorthosite layers due to supercooling and rapid nucleation is a theory first proposed by Maaloe (1978), based on studies carried out on the Skaergaard intrusion. The model suggests supercooling of a magma, which would result in rapid nucleation and the simultaneous supersaturation of the various stable mineral phases.

In a study carried out by Irvine *et al*. (1983) regarding the J-M Platinum-Palladium Reef of the Stillwater Complex, the formation of the anorthosite layers was attributed to double-diffusive convection. Generation of these convection cells resulted from multiple injections of magma. The large variations in the proportions of the various minerals present represented mineralogical breaks caused by additional injections of magma. The model proposed the injection of a plagioclase-saturated magma with the subsequent development of anorthosite layers at the top of the double-diffusive convective cell. Irvine *et al*. (1983) also discussed the possible relevance of this model to the formation of the Merensky Reef in the Bushveld Complex.

Eales *et al.* (1990) investigated the anorthosite layers of the Critical Zone and attributed the cyclic reversals in the mineralogy and changes in the mineral crystallisation to magma replenishment. According to Eales *et al.* (1990), the formation of the anorthosite layers resulted from differentiation of a magma to form pyroxenite, norite and finally anorthosite. In order to crystallise pyroxene again, and the following anorthosite layer, a new batch of magma would need to be injected.

The lateral continuity of the Upper Zone anorthosite layers led to the suggestion of changes in a large-scale variable. Naslund & McBirney (1996) discussed the effect of changes in pressure and the generation of anorthosite layers. With a decrease in pressure, the liquidus temperature of plagioclase and pyroxene would decrease at different rates (Cawthorn & Ashwal, 2009). According to Naslund & McBirney (1996) and Cawthorn & Walraven

(1998), an eruption would trigger a considerable decrease in pressure leaving the magma at superheated conditions. Due to the different rates of the shifting liquidus between plagioclase and pyroxene, the first mineral to crystallise would be plagioclase until the co-tectic is reached.

Scoon & Mitchell (2012) proposed the formation of the anorthosite layers by means of disequilibrium partial melting. Additions of hotter pulses of magma into a crystal mush would result in the melting of the mafic mineralogy and the "survival" of plagioclase as a refractory material (Naslund, 1986). Mitchell & Manthree (2002) have previously investigated the formation of the Critical Zone anorthosites by disequilibrium partial melting.

Bédard *et al*. (2007) presented a study into the Jurassic Ferrar dolerite sills of the McMurdo Dry Valleys of Antarctica that showed the presence of large anorthosite-rich layers that were of uniform plagioclase composition compared to the hanging and footwall lithologies. The authors proposed a model whereby the homogenisation of the plagioclase compositions was achieved through local sourcing of plagioclase from the surrounding crystal mush and consequently the enrichment of pyroxene. The result would be the near identical An composition of the anorthosite sill with the hanging wall and footwall.

In a study carried out by Cawthorn & Ashwal (2009), models concerning the formation of anorthosite layers were reviewed. Using the density of sampled rock types, the various mineral proportions were determined. A number of the above-mentioned models were re-examined in their study. The model proposed by Cawthorn & Ashwal (2009) noted that the formation of the anorthosite layers within the Upper Zone would require an extreme form of differential settling after periods of pulsed crystallisation of plagioclase and pyroxene. Compared to the model proposed by Wager & Brown (1968) the periods of quiescence would not have been as extensive as in the Skaergaard layers and complete separation between mafic minerals and plagioclase would not be possible. As a result, more leucocratic rocks types border the upper and/or lower boundaries of many of the anorthosite layers.

According to Cawthorn & Ashwal (2009), the model set out by Maaloe (1978) involving the supersaturation of plagioclase would result in the prolific crystallisation of smaller plagioclase grains. Additionally, supercooling within the Skaergaard intrusion is plausible; however, the calculated rate of cooling within the Rustenburg Layered Suite, according to Cawthorn & Walraven (1998), is significantly slower. As a result, supercooling within the mafic series is highly unlikely.

Cawthorn & Ashwal (2009) discussed the generation of double-diffusive convection cells by multiple magma injections (Irvine *et al*., 1983). The model involved the injection of a plagioclase-saturated melt at the base of a resident crystallising mush. The mush, described as containing predominantly plagioclase, pyroxene and possible magnetite, would then produce an anorthosite layer at the base of the chamber. In order to be plausible, the An% of the anorthosite layer and the footwall would need to vary by more than 2%. Cawthorn & Ashwal (2009) incorporated data from Tegner *et al*. (2006) and observed that the An% very seldom varied more than 2%.

According to Cawthorn & Ashwal (2009), the cyclic mineralogy of the Upper Zone makes the application of the theory from Eales *et al.* (1990) plausible. However, additions of a plagioclase-saturated melt would result in abrupt contacts as well as drastic changes in the mineral compositions. Despite the mineralogical cyclicity, no significant reversals in the mineral compositions, as seen in the Critical Zone, were observed. In addition to this, the cycles within the Upper Zone transition through magnetitite-gabbronorite-anorthosite, not pyroxenite-norite-anorthosite.

The formation of the anorthosite layers by magma addition has been argued against based on the unlikely event that the incoming magma pulses contain plagioclase compositions similar to the resident crystal mush. In the model described by Bédard *et al*. (2007), the incoming magma sourced plagioclase from the resident crystal mush and subsequently formed anorthosite layers with identical plagioclase compositions. However, Cawthorn & Ashwal (2009) pointed out that enrichment of pyroxene would result through the removal of plagioclase from the crystal mush. No pyroxene-rich rocks are found either above or below the Upper Zone anorthosites.

Models of magnetitite layer formation

Numerous magnetitite layers have been identified in different portions of the Upper Zone. Twenty-one magnetitite layers identified by Molyneux (1974) are shown in Figure 3 (represented by the numbers 1-21) and Figure 4 (represented by the triangular symbols on the right of the figure). Tegner *et al*. (2006) identified twenty-six magnetitite layers and six nelsonite layers (titanium-magnetite-apatite rich layers). The most prominent feature of the Upper Zone cyclicity is the sharp contact between the underlying anorthosite and the overlying magnetitite layers which show a gradual transition into gabbro and then into anorthosite again. The sharpness of the contact is however variable. The thickness of the layers varies between 2 and 710 cm thick, with some layers containing economic concentrations of vanadium.

Wager & Brown (1968) proposed that the magnetitite layers formed through differential density settling. This model, however, is inapplicable to the magnetitite layers of the Upper Zone. Settling out of heavier minerals after cotectic crystallisation of plagioclase and mafic minerals would result in a gradational contact transition onto into rocks containing an intermediate density of cumulus pyroxene followed by cumulus plagioclase. The lithologies overlying the magnetitite layers differ in that there is no overlying cumulus pyroxene, only cumulus plagioclase.

A shift of the oxygen fugacity within a system would affect the crystallisation of magnetite and not that of the plagioclase crystallising before and after the magnetitite layers (Klemm *et al.*, 1985). However, a mechanism to create such a shift in the oxygen fugacity and create the observed contacts is not commonly accepted (Cawthorn & Ashwal, 2009).

Studies published by Reynolds (1985*a*, *b*) proposed the formation of magnetitite layers by means of liquid immiscibility. A clear contrast in both the densities and the viscosities between the two melts would be evident. The variations between these two variables would result in the percolation of the ferric melt through the silica melt, leading to the formation of two distinct layers separated by a sharp contact. However, more gradational contacts are observed in the magnetitite layers of the Upper Zone.

According to Cawthorn & McCarthy (1980), changes in pressure, as opposed to geochemistry, would result in the formation of magnetitite layers. The observed fluctuations in the Cr concentrations are achieved through crystallisation of magnetite at the base of the magma chamber rather than crystallisation and settling out from the magma. In addition, the lateral consistency of these layers implies a model capable of causing a large-scale phase boundary shift towards the crystallisation of magnetite.

The works of Cawthorn & Ashwal (2009) and Cawthorn & McCarthy (1980) agree that this model involves a large-scale effect of the mechanism resulting in the formation of the magnetitite layers. Changes in pressure resulting from tectonic forces could cause a shift of the liquidus crystallising out only magnetite.

Despite the near-homogenous Sr^{87}/Sr^{86} data, the formation of the Upper Zone due to magma mixing remains contentious. The cyclic mineralogy of the Upper Zone, in addition to the sharp contacts observed beneath some magnetitite layers supports magma mixing. Harney *et al.* (1990) and Harney *et al.* (1996) proposed the formation of magnetitite layers by one of two models: firstly, from magma mixing by the addition of small volumes of magnetite-rich magma, which would not drastically affect the general isotopic ratios; and secondly, by the collapse of a density-separated stratified column. With magma additions, the liquid mixed in with the residual magma would be less differentiated and therefore reversals in the An% should be evident. Although cyclic reversals in An% throughout the Upper Zone are evident, Tegner *et al.* (2006) noted that the positions at which the reversals were identified showed no distinct relationship with the position of the magnetitite layers.

Zhang *et al.* (2012) proposed a highly evolved; Fe-Ti-rich parental magma was responsible for the deposits of the Baima Intrusion in China. The formation of these deposits from this parental magma would require a system closed to oxygen and extreme silicate fractionation. Subsequently, this would allow for the crystallisation of Ti-rich Fe deposits as the magma began to rise to shallower depths. Multiple pulses of magma led to the crystallisation and crystal settling which then led to the formation of stratiform Ti-Fe-rich oxides at the base of the intrusion. Scoon & Mitchell (2012) proposed a similar mechanism for the formation of the Upper Zone, in which each magnetitite layer or cluster of smaller layers would represent a separate injection of a crystal rich mush. Rapid crystallisation within these intruded sills would result in the formation of dense crystal slurries rich in Ti-rich oxides that would then settle to form magnetitite layers.

Chapter 3 – Methodology

Sampling

The Bierkraal boreholes were drilled through the Upper Zone in the Western Limb of the Rustenburg Layered Suite, where the three boreholes combined cover the entirety of the 2.1 km thick Upper Zone. The two most pronounced cycles, according to the subdivisions of Tegner *et al.* (2006), are Cycles V and VI. Thirty samples were taken from BK1; fifteen from Cycle V and fifteen from Cycle VI (Table 2). The sampling positions were determined through core logging and through the examination of pre-existing whole rock data.

The Rustenburg Layered Suite in BK1 extends from a depth of ~1650 m up to a depth of ~430 m, where the Lebowa Granite Suite caps the borehole. Prior to sampling, BK1 was logged in extensive detail in order to identify the relevant cycles. Core logging revealed three main rock types namely: magnetitite, gabbro and anorthosite.

Cycle V is from ~1460 m to ~1105 m and Cycle VI from ~1100 m to ~900 m. Both cycles appeared to contain similar lithologies. Changes in the proportions of plagioclase, olivine and pyroxene in hand specimen were obvious, but the identification of apatite was impossible due to the relatively small grain size. Unfortunately, some uncertainty as to the exact depth of sampling exists due to the lack of core loss information throughout BK1, but the sampled depths are correlated with those used by Tegner *et al.* (2006). Core loss was calculated by measuring the exact amount of core present in each tray versus the recorded depths from which the core was extracted. The estimated loss varied from tray to tray with calculations estimating losses between 20 cm and reaching as high as 100 cm in highly fractured sections of the core.

The use of whole rock data allowed for the identification of potential changes in the modal mineralogy. Whole rock XRF data was provided courtesy of Professor R.K.W. Merkle of the University of Pretoria. In Figure 7, whole rock XRF data for CaO is shown with the CaO of plagioclase from Tegner et al. (2006) and the CaO of plagioclase from this study.

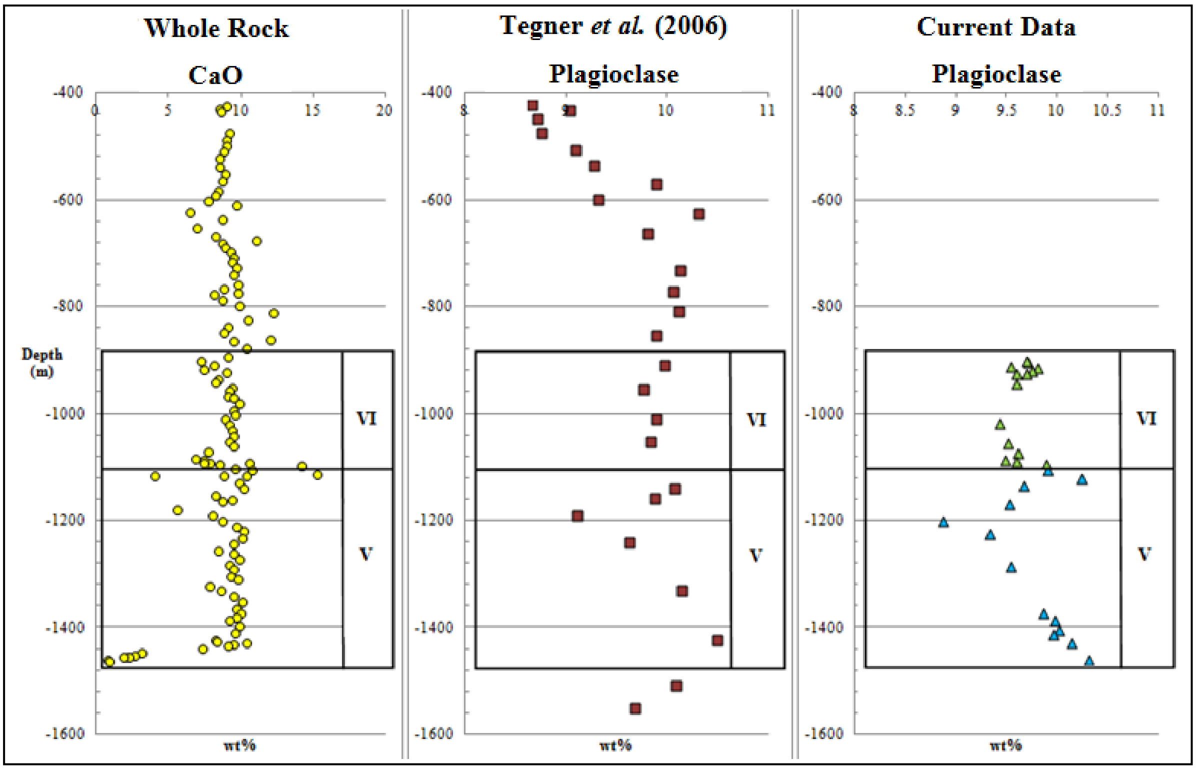

Figure 7. Comparison of whole rock CaO, plagioclase CaO (Tegner *et al.*, 2006) and plagioclase CaO from this study. Cycles V and VI are indicated by the boxes.

Table 2. Samples collected from Cycles V and VI from BK1 of the Upper Zone.

CT_5	Sample #	Depth (m)	Description	CT_6	Sample #	Depth (m)	Description
	1	-1105.5	Gabbro		1	-902.3	Mottled anorthosite
	2	-1119.3	Magnetite-rich gabbro		2	-904.5	Mottled anorthosite
	3	-1133.85	Gabbro		3	-911.66	Anorthite-rich gabbro
	4	-1155.92	Gabbro		4	-914.99	Anorthosite
	5	-1166.52	Mottled anorthosite		5	-918.69	Gabbro
	6	-1179.8	Anorthite-rich gabbro		6	-923.61	Anorthosite
	7	-1199.75	Gabbro		7	-925.91	Anorthosite
	8	-1223.85	Gabbro		8	-942.4	Gabbro
	9	-1285.65	Gabbro		9	-990.09	Gabbro
	10	-1371.05	Gabbro		10	-1016.5	Gabbro
	11	-1385.04	Gabbro		11	-1053.67	Gabbro
	12	-1403.32	Gabbro		12	-1074.04	Gabbro
	13	-1411.03	Gabbro		13	-1085.54	Gabbro
	14	-1427.95	Gabbro		14	-1090	Gabbro
	15	-1458.12	Magnetite-rich gabbro		15	-1094	Gabbro

Microscopy

Polished thin sections were prepared from the 29 samples collected throughout cycles V and VI at the University of Hanover courtesy of Dr B. Charlier. The petrographic study involved mineral identification, estimation of modal proportions of the main mineral assemblage, examination of important textural relations between minerals and textural changes.

The determination of the modal proportions of each sample was carried out using a form of spectral analysis. Spectral analysis involves the quantification of each of the mineral proportions based using the colour of the mineral in standard light (i.e. hand specimen). Each thin section was scanned at 2400 dpi. Each image was then imported into Adobe Photoshop CS4 and cropped so that only the rock was analysed. The total pixel count was used to determine the proportion of each mineral in the rock. An example of this method is given in the table below.

Table 3. **Scanned image of sample CT5_10 (left) and the mineral proportion estimation using the pixel count for each mineral.**

		CT_10	
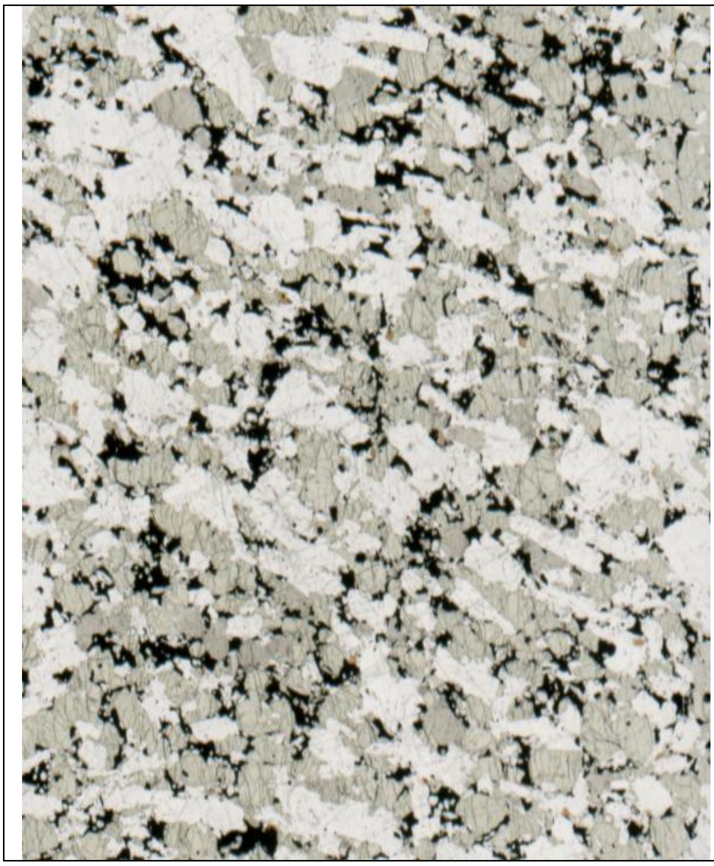		**Pixels**	**Proportion**
	Magnetite	258397	9.9
	Plagioclase	1580463	60.3
	Apatite	39420	1.5
	Olivine	648545	24.8
	Pyroxene	69458	2.7
	Biotite	23722	0.9
	Amphibole	0	0
	Silica	0	0
	Total	**2620005**	**100**

In Adobe Photoshop, a number of tools were used to enhance and isolate each of the individual minerals. The first of these tools adjusted the contrast of the image to enhance the discrimination between pyroxene and olivine. The second tool enabled the isolation of each mineral based on its colour. In order to distinguish between different minerals a particular "tolerance" was assigned to each mineral. Plagioclase and amphibole was assigned a tolerance of 40, olivine, apatite and silica 10, pyroxene 30 and finally biotite and magnetite 70. Using these features, the number of pixels making up each of the respective minerals was determined and calculated as part of the total pixels of the image.

The grain size variation was calculated as follows: Each thin section was divided into a 4 by 5 grid (total of 20 blocks). Within each block between three and five grains of each of the respective minerals were measured and recorded. In the case of inequant grains such a plagioclase, only the long axis was measured. The median was considered to be the most representative of the grain size variation and used in conjunction with the upper and lower and minimum and maximum values in box-whisker plots, as seen for instance in Figure 15.

Electron Microprobe

Major element data was collected for each of the thin sections using a JEOL JXA 8230 Superprobe, with four WD spectrometers at the Department of Geology at Rhodes University. The analytical conditions employed were an acceleration voltage of 15kV, a probe current of 20nA; counting times were at ten seconds on peaks and five seconds on background, and the beam spot size less than 1 micron. Characteristic x-rays were measured and the ZAF matrix correction was used for quantification.

Examination and mapping of each thin section took place to indentify suitable grains for each mineral phase. The number of grains analysed for each mineral varied between minerals based on the proportions of the relative mineral. In extreme cases, low apatite bearing samples for example, a minimum of five grains per slide for each mineral were analysed. A single spot at the core of each mineral was analysed except pyroxene. Exsolution of an oxide phase along the cleavage planes required additional points on a single mineral.

The following X-ray lines, spectrometer crystals and standards (in brackets) were used for plagioclase & silica: SiKα, TAP (Plag-An65_SPI); CaKα, PETJ (Plag-An65_SPI); TiKα, PETJ (Rutile_SPI); NaKα, TAP (Plag-An65_SPI); AlKα, TAP (Almandine_SPI);

FeKα, LIF (Almandine_SPI); KKα, PETL (Biotite_SPI); MnKα, LIFL (Rhodonite_SPI); BaLα, PETL (Barite_SPI); MgKα, TAPL (Olivine_SPI); SrLα, PETL (SrTiO3).

Olivine: SiKα, TAP (Almandine_SPI); CaKα, PETJ (Cr_Diopside_SPI); MgKα, TAP (Olivine_SPI); AlKα, TAP (Almandine_SPI); FeKα, LIF (Almandine_SPI); MnKα, LIFL (Rhodonite_SPI); NiKα, LIFL (Pentlandite_SPI); TiKα, PETL (Rutile_SPI); CrKα, PETL (Chromium_Oxide_SPI).

Pyroxene: SiKα, TAP (Almandine_SPI); CaKα, PETJ (Cr_Diopside_SPI); TiKα, PETL (Rutile_SPI); NaKα, TAP (Albite_SPI); AlKα, TAP (Almandine_SPI); FeKα, LIF (Almandine_SPI); KKα, PETL (Biotite_SPI); MnKα, LIFL (Rhodonite_SPI); CrKα, PETL (Chromium_SPI); MgKα, TAPL (Olivine_SPI).

Apatite: SiKα, TAP (KP Garnet); CaKα, PET (KP Garnet); PKα, PETJ (Apatite_SPI); MgKα, TAP (Dolomite_SPI); AlKα, TAP (Almandine_SPI); FeKα, LIF (Almandine_SPI); ClKα, PETL (Tugtupite1); MnKα, LIFL (Rhodonite_SPI); BaLα, PETL (Barite_SPI); FKα, TAPL (MgF2); NaKα, TAPL (Albite_SPI); SrLα, PETL (Celestite_SPI).

Biotite & amphibole: SiKα, TAP (Olivine_SPI); CaKα, PETJ (Cr_Diopside_SPI); TiKα, PETL (Rutile_SPI); NaKα, TAP (Albite_SPI); AlKα, TAP (Almandine_SPI); FeKα, LIF (Almandine_SPI); KKα, PETL (Biotite_SPI); MnKα, LIFL (Rhodonite_SPI); CrKα, PETL (Chromium_SPI); FKα, TAPL (MgF2); ClKα, PETL (Tugtupite1); MgKα, TAPL (Olivine_SPI).

The aim of the project was to obtain a greater understanding behind the cyclic variations in the main mineralogy (excluding opaque minerals) present throughout the Upper Zone, therefore the grains selected included plagioclase, olivine, orthopyroxene, clinopyroxene and apatite. Other minerals such as biotite, amphibole and silica were analysed due to their relative abundance. In Table 4, a list of all the elements measured for each of the respective minerals is presented.

Table 4. **Compounds analysed for each mineral.**

	Compounds Analysed														
Plagioclase	SiO_2	Al_2O_3	CaO	MgO	MnO	FeO	TiO_2	Na_2O		K_2O	SrO	BaO			NiO
Olivine	SiO_2	Al_2O_3	CaO	MgO	MnO	FeO	TiO_2		Cr_2O_3						
Orthopyroxene	SiO_2	Al_2O_3	CaO	MgO	MnO	FeO	TiO_2	Na_2O	Cr_2O_3	K_2O					
Clinopyroxene	SiO_2	Al_2O_3	CaO	MgO	MnO	FeO	TiO_2	Na_2O	Cr_2O_3	K_2O					
Apatite	SiO_2	Al_2O_3	CaO	MgO	MnO	FeO		Na_2O			SrO	BaO	F	Cl	P_2O_5
Biotite	SiO_2	Al_2O_3	CaO	MgO	MnO	FeO	TiO_2	Na_2O	Cr_2O_3	K_2O			F	Cl	
Amphibole	SiO_2	Al_2O_3	CaO	MgO	MnO	FeO	TiO_2	Na_2O	Cr_2O_3	K_2O			F	Cl	
Silica	SiO_2														

Chapter 4 – Petrography

The results include the identification of the primary mineralogy, the relative proportions of each mineral, the characteristic shape and size distribution of each mineral followed by a petrogenetic sequence for each sample. The geochemical data obtained through EPMA is discussed in Chapter 5.

Sampling of Cycle V and Cycle VI includes a range of rock types but the general lithology includes two magnetite-rich gabbros, nineteen gabbros; comprising of olivine gabbro and plagioclase-rich gabbro, and finally six anorthosites. Each sample is discussed in terms of the depth rather than sample name.

Figure 8 below shows the rock types sampled in Cycle V as well as the depths at which the samples were taken. On the right-hand side of the figure the relative proportions of each mineral in each sample is provided. Cycle V consists of twelve gabbros, two magnetite-rich gabbros and one anorthosite. A magnetite-rich gabbro is situated at the bottom of Cycle V at 1458.12 m. Above this gabbros dominate the next ~250 m. In hand specimen the gabbros were observed to increase in plagioclase content as depth decreases. An anorthosite was intersected at 1166.52 m. Above this the rock type transitions back into a plagioclase-rich gabbro. At 1119.3 m, a magnetite-rich gabbro was intersected again, with another overlying gabbro sample overlying at 1105.5 m.

The proportions of plagioclase and magnetite are inversely related when examining the gabbro samples; the higher the proportion of plagioclase, the lower the proportion of magnetite. The proportions of pyroxene increase above the magnetite-rich gabbro at 1458.12 m until the anorthosite is encountered at 1166.52 m. The gabbro above this is contains considerably higher proportions of pyroxene than lower gabbros. These proportions decrease again in the next magnetite-rich gabbro.

Biotite is present throughout the whole of Cycle V, and apatite is present in the gabbros from 1458.12 m through to 1285.65 m. Above this apatite is intermittently present in the gabbro samples but only in small quantities. The proportion of apatite appears to increase again above the magnetite-rich gabbro at 1119.3 m. An additional interstitial mineral was identified within the anorthosite sample at 1166.52 m. The amphibole identified in the gabbros at 1223.85 m and 1105.5 m was secondary and was found as thin veins and/or layers within the sample.

An additional interstitial mineral was identified in the anorthosite at 1166.52 m. Initial observations under plane polarised light and crossed polarised light suggested quartz however the interference figures revealed both uniaxial and biaxial positive. Additional analysis is required to confirm the structure of the silica polymorph.

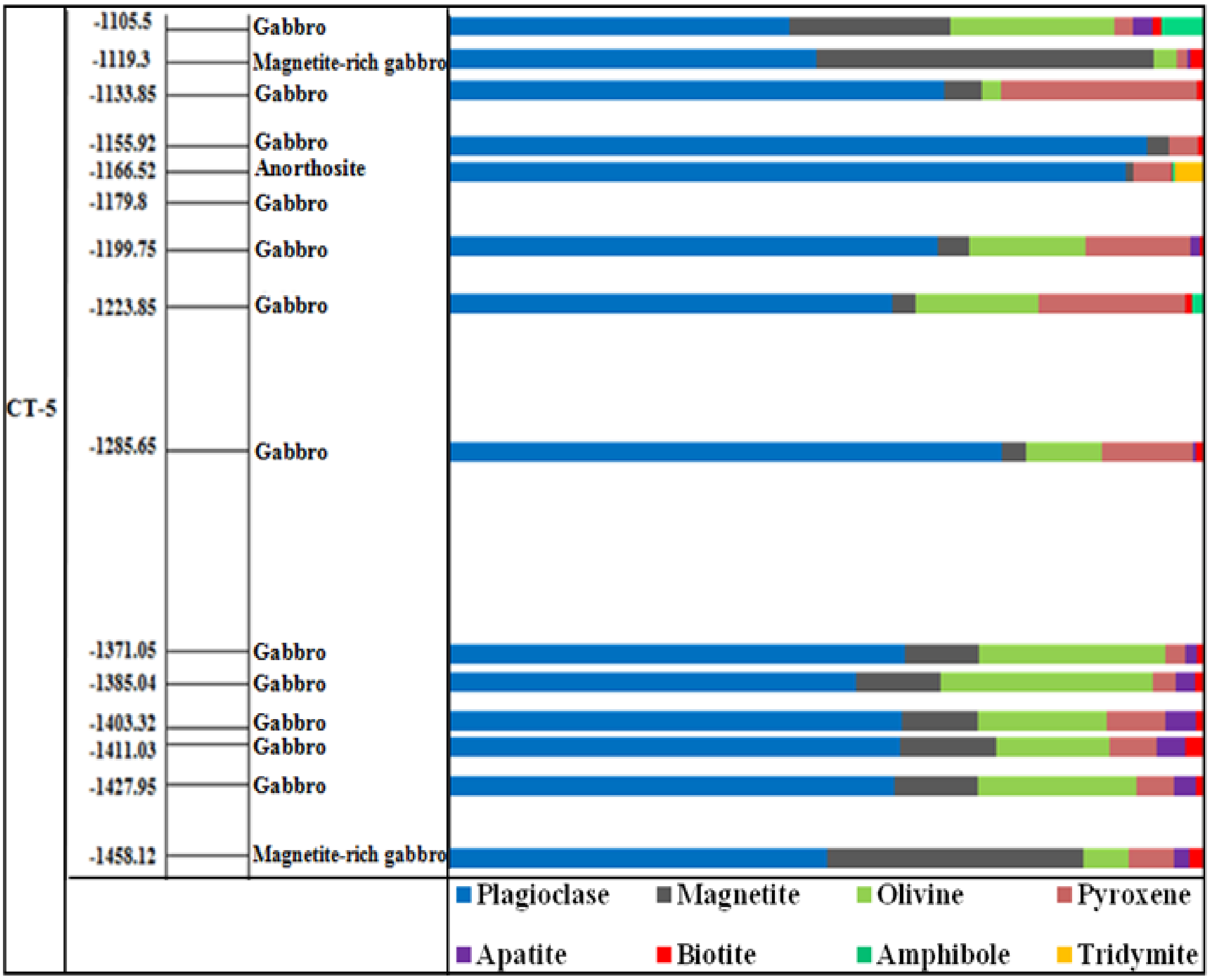

Figure 8. **Illustration of the sampling heights for Cycle V (left). Sample 15 is at the bottom of the cycle with Sample 1 at the top of the cycle. The mineralogical proportions of each sample are provided in the bar on the right of each sample.**

In Figure 9 below, the sampled rock types at the respective depths for Cycle VI are shown. The proportions of the primary mineral phases within each sample are provided again on the right-hand side of the figure. Cycle VI consists of ten gabbros and five anorthosites. No magnetite-rich gabbros were found throughout Cycle VI.

Cycle VI consist of mainly gabbros from the bottom at 1094.0 m of the cycle through to 942.4 m. Anorthosites make up the majority of the samples at the top of Cycle VI with only two plagioclase-rich gabbros being sampled in between the anorthosite samples. The anorthosites extend from 925.91 m through to 902.3 m. The two gabbros are situated at 918.69 m and 911.66 m.

The gabbros making up the bottom section of Cycle VI contain less plagioclase and more olivine compared the gabbros from Cycle V. A single gabbro at 1053.67 m contained more plagioclase and less olivine making the two mineral phases inversely proportional. Higher proportions of magnetite are observed in the gabbros at the bottom of the cycle. The proportion of pyroxene in the gabbros decreases with depth. The proportions decrease relative to the amount of plagioclase in the anorthosites. The amount of amphibole is higher in Cycle VI and is found in the anorthosites, not in the gabbros. The amphibole is interstitial and appears to be crystallising at the same time as pyroxene. Apatite is limited to the gabbro samples at the bottom of Cycle VI. High proportions of apatite are found at 1094.0 m and decrease steadily towards 925.91 m. Above this, no apatite was identified in the anorthosites or the two gabbro samples. Varying proportions of biotite were identified throughout Cycle VI. The silica polymorphs were identified once again in all the majority of the anorthosite samples, with large amounts observed at 904.5 m and 902.3 m.

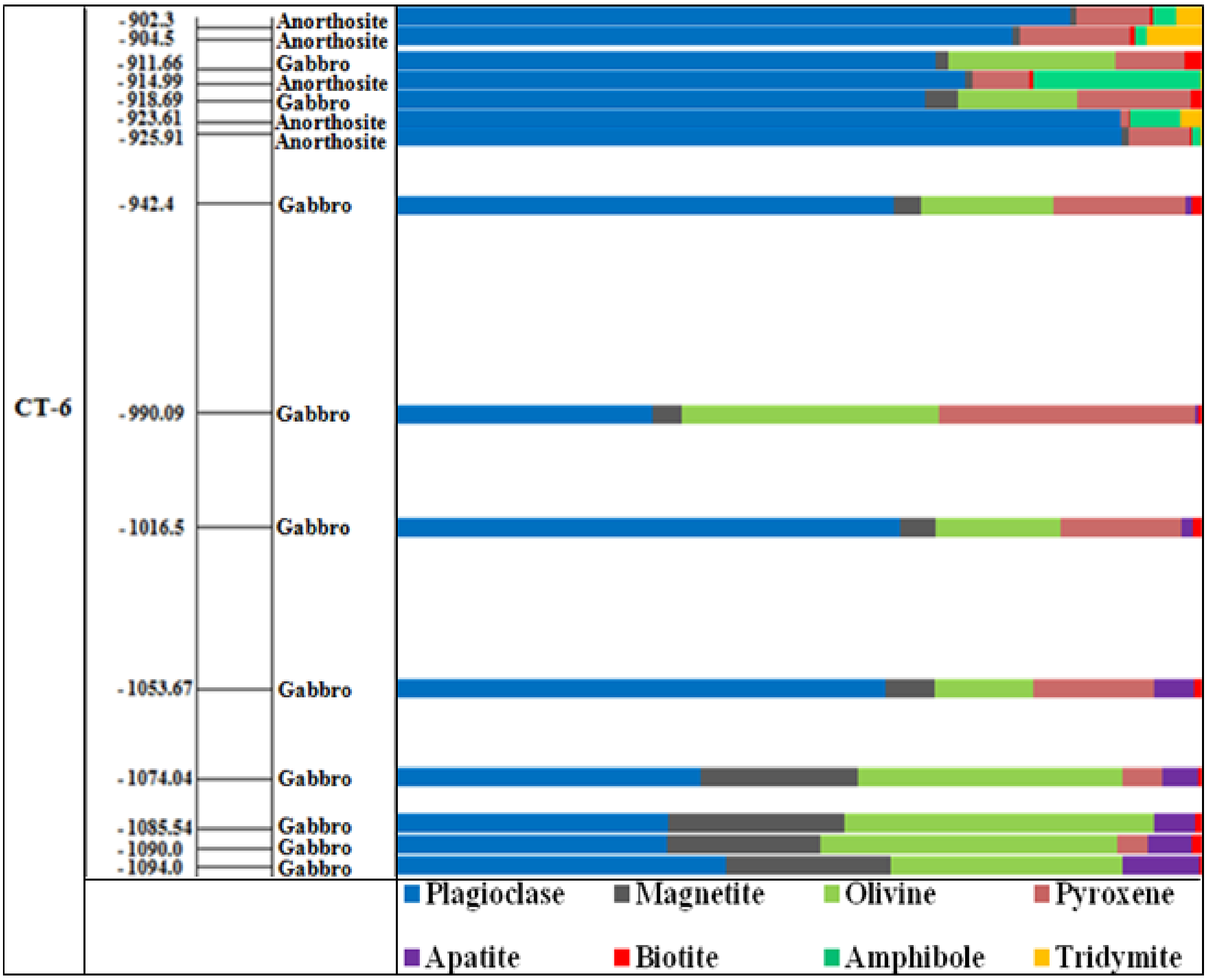

Figure 9. **Illustration of the sampling heights for Cycles VI (left). Samples 15 start at the bottom of the cycles and move up to samples 1 at the top of the cycle. The mineralogical proportions of each sample are provided on the right of each sample.**

Plagioclase

Microscopy

Plagioclase was identified throughout the gabbro and anorthosites from both Cycle V and Cycle VI. Plagioclase was present in one of two habits, large tabular grains or much smaller, rounded grains. The tabular grains exhibited typical polysynthetic twinning (Figure 10). The second habit of plagioclase occurs in clusters, generally situated between two or three larger tabular grains of plagioclase (Figure 10).

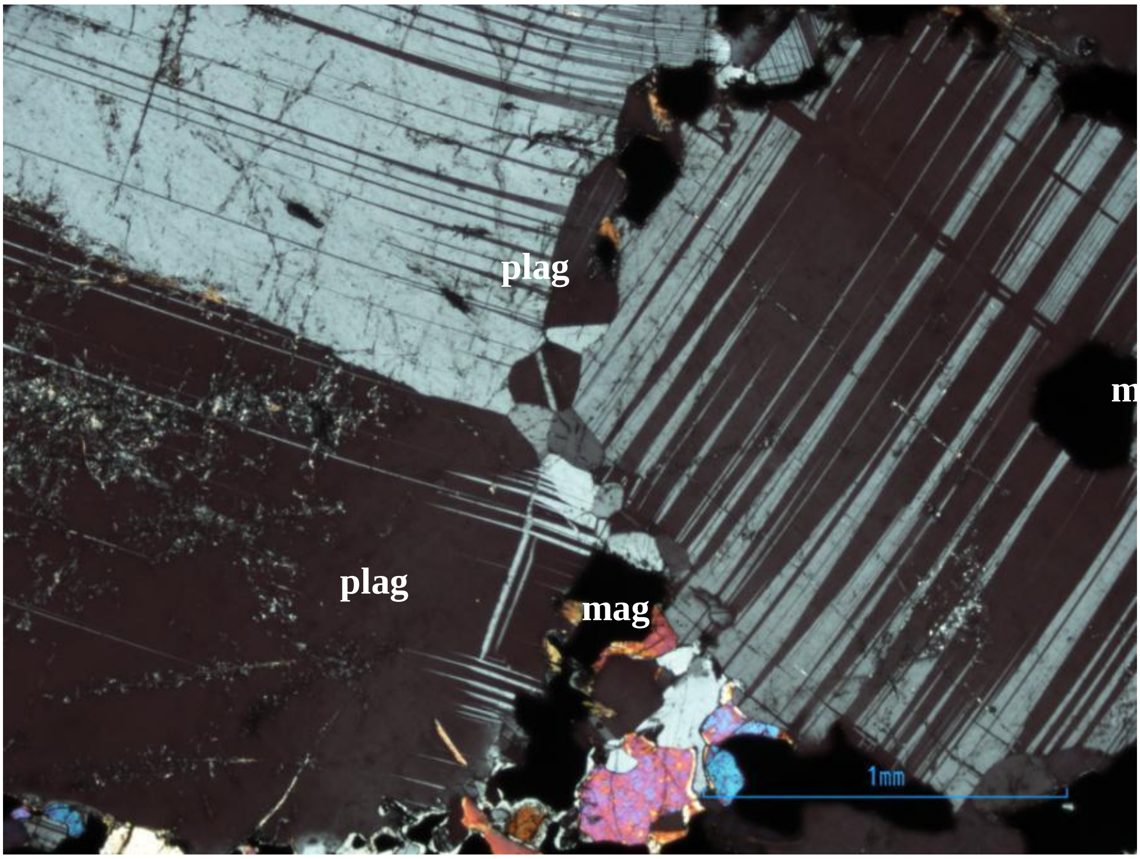

Figure 10. **XPL image from a magnetite-rich gabbro (1458.12 m) showing the relationship of small grains of plagioclase at the grain boundaries between larger, tabular grains of plagioclase.**

The petrogenetic sequence of the gabbros varies from sample to sample. In a gabbro from 911.66 m depth large grains of plagioclase were surrounded by olivine (Figure 11Figure a). In a gabbro from 1427.95 m depth, large grains of pyroxene were overgrown by plagioclase (Figure 11b). Throughout the majority of the samples, olivine was observed to surround plagioclase usually observed as a rim around plagioclase. Where present, apatite was found as inclusions in plagioclase as well as in all other minerals.

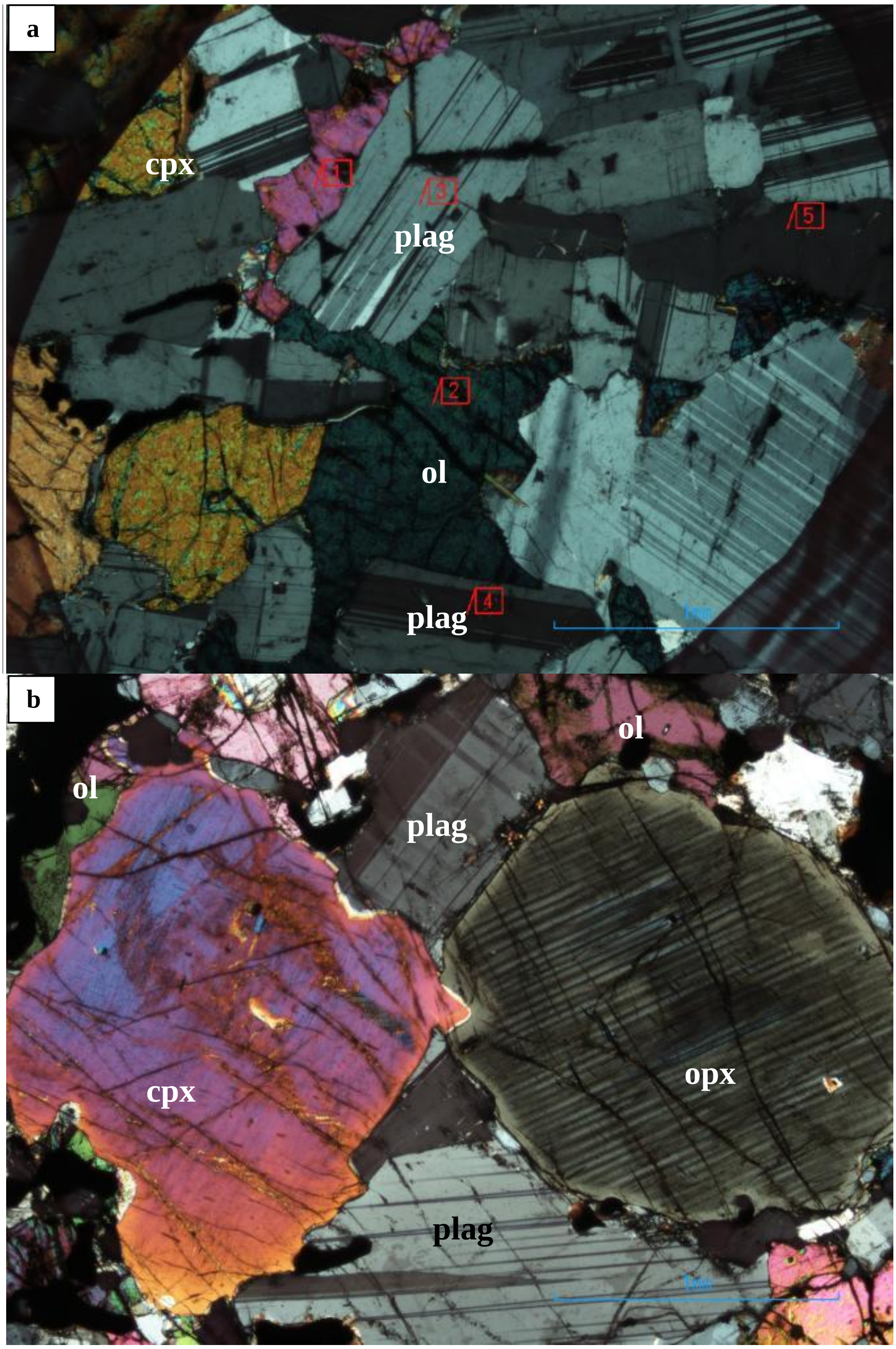

Figure 11. **a. XPL image from a gabbro (911.66 m) showing the overgrowth of plagioclase by olivine. b. XPL image from a gabbro (1427.95 m) showing the overgrowth of pyroxene by plagioclase. Olivine can also be seen to overgrow cpx and opx.**

Platy grains of biotite were observed at the grain boundaries between interstitial magnetite and plagioclase (Figure 12a and b).

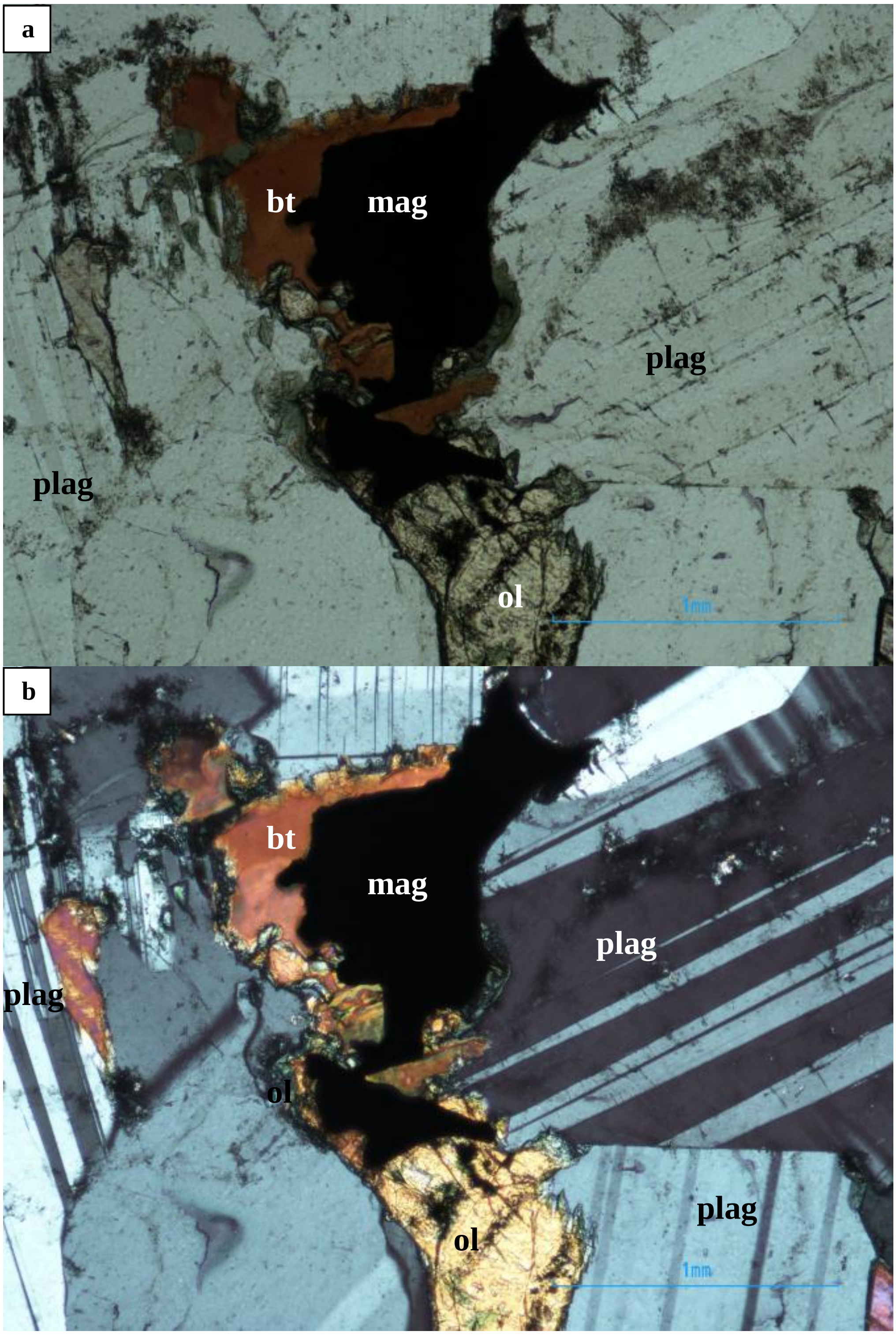

Figure 12. a. PPL image from a gabbro (1133.85 m) showing the grain boundary growth of biotite between magnetite and plagioclase. b. XPL image from a gabbro (1133.85 m) showing the grain boundary growth of biotite around magnetite.

In the anorthosite samples, plagioclase was present as large tabular grains with interstitial pyroxene and sometimes the silica (Figure 13). Magnetite was also present in small amounts but as an interstitial mineral and as smaller, subhedral grains (Figure 13). Once again, biotite was present and observed within the interstitial spaces between plagioclase grains.

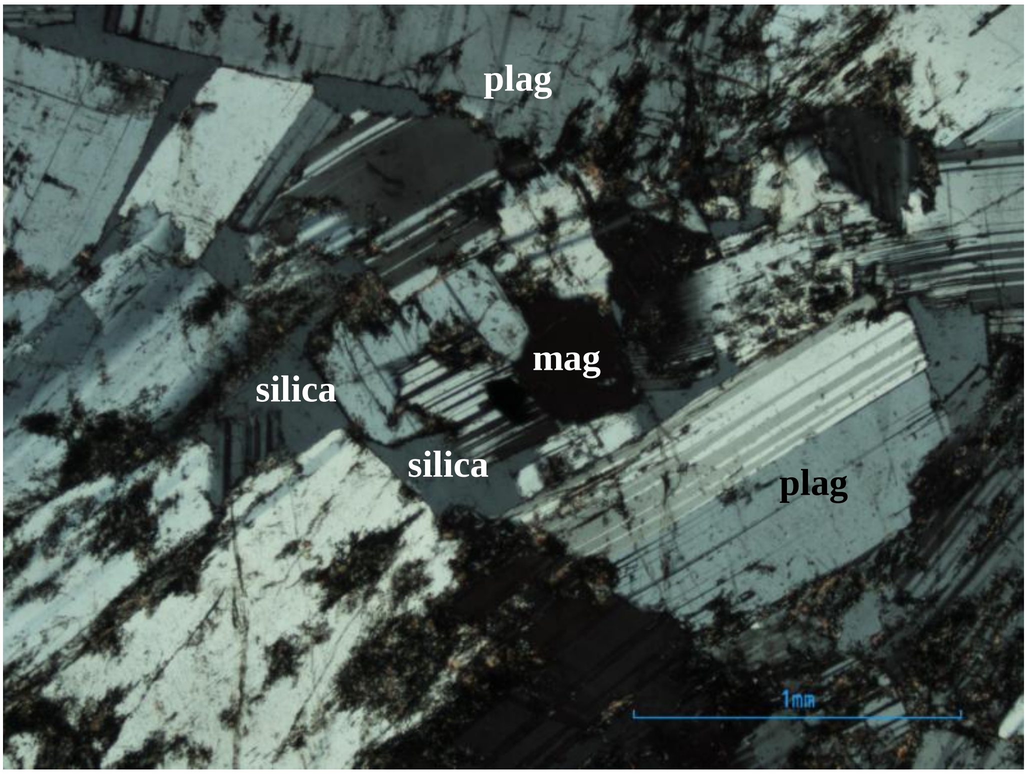

Figure 13. XPL image from an anorthosite from 1166.52 m depth showing interstitial growth of silica and the overgrowth of magnetite by plagioclase.

A number of plagioclase grains showed unusual textures in the magnetite-rich gabbros from Cycle V. In Figure 14a, a deformed tabular-shaped plagioclase grain is visible. The presence of the smaller, more rounded grains of plagioclase usually accompanied these deformed grains. The bulk of the larger plagioclase grains showed some form of preferred horizontal orientation. A number of these grains showed deformation similar to that in the figure below. In the magnetite-rich gabbro from 1119.3 m depth, symplectites were observed between plagioclase, magnetite and what appeared to be olivine (Figure 14b). The symplectites were observed at the grain boundaries between tabular grains of plagioclase. These symplectites were only observed in this sample.

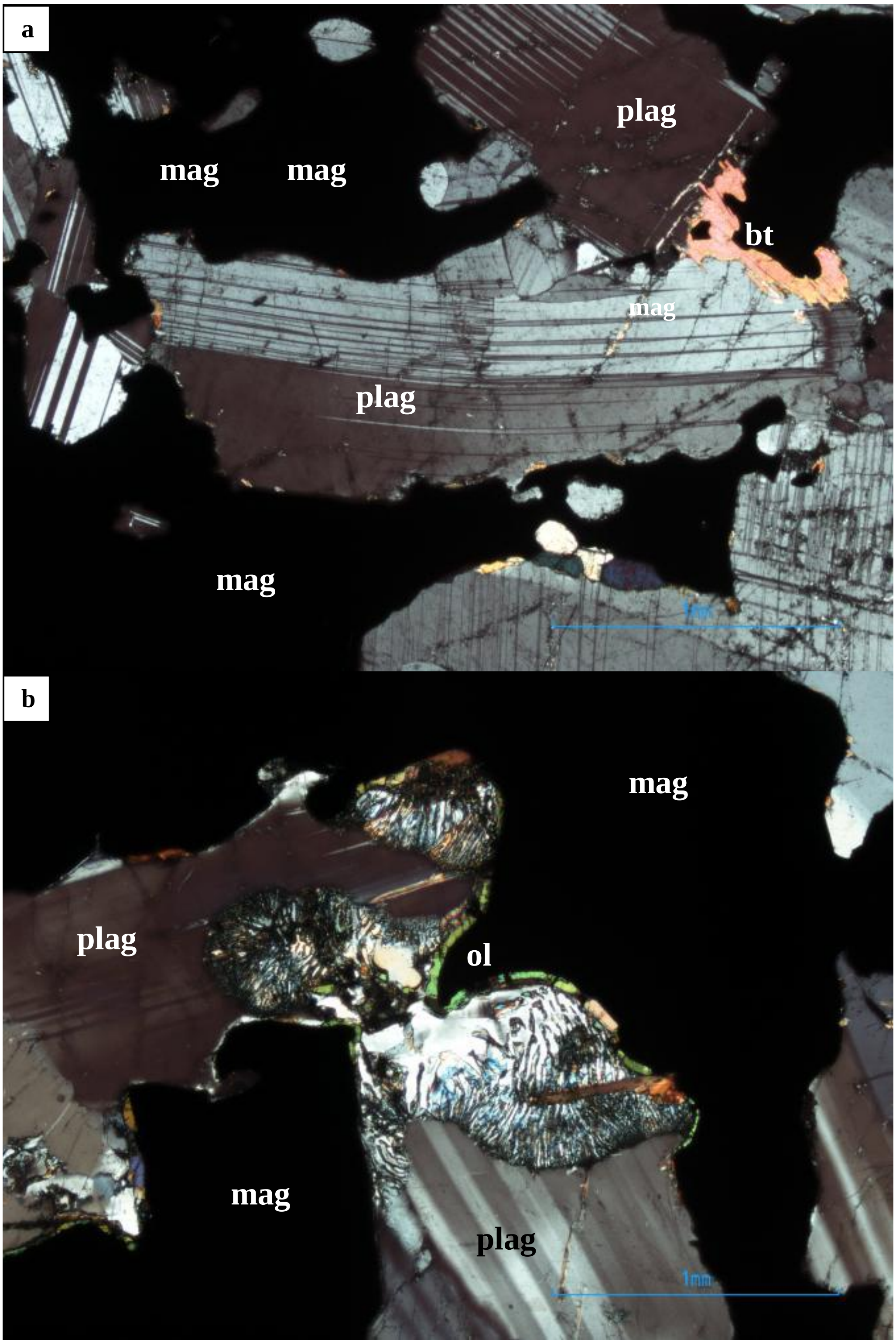

Figure 14. a. XPL image from a magnetite-rich gabbro at 1458.12 m depth showing deformation of a tabular plagioclase grain. b. XPL image from a magnetite-rich gabbro at 1119.3 m depth showing a symplectite texture propagating into two tabular plagioclase grains.

Grain shape and size

The grain size variation of the plagioclase grains in Cycle V is given in Figure 15. The highest median grain size of the plagioclase grains was 1.75 mm in an anorthosite at 1166.52 m depth. The lowest median grain sizes were recorded in the gabbros in the middle portion of the cycle. Grain sizes of 0.9 mm were recorded at 1053.67 m, 1016.5 m and 990.09 m depth. The maximum grain size of 4mm was recorded in an anorthosite at 923.61 m depth. The smallest grain size of 0.1 mm was measured in the gabbros at 1155.92 m, 1133.85 m and 1105.5 m depth.

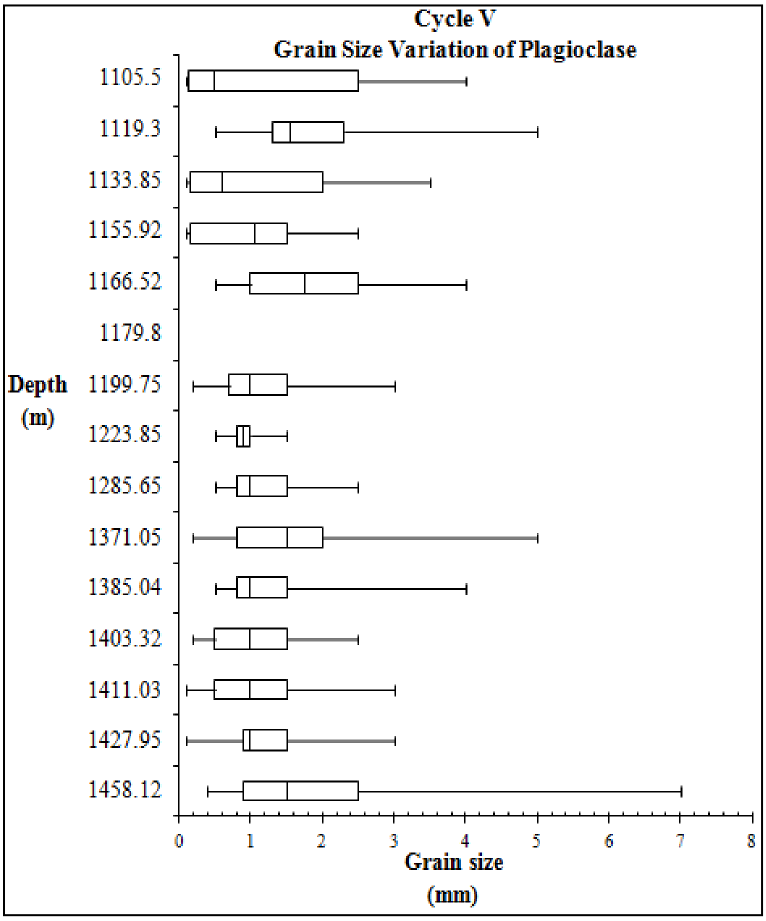

Figure 15. Box and whisker plot showing the grain size variation for plagioclase recorded for Cycle V.

The overall median grain size of the plagioclase grains from Cycle VI (Figure 16) is larger than Cycle V. The highest median grain size was 2.25 mm in an anorthosite at 923.61 m depth. The lowest median grain size of 0.5 mm was recorded in a gabbro at the top of the cycle at 1105.5 m depth. The maximum grain size of 7 mm was recorded in a magnetite-rich gabbro at 1458.12 m depth. The smallest grain size of 0.2 mm was recorded in a gabbro at the bottom of the cycle positioned 1090.0 m depth.

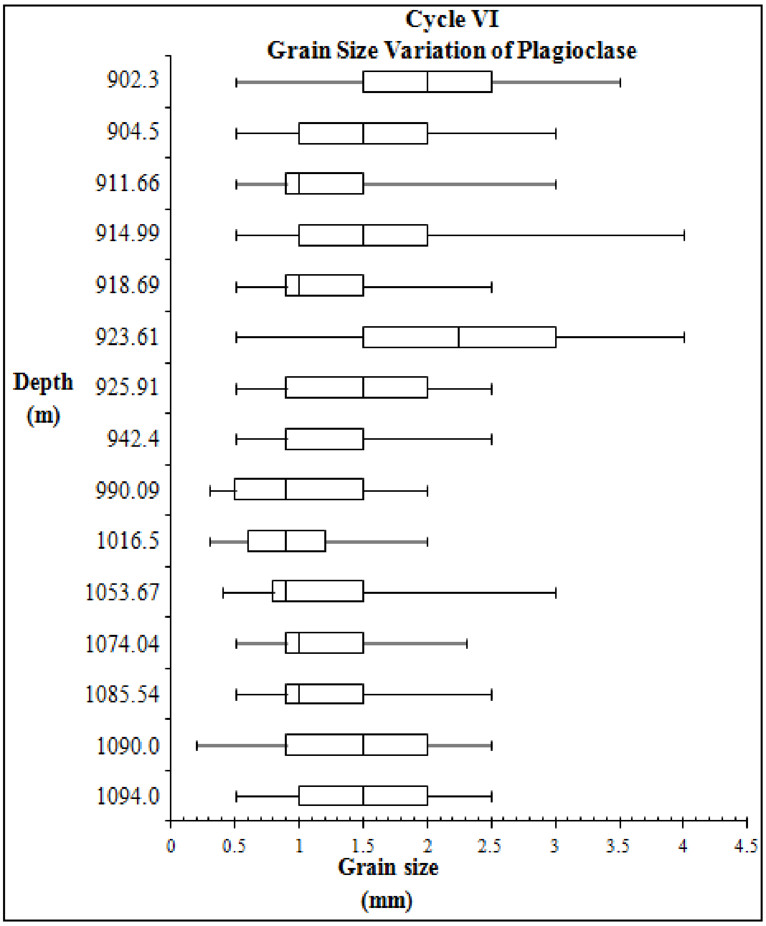

Figure 16. **Box and whisker plot showing the grain size variation for plagioclase recorded for Cycle VI.**

Magnetite

The term magnetite has been used in a general sense but includes all opaques present throughout the two cycles. Magnetite, although not analysed for in this study, is an important mineral in Cycle V and Cycle VI. The textural relationships between the silicates and magnetite are important, as these will provide information about the paragenetic sequence.

Magnetite was identified in every sample including the anorthosites. The bulk of the magnetite within each sample was identified as interstitial (Figure 17a). However, a number of anorthosite and gabbro samples showed small, round grains of magnetite most commonly included in plagioclase, olivine and pyroxene (Figure 17b).

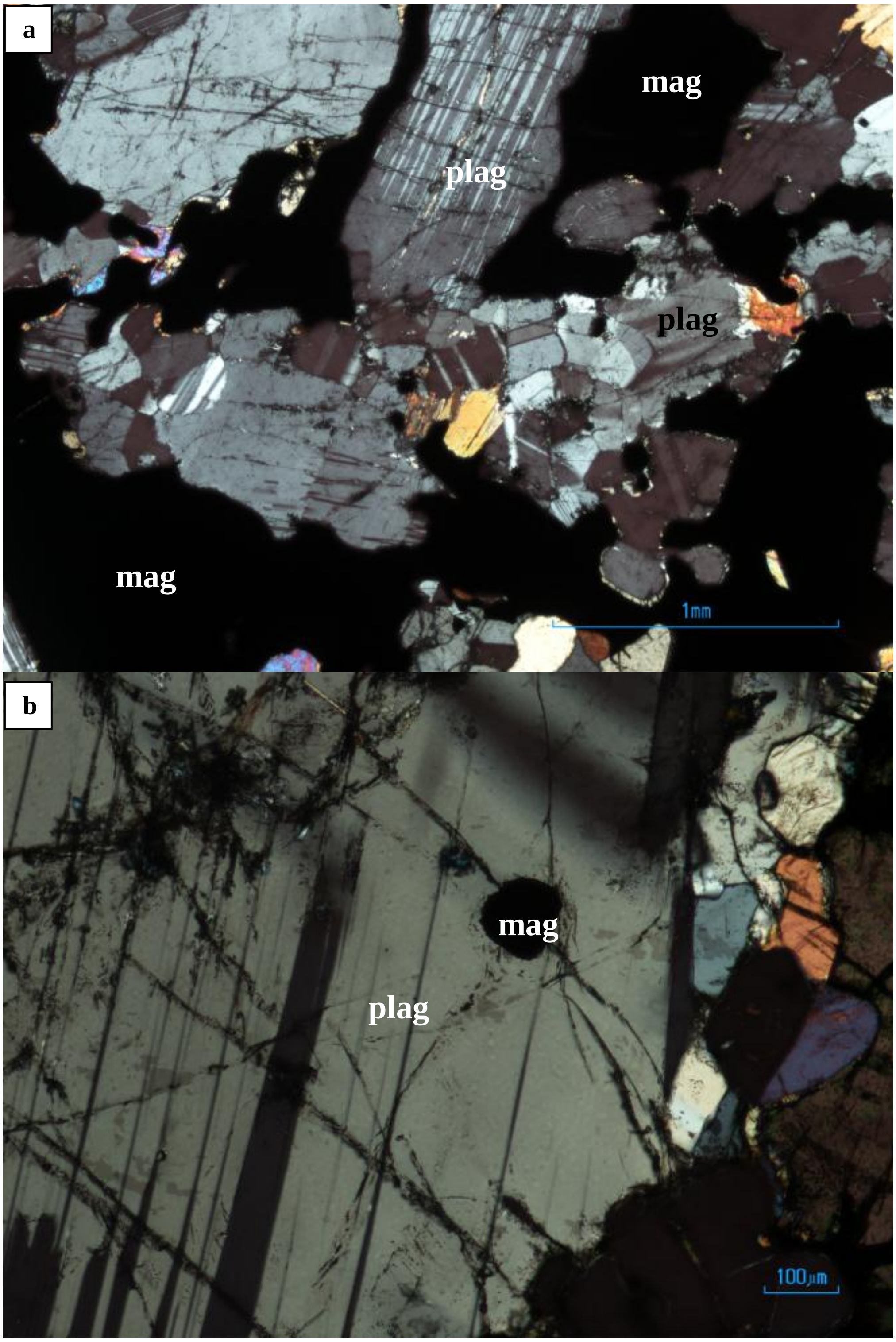

Figure 3. **a. XPL image from a magnetite-rich gabbro (1458.12 m) showing interstitial magnetite. b. XPL image from a gabbro (1427.95 m) showing a small, round grain of magnetite included in plagioclase.**

Inclusions of magnetite were observed in plagioclase, olivine and pyroxene. The more anhedral interstitial magnetite was commonly associated with biotite. Either biotite was seen surrounding the magnetite grain (Figure 18a) or the biotite was identified in the interstitial spaces between magnetite and plagioclase (Figure 18b). Euhedral grains of apatite are found within the interstitial magnetite in the magnetite-rich gabbros.

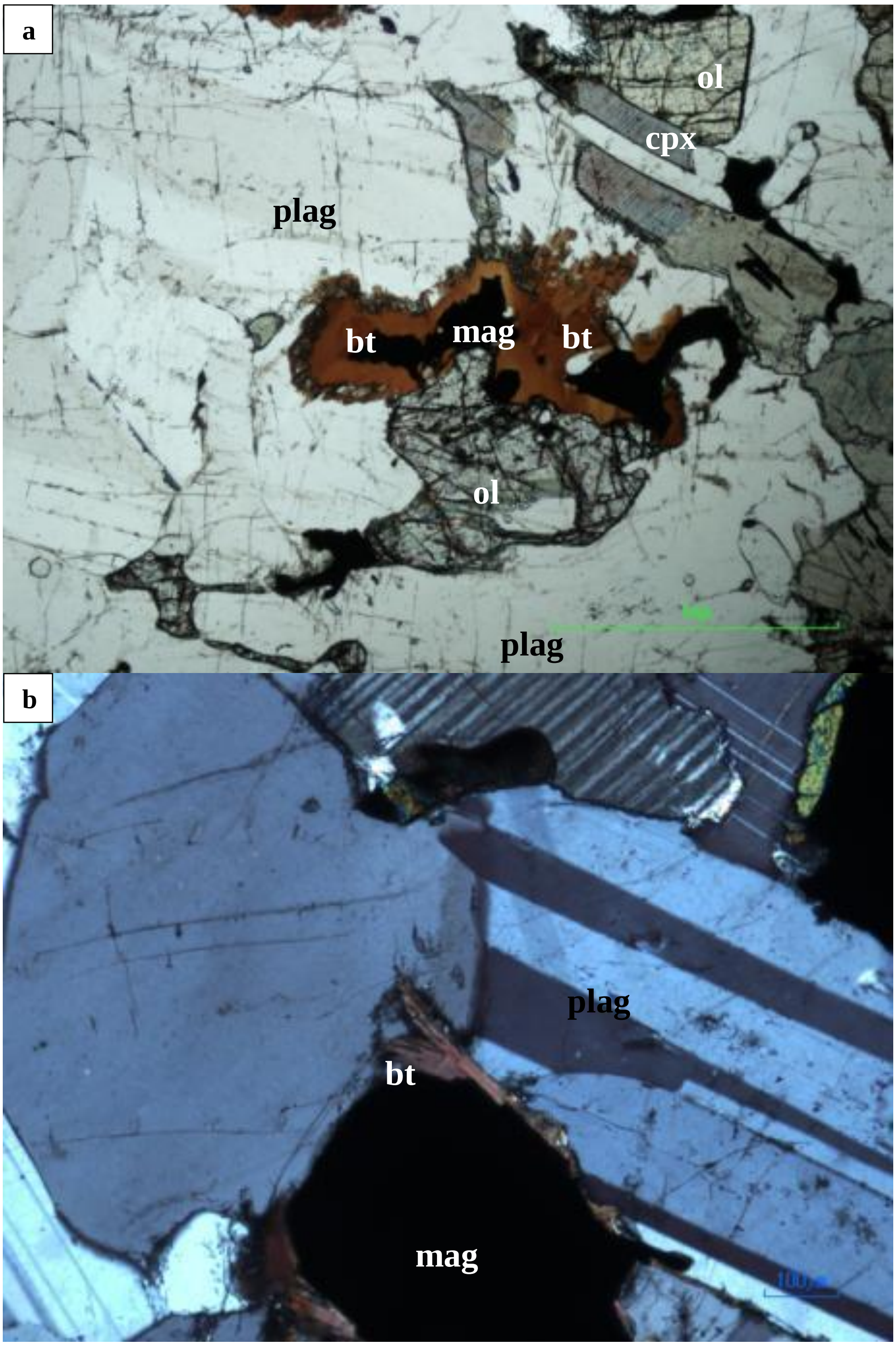

Figure 4. **a. PPL image of biotite surrounding magnetite in a sample taken from Cycle VI. b. XPL image of platy grains of biotite in the interstitial spaces between magnetite and plagioclase.**

Two altered samples were determined as gabbro based on the presence of plagioclase, magnetite and apatite. The altered gabbros originated from 1155.92 m and 990.09 m. In both samples, altered grains of subhedral to euhedral magnetite were observed. Examples of these can be seen in Figure 19 below.

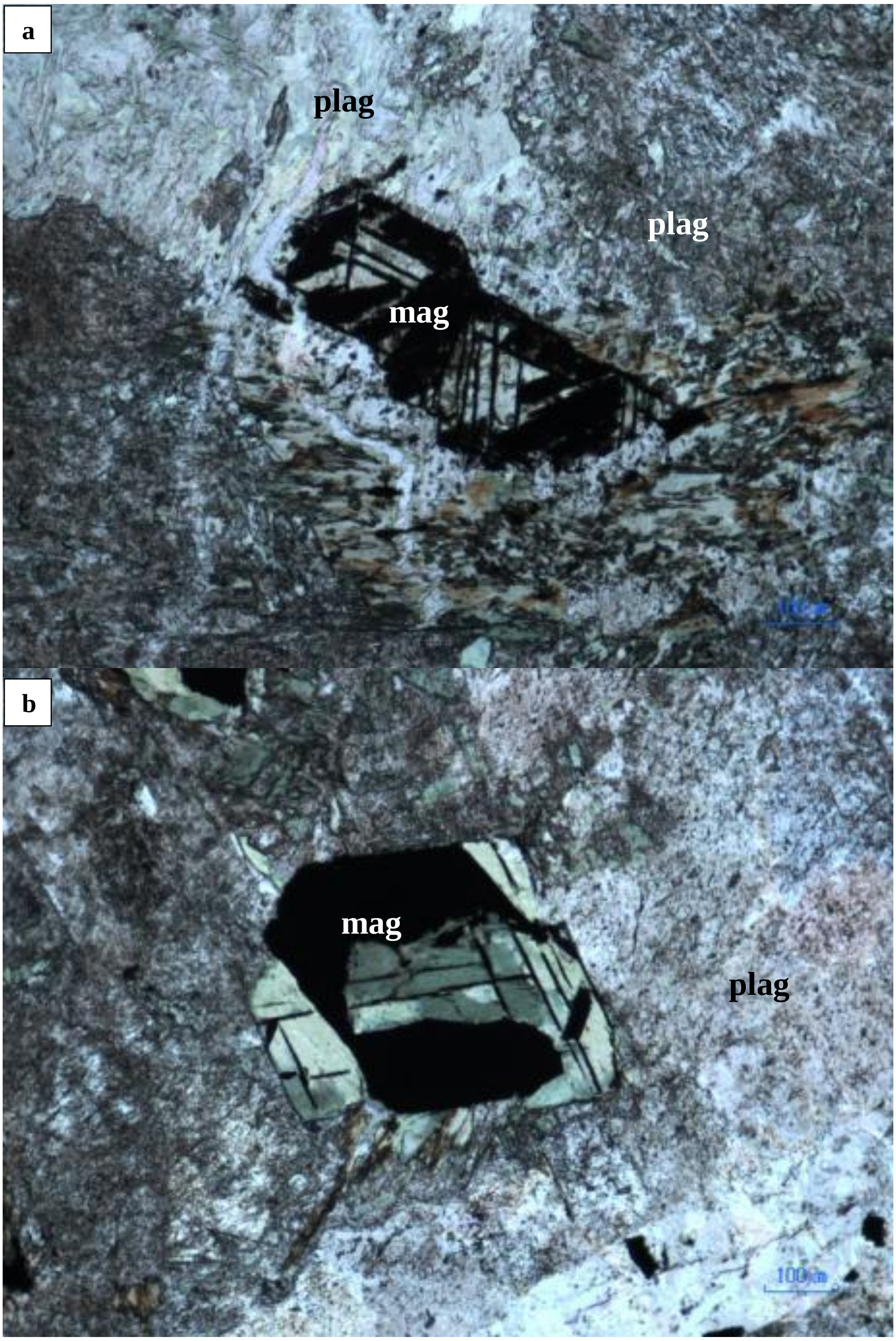

Figure 19. Altered euhedral grains of magnetite in gabbros from 1155.92 m from Cycle V (a) and 990.09 m from Cycle VI (b).

Olivine

Microscopy

All gabbros contained varying proportions of olivine as illustrated in Figure 8 and Figure 9. The olivine was identified as fayalite based on the pale yellow to pale orange pleochroism, low 2V angle and the biaxial negative interference figure. Some gabbros contained significantly high amounts of olivine leading to the name olivine-gabbro for some samples. No olivine was identified in the anorthosites.

Olivine is observed to overgrow plagioclase in some samples but is found as inclusions in plagioclase in other samples (Figure 20a). Similar observations were made between olivine and pyroxene. In Figure 11b, olivine is overgrowing clinopyroxene, whereas in Figure 20b, clinopyroxene includes two small grains of olivine. The alternating petrogenesis between samples does not appear to be systematic. Magnetite was found as small cubic or rounded grains included in olivine, but was also observed to overgrow olivine in the majority of the gabbros. Olivine was observed to overgrow biotite and include apatite.

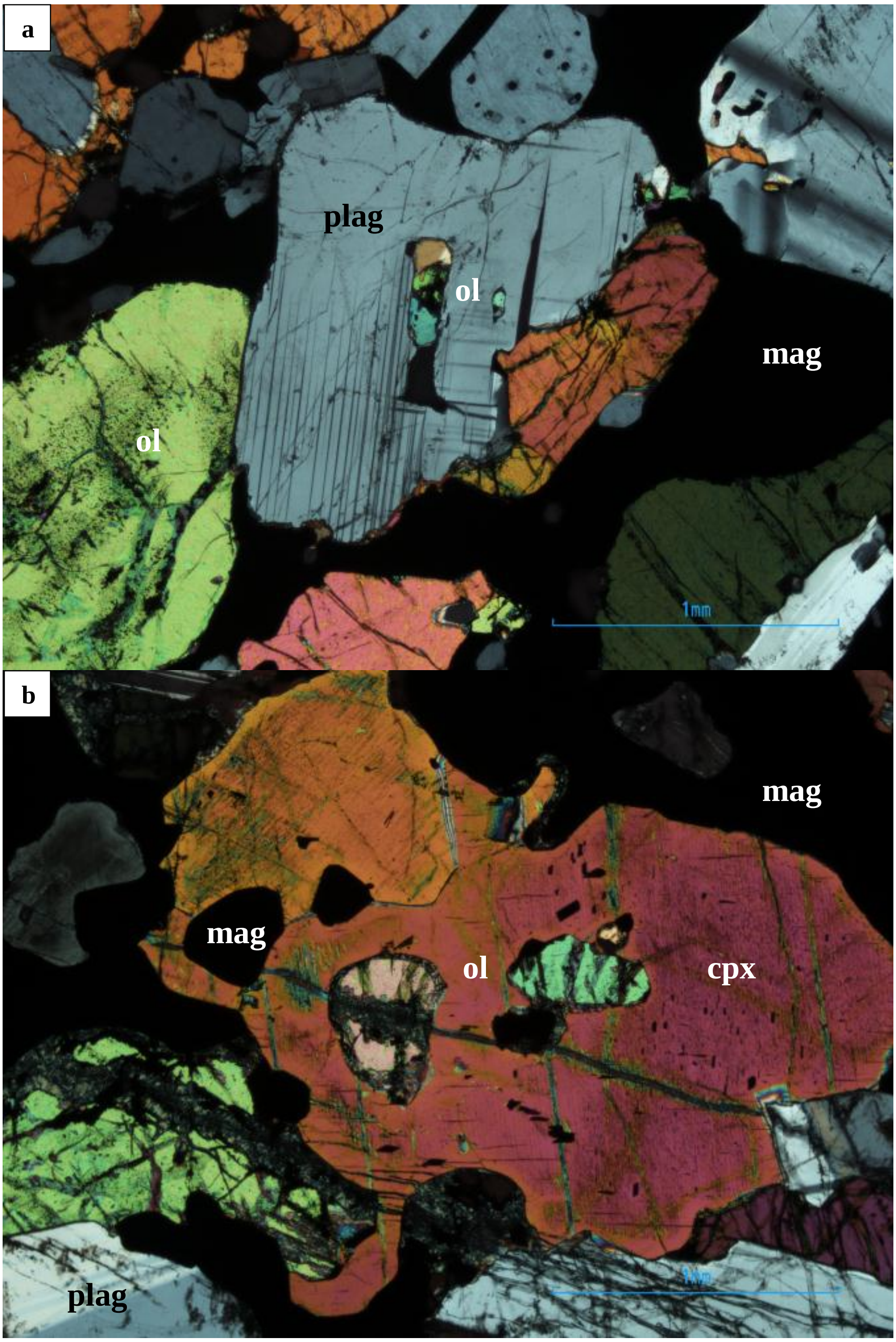

Figure 20. a. XPL image from a gabbro at 1094.0 m depth showing the inclusion if olivine in plagioclase. b. XPL image from a gabbro at 1105.5 m depth showing the inclusion of two small grains of olivine by clinopyroxene.

Grain shape and size

The grain size variation of the olivine in Cycle V is shown in Figure 21.The highest median grain size in the gabbros was 1.3 mm at 1427.95 m depth. The lowest median grain size was recorded at 1458.12 m depth. The maximum grain size of 3.6 mm was recorded at 1411.03 m depth. The smallest grain sizes of 0.1mm was recorded in the gabbros at 1458.12 m, 1403.32 m, 1371.05 m and 1223.85 m depth.

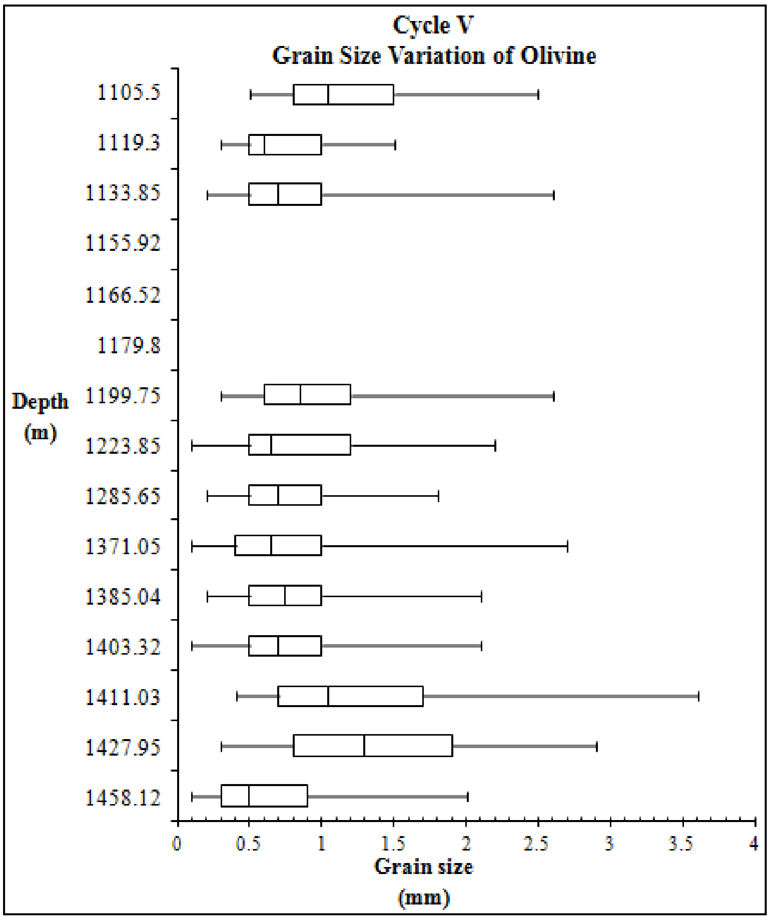

Figure 21. Box and whisker plot showing the grain size variation for olivine recorded for Cycle V.

The grain sizes of the olivine from Cycle VI (Figure 22) are relatively similar to Cycle V. The highest median grain size was 1.05 mm at 1094.0 m and 1074.04 m depth. The lowest median grain size was recorded at 1016.5 m depth. The maximum grain size of 3.0 mm was recorded at 1090.0 m depth. The smallest grain sizes of 0.1 mm was recorded at 911.66 m depth.

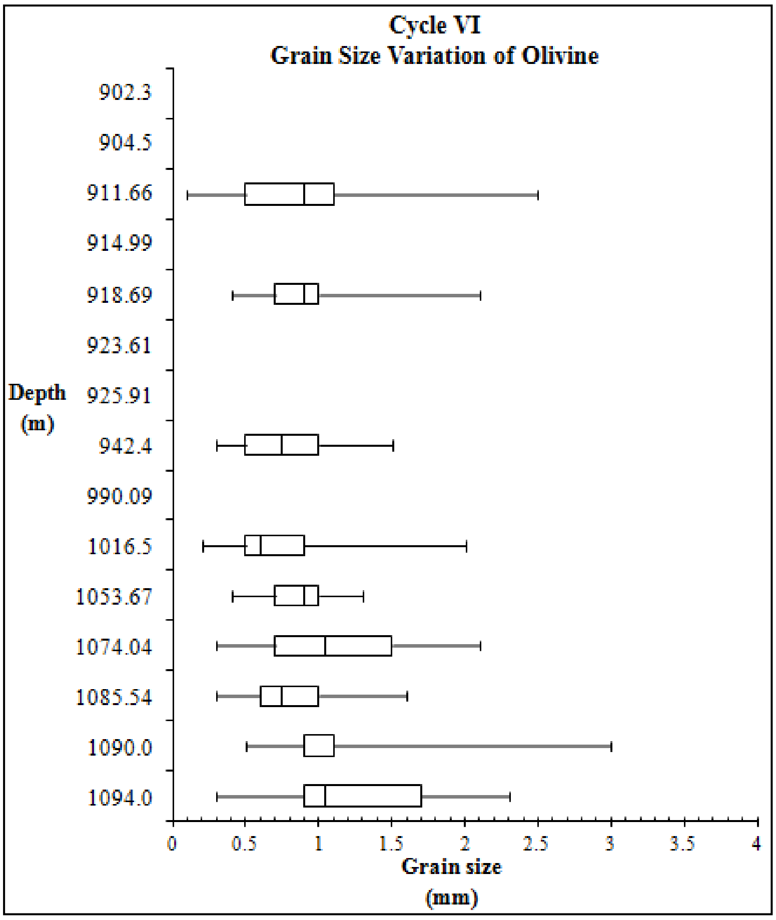

Figure 22. **Box and whisker plot showing the grain size variation for olivine recorded for Cycle VI.**

Pyroxene

Microscopy

Both clinopyroxene and orthopyroxene were identified in Cycle V and Cycle VI (Figure 11b). Not all rocks contained pyroxene and those that did, did not necessarily contain both clinopyroxene and orthopyroxene. Clinopyroxene was the most predominant of the two pyroxenes; however one anorthosite at 925.91 m depth contained only orthopyroxene (Figure 23).

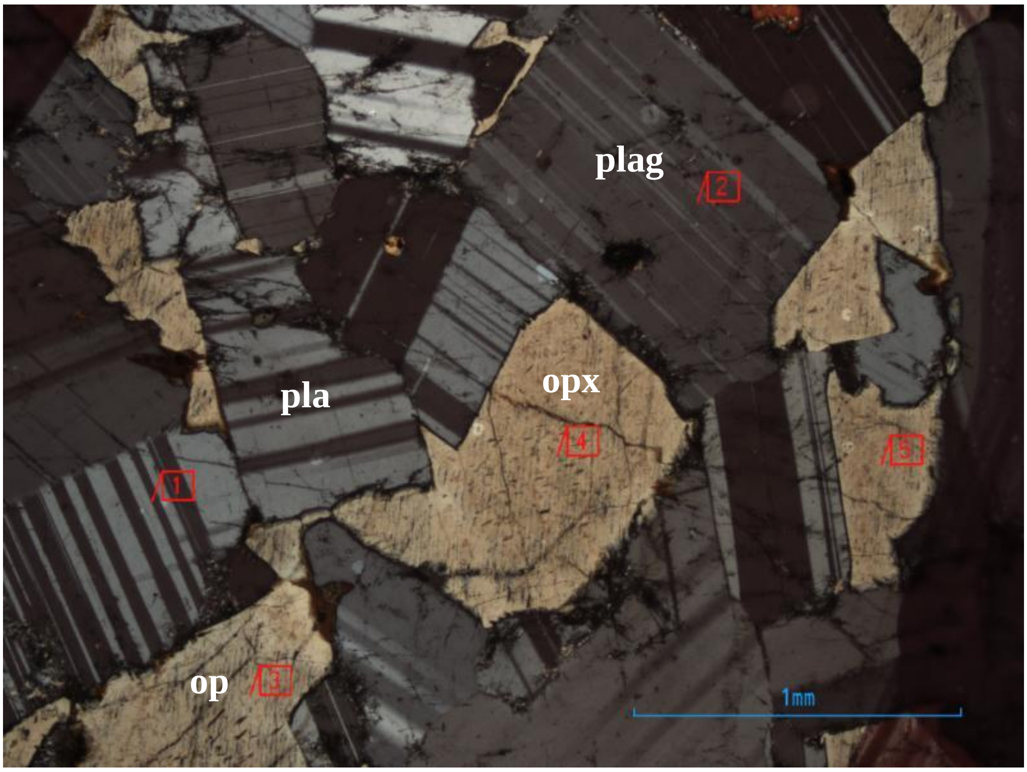

Figure 23. **XPL image of an anorthosite from 925.91 m depth showing the poecilitic interstitial texture of the orthopyroxene.**

The petrogenetic sequence of the pyroxenes has been indirectly discussed under the plagioclase and olivine sections. To reiterate, the relationship between plagioclase, olivine and the pyroxenes varies from sample to sample. In Figure 11b, plagioclase overgrows both orthopyroxene and clinopyroxene. In Figure 24, both orthopyroxene and clinopyroxene overgrow plagioclase. The relationship between orthopyroxene and clinopyroxene is more ordered. In the samples where both orthopyroxene and clinopyroxene are present, the former is always overgrown by the latter.

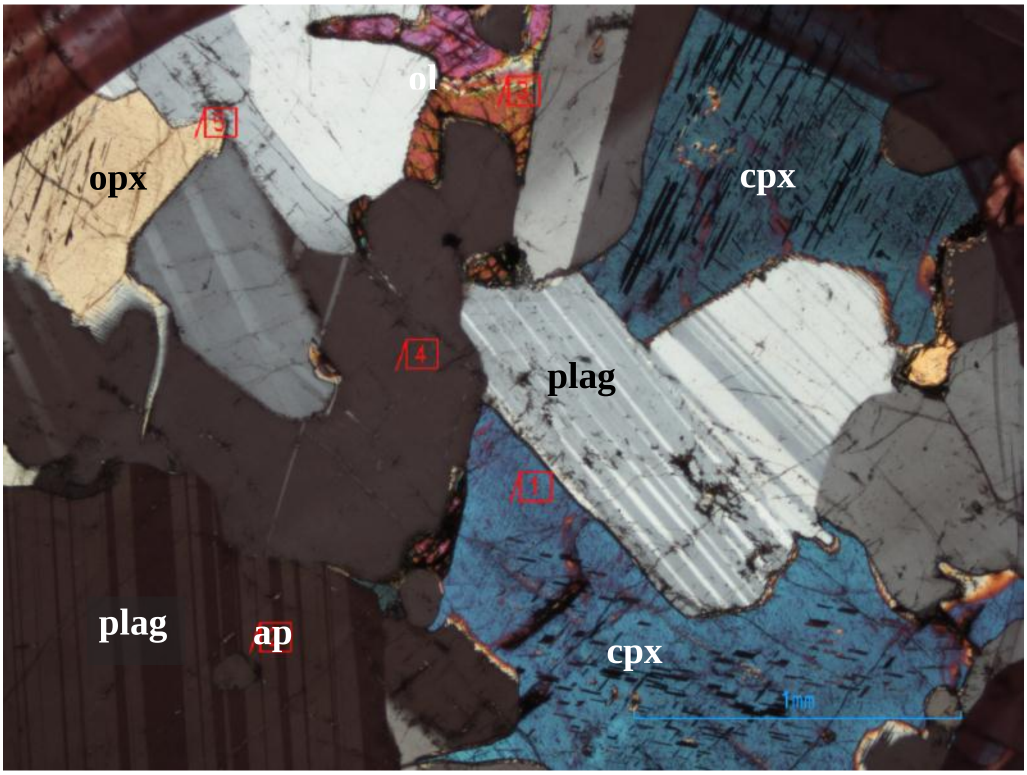

Figure 24. **XPL image of a gabbro from 942.4 m depth showing the overgrowth of plagioclase by orthopyroxene and clinopyroxene.**

Magnetite was found as small cubic or rounded grains included in both clinopyroxene and orthopyroxene. Inclusions of apatite were identified within pyroxene with biotite crystallising within the interstitial spaces between plagioclase and pyroxene. In the anorthosites, orthopyroxene and/or clinopyroxene were interstitial. A number of the pyroxene grains showed exsolution along cleavage planes (Figure 24). The textural relationship between amphibole and pyroxene in the anorthosites in Cycle VI is discussed under the amphibole section.

Grain shape and size

The median grain sizes show no particular trend throughout Cycle V (Figure 25). The lowest medians of 0.3 mm and 0.25 mm were recorded in the magnetite-rich gabbros at 1458.12 m and 1119.3 m depth respectively. The median grain size throughout the remainder of the gabbros was between 0.6 mm and 0.9 mm. No pyroxenes were identified in the altered gabbro at 1155.92 m depth. The maximum grain size becomes steadily higher with a decrease in depth. The largest grain was 2.3 mm at 1105.5 m depth.

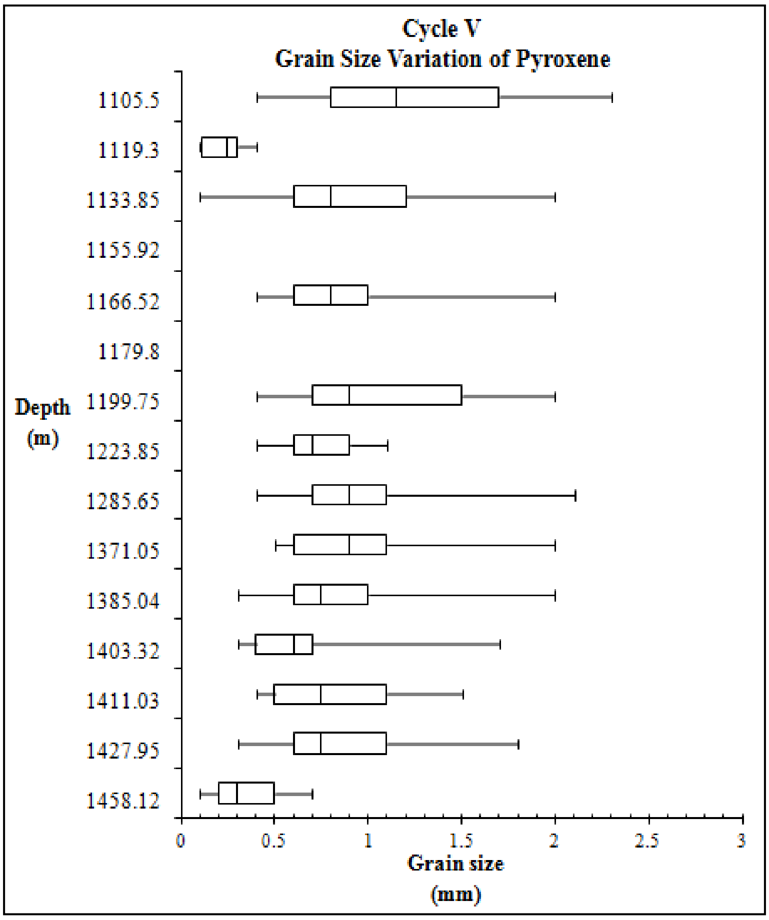

Figure 25. **Box and whisker plot showing the grain size variation for pyroxene recorded for Cycle V.**

The median grain sizes of the pyroxenes from Cycle VI (Figure 26) in the gabbros from 1074.04 m to 942.4 m depth vary between 0.9 mm and 1.1 mm. The gabbro at 990.009 m depth contained the smallest grain sizes with the median recorded as 0.5 mm. The gabbros at 918.69 m and 911.66 m were 1.15 mm and 0.9 mm respectively. The pyroxenes in the anorthosites that dominate the top of Cycle VI consisted of similarly sized grains between 1 mm and 0.9 mm.

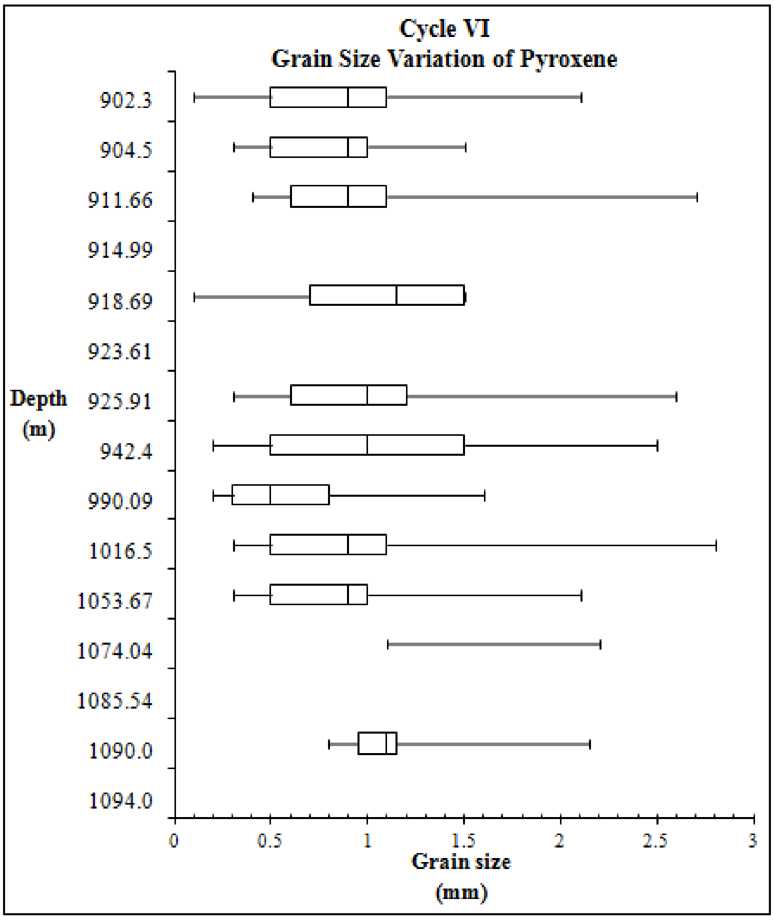

Figure 26. **Box and whisker plot showing the grain size variation for pyroxene recorded for Cycle VI.**

Apatite

Microscopy

Cumulus apatite was found in most of the gabbros throughout Cycle V and Cycle VI. The grains varied in size but the majority were subhedral to euhedral. In the gabbros containing apatite, cumulus grains were found as inclusions in plagioclase, olivine, pyroxene and magnetite (Figure 27a). Overgrowths of apatite by biotite were observed in a few samples (Figure 27b).

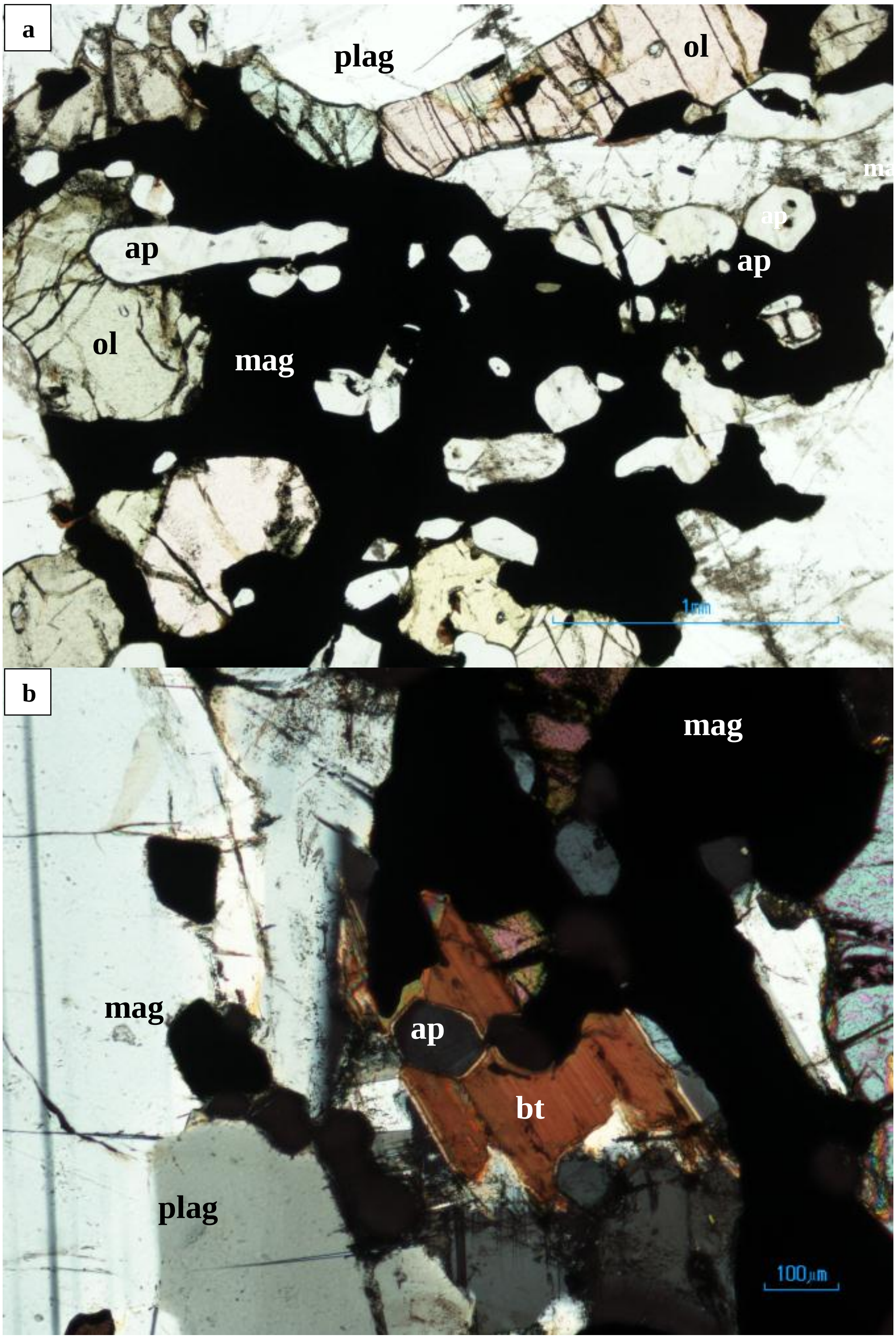

Figure 5. **a. PPL image from a gabbro at 1085.54 m depth showing the inclusion of apatite in magnetite, plagioclase and olivine. b. XPL image from a gabbro at 1403.32 m depth showing biotite surrounding a cumulus grain of apatite.**

Grain shape and size

The median grain sizes of the apatite in Cycle V (Figure 28) show minor variation throughout the apatite-containing gabbros. The highest median grain sizes were 0.1 mm in gabbros at 1458.12 m, 1411.03 m, 1403.32 m, 1385.04 m, 1371.05 m and 1199.75 m. The lowest median grain size was at 1223.85 m. The maximum grain size of 0.9 mm was at 1403.32 m depth. The smallest grain size of 0.03 mm was recorded in the gabbros at 1411.03 m, 1403.32 m, 1371.05 m and 1285.65 m depth.

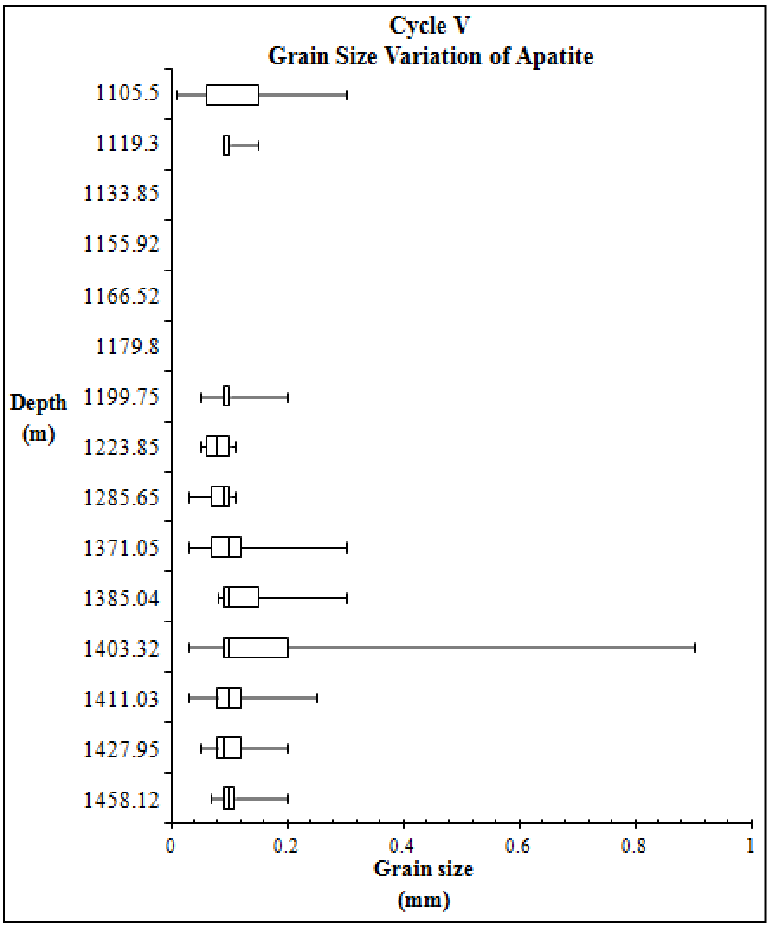

Figure 6. **Box and whisker plot showing the grain size variation for apatite recorded for Cycle V.**

Although apatite is not as prevalent in Cycle VI (Figure 29), the grain sizes were larger. The highest median grain size of 0.15 mm was recorded in samples 1090 m, 1085.54 m and 990.09 m. The lowest median grain size of 0.09 mm was at 1016.5 m and 942.4 m depth. The largest grains were recorded at 1094 m and 1085.54 m depth, while the smallest occurred at 1074.04 m and 1016.5 m depth.

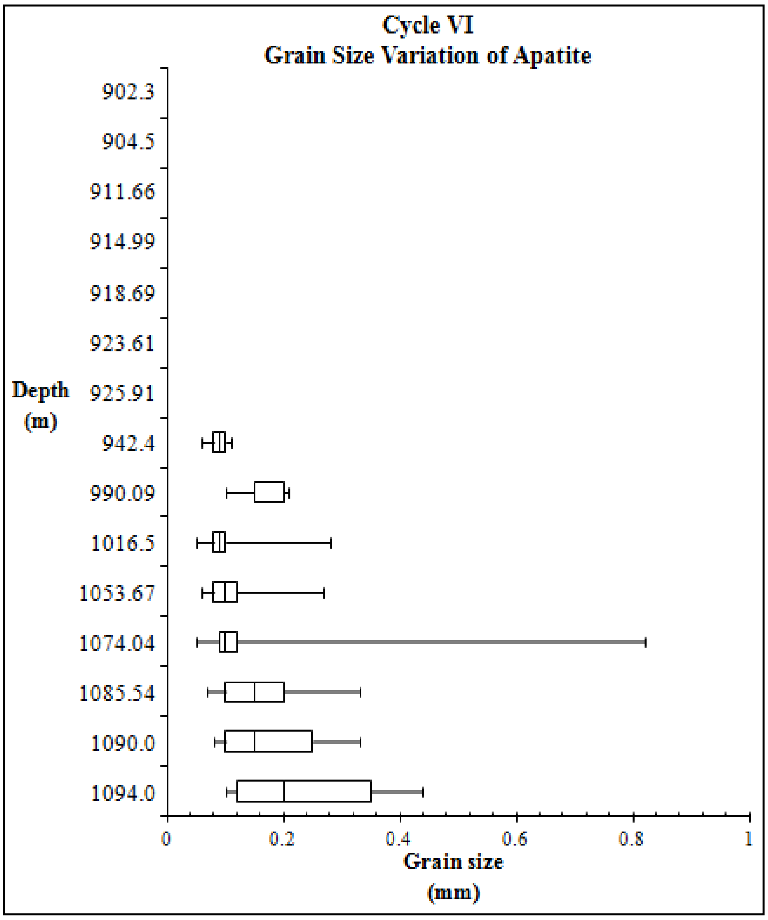

Figure 7. **Box and whisker plot showing the grain size variation for apatite recorded for Cycle VI.**

Biotite

Microscopy

Biotite was observed throughout all rock types from Cycle V and Cycle VI, gabbros and anorthosites, most commonly with plagioclase and magnetite. Biotite occurred within the interstitial spaces between magnetite and plagioclase. Biotite can be seen in Figure 14a, Figure 18a and b associated with plagioclase and magnetite and in Figure 27b associated with plagioclase, magnetite and apatite. Observations of biotite within the interstitial spaces between olivine and pyroxene (Figure 30).

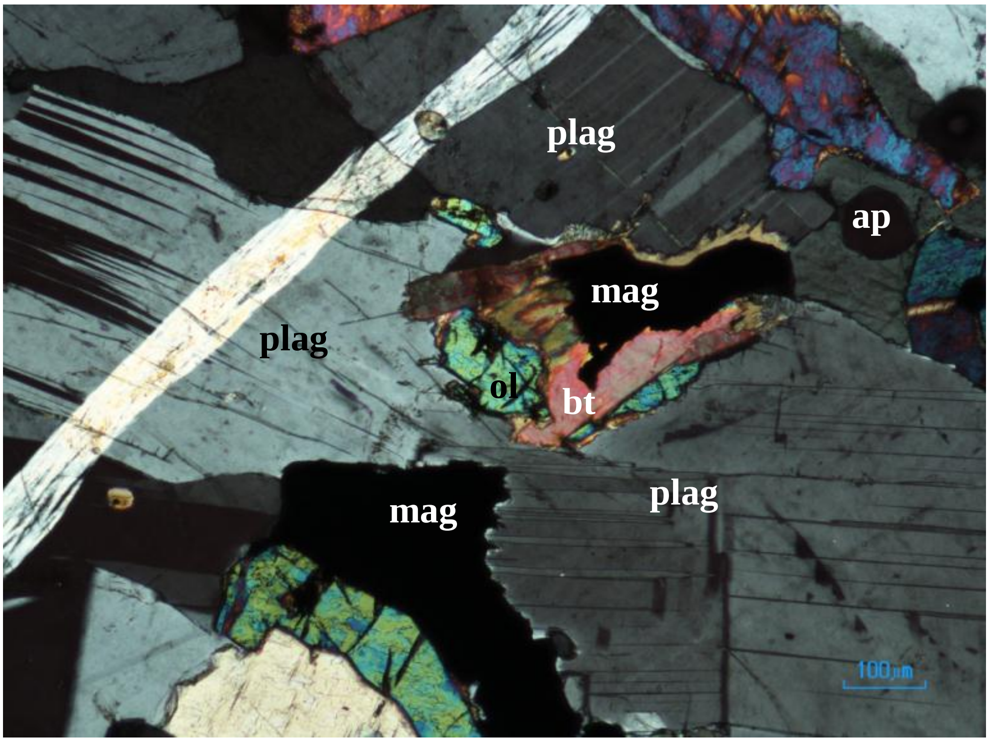

Figure 30. **XPL image from at gabbro at 1199.75 m depth showing the presence of biotite between magnetite and olivine.**

Amphibole

Microscopy

Amphibole occurs in two different forms when comparing Cycle V and Cycle VI. The textures observed in Cycle V occur mainly in the form of reaction rims surrounding magnetite grains in a gabbro from 1105.5 m (Figure 31a) or clinopyroxene in the anorthosite at 1166.52 m (Figure 31b). The largest amount of amphibole in Cycle V occurs as an amphibole rich vein. These veins were limited to two gabbros 1105.5 m (Figure 31c) and 1223.85 m (Figure 31d). Visible in these figures is the presence of a series of green veins running throughout the rock.

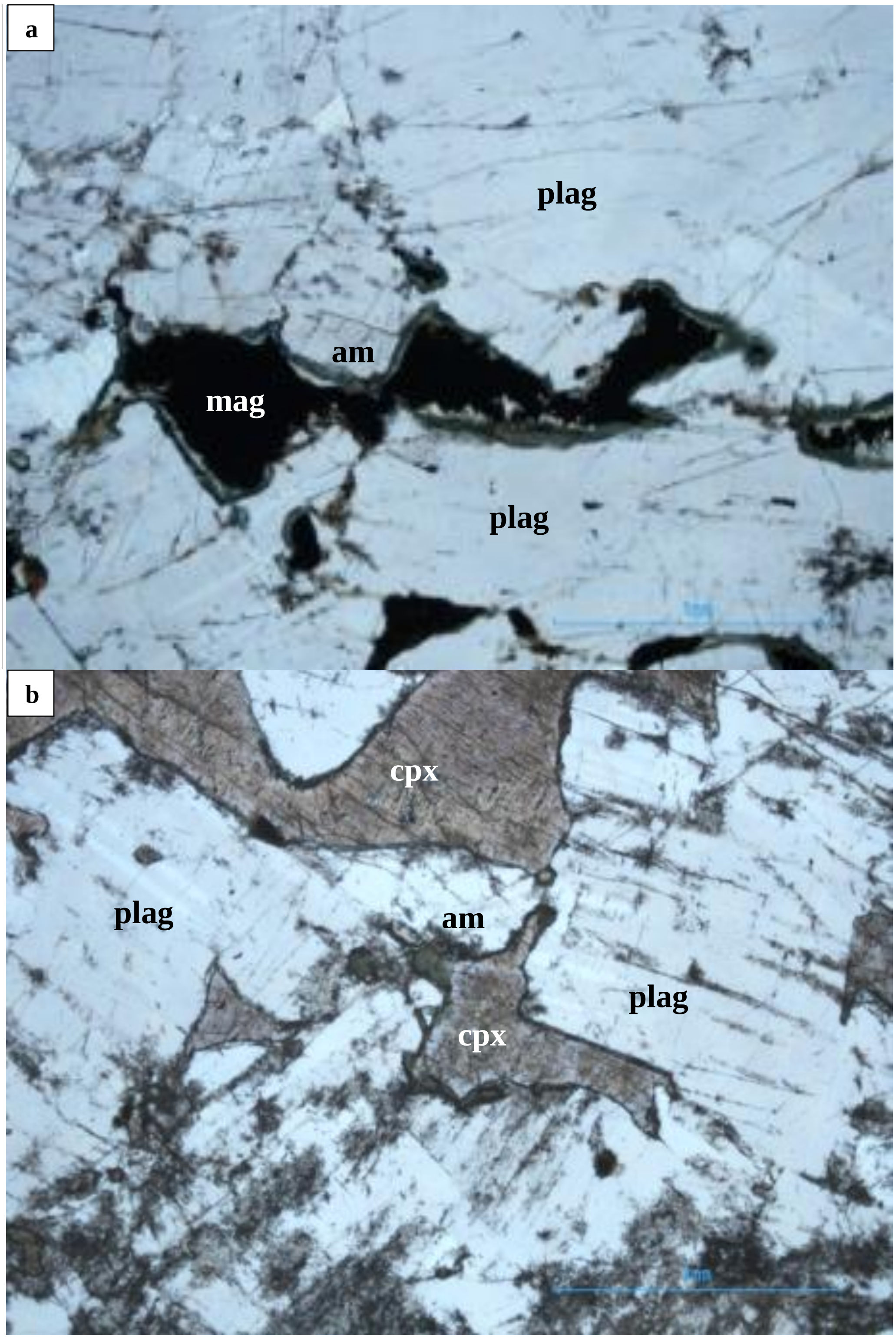

Figure 31. a. Amphibole rim around magnetite grain. b. Amphibole rim around clinopyroxene grains in an anorthosite from 914.99 m.

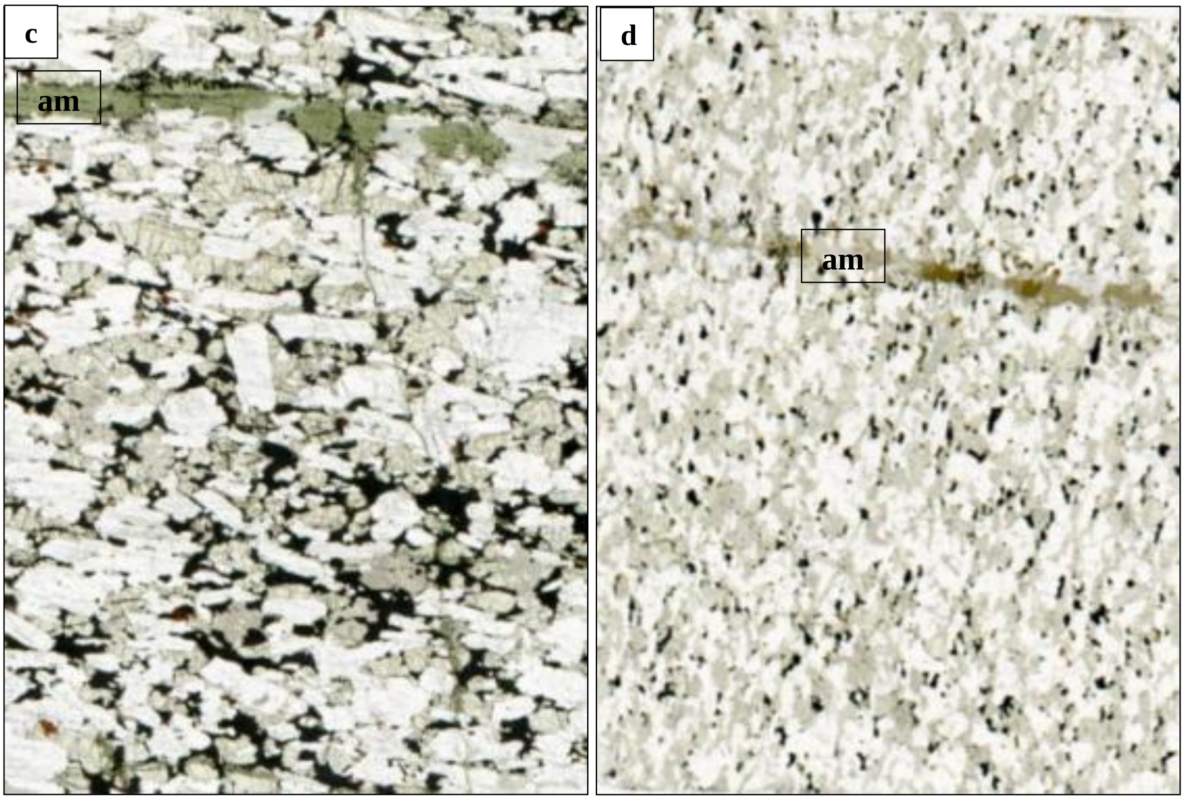

Figure 31. **c. Scanned image of a gabbro from 1105.5 m. d. Scanned image of a gabbro from 1223.85 m.**

Referring to Figure 31c and d, the amphibole “layer” can be seen propagating across the thin section. The presence of this layer appears to have had little effect on the mineralogy above and below it, although small cumulus grains of magnetite were seen to be accumulating above the amphibole layer and near horizontal plagioclase grains lying on top of the layer.

The majority of amphiboles present in Cycle VI were identified as pargasite based on the strong brown-green-turquoise pleochroism under plane polarised light. Smaller amounts of amphibole were found as reaction rims in the gabbro samples of Cycle VI but the greatest amount of amphibole was identified within the anorthosites (Figure 32a). The clinopyroxene in an anorthosite from 914.99 m shows an unusual, poorly defined texture that can be seen in Figure 32b. Despite the pargasite having crystallised around the clinopyroxene, the two minerals appear to have crystallised synchronously.

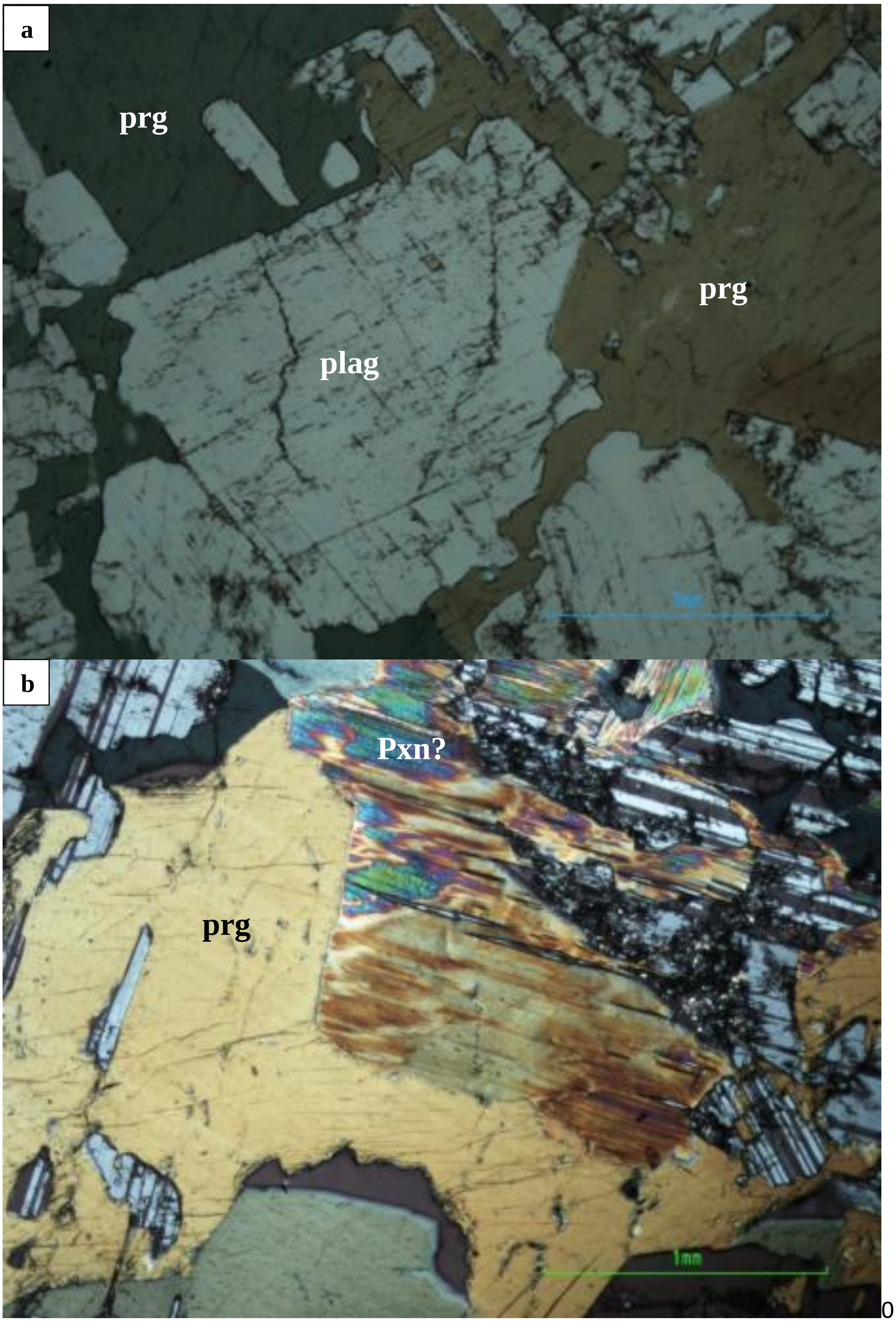

Figure 32. a. PPL image illustrating the interstitial texture of pargasite within anorthosite (914.99 m). b. XPL image illustrating the replacement of clinopyroxene by pargasite (914.99 m).

Silica

Microscopy

A mineral was observed to have low relief and no pleochroism under plane polarised light. Under crossed polarised light the interference colours showed a range and first order colours. The initial observations would suggest the mineral was quartz however, the interference figure revealed both uniaxial and biaxial positive interference figures. Additional XRD or RAMAN analysis of the silica mineral is essential to determine the state of the silica mineral.

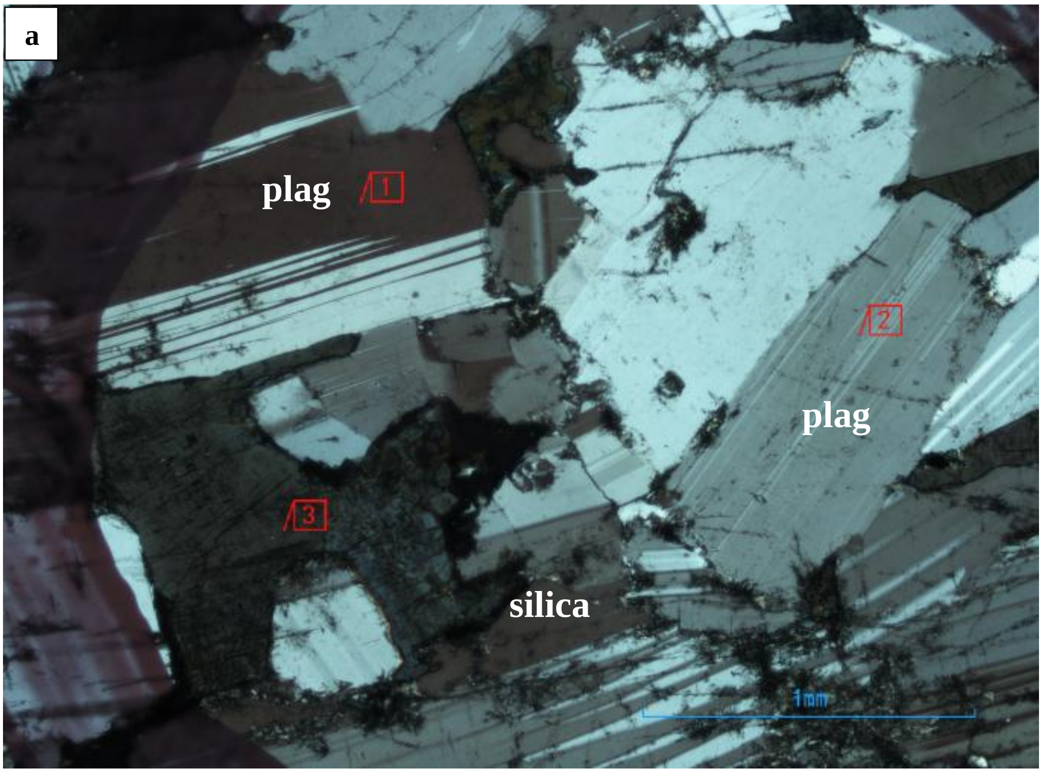

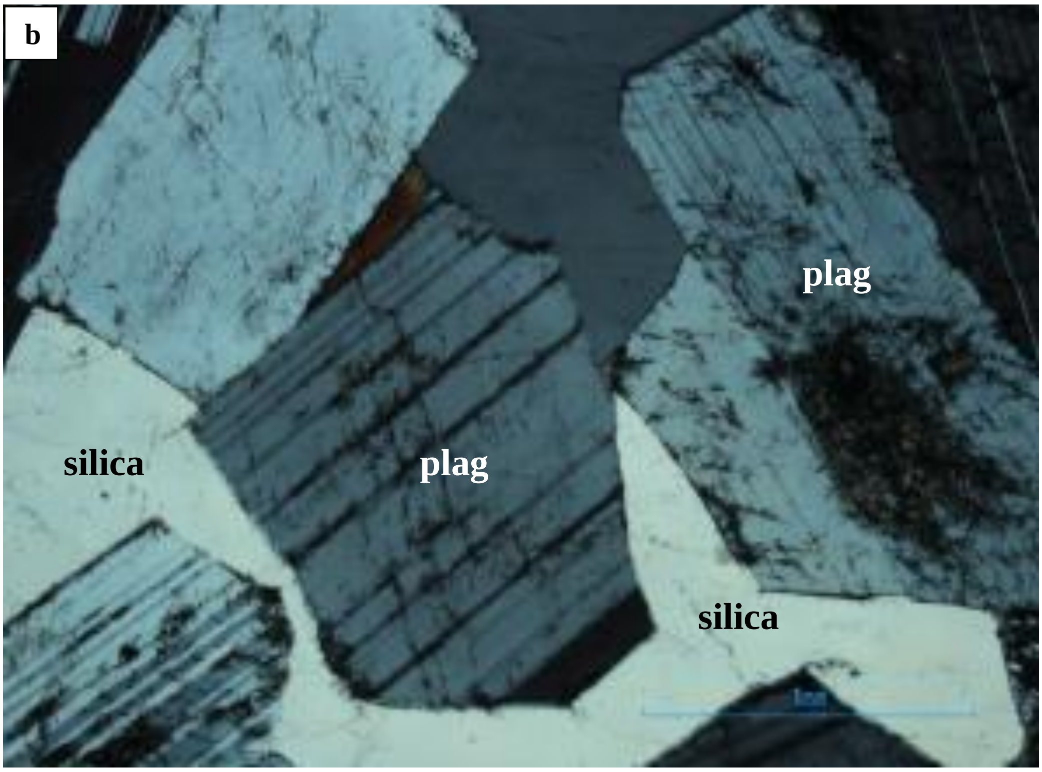

Figure 33. **XPL images of interstitial silica from two anorthosites from a. 1166.52 m and, b. 923.61 m.**

Summary

The general paragenetic sequence of the gabbros varies with depth, which may suggest that a number of phases were crystallising within short time spans of one another. Plagioclase, olivine, pyroxene, magnetite and apatite crystallised from the bulk magma. Although magnetite appears to be interstitial, oxides crystallising later on in the crystal mush layer could overgrow early formed grains of magnetite.

The paragenetic sequence of the magnetite-rich gabbros is different as the two rocks contain different minerals. The magnetite-rich gabbro at the bottom of Cycle V has the paragenetic sequence of plagioclase, magnetite, apatite, and the simultaneous crystallisation of olivine, clinopyroxene and orthopyroxene followed by biotite. The magnetite-rich gabbro at the top of Cycle V has the paragenetic sequence of magnetite, biotite, clinopyroxene and simultaneous crystallisation of plagioclase and olivine.

The paragenetic sequence of the anorthosites for Cycle V and Cycle VI remains relatively consistent. The single anorthosite from Cycle V contained large grains of plagioclase with interstitial orthopyroxene and minor clinopyroxene and magnetite. Amphibole was found as alteration around clinopyroxene and magnetite (Figure 31)). Three out of the five anorthosites from Cycle VI were identical to the anorthosite in Cycle V.

Chapter 5 – Analytical Results

All analytical data from this study, which are presented graphically in this chapter, is presented in the appendix. The analytical procedure was highlighted in Chapter 3.

Plagioclase

The An% for Cycle V is presented in Figure 34. The data shows a wide spread in between andesine and labradorite, with a larger proportion of the data plotting as andesine. No analyses from Cycle V contained more than 5% K_2O.

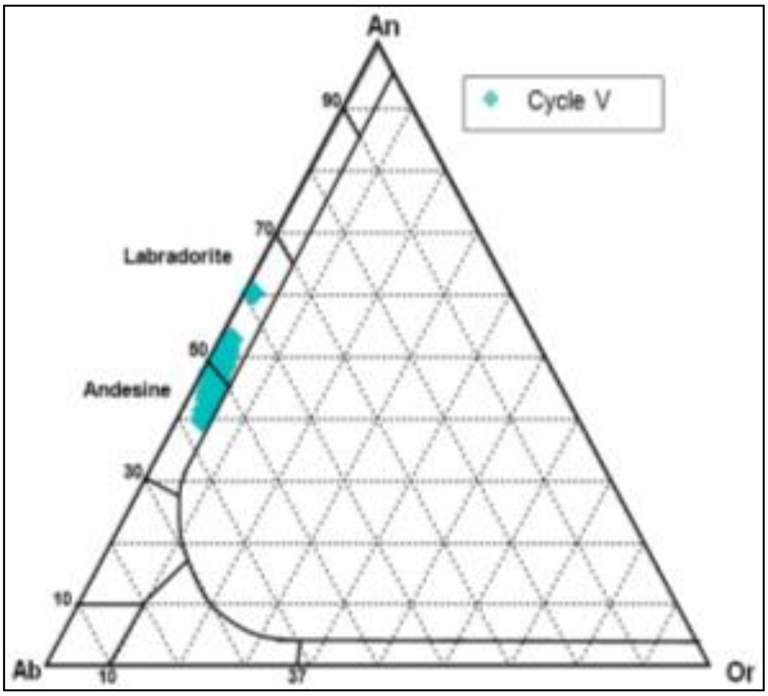

Figure 34. Ternary plots illustrating the compositions of the feldspars analysed in Cycle V.

A single data point can be seen at 60% anorthite. The grain analysed originated from a depth of 1403.32 m and showed no distinct variation in size but did appear to be somewhat zoned (grain 1 in Figure 35). The core of the grain displayed no albite twinning, but the outer edges did.

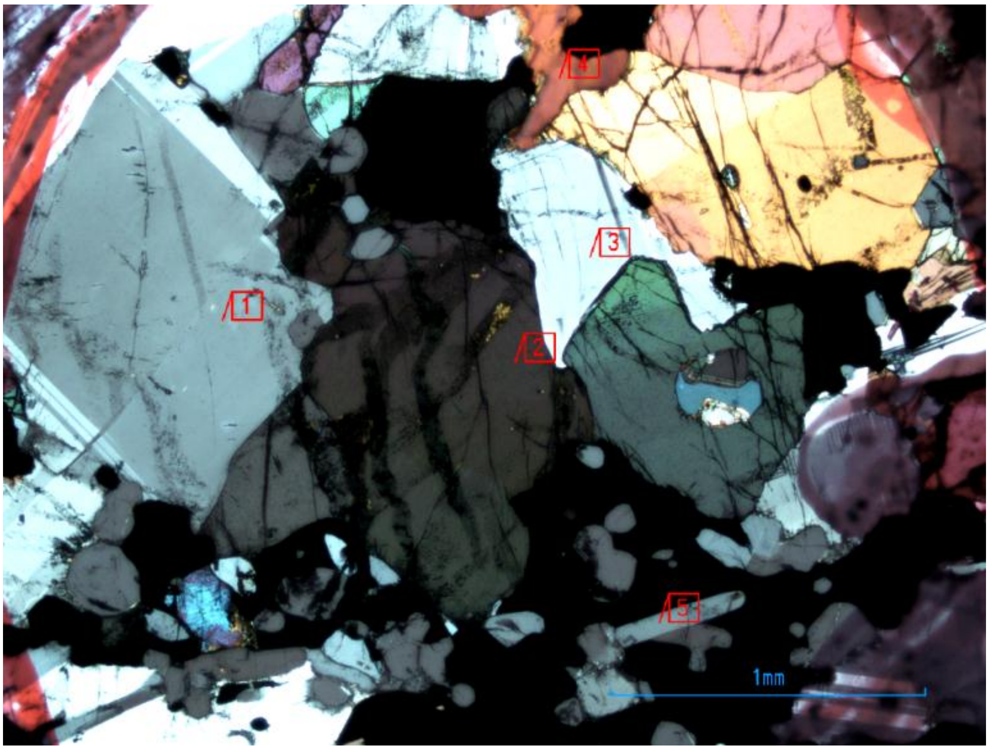

Figure 35. **XPL image of the labradorite grain (labelled 1) analysed at 1403.32 m.**

The plagioclase analyses for Cycle VI showed less variation than in Cycle V. The majority of the analyses plotted as andesine (between 50-60% albite) and a few points as labradorite (>50% anorthite). The percentage of K_2O is in general higher in Cycle VI compared to Cycle V.

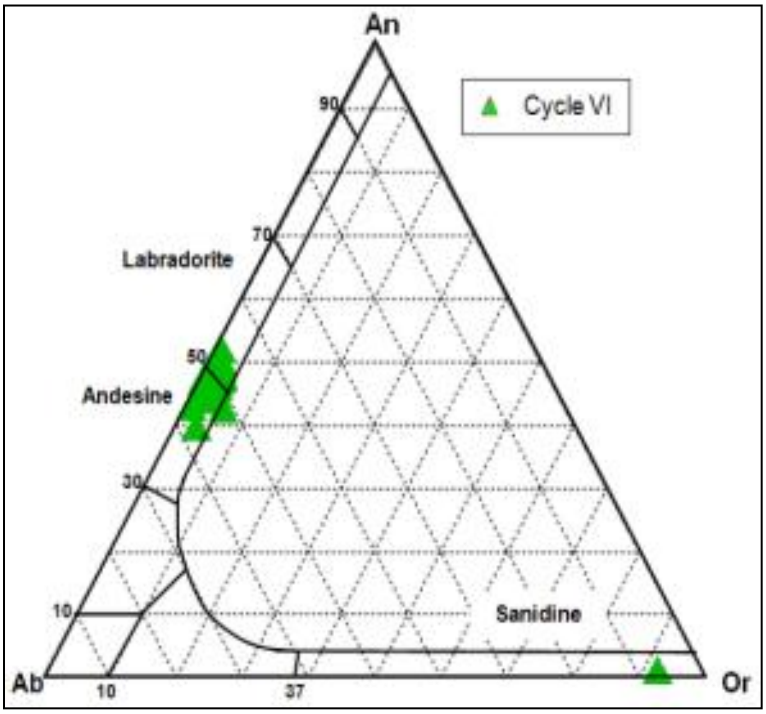

Figure 36. **Ternary plots illustrating the compositions of the feldspars analysed in Cycle VI.**

The analyses contained between 1-2% higher K_2O in Cycle VI with a single grain plotting as sanidine. The analysed grain originated from a depth of 911.66 m. The orthoclase grain can be seen in Figure 37 below.

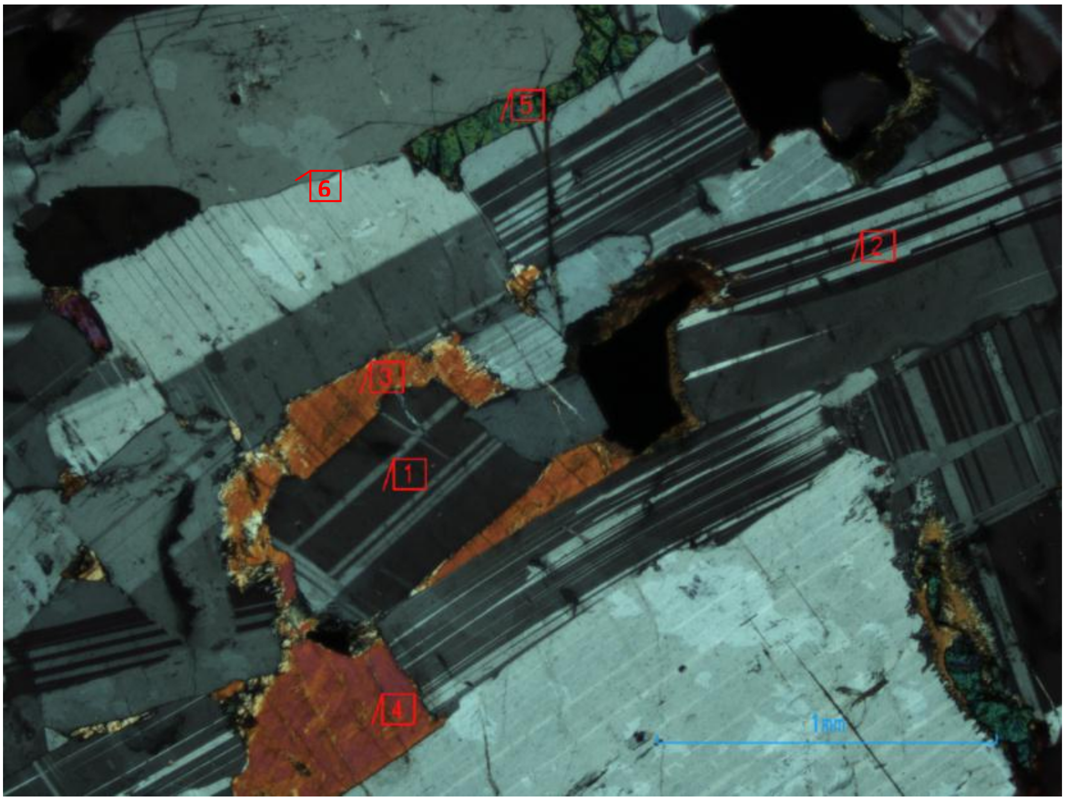

Figure 37. XPL image of the sanidine grain (labelled 6) analysed at 911.66m.

The fluctuation in An% with a decrease in depth is shown in Figure 38. A general observation shows two possible trends within the data, as indicated by the two red lines. Both trends show higher An% at the bottom and top of the trend, and lower values in the middle. The two separate trends are of Cycles V and VI.

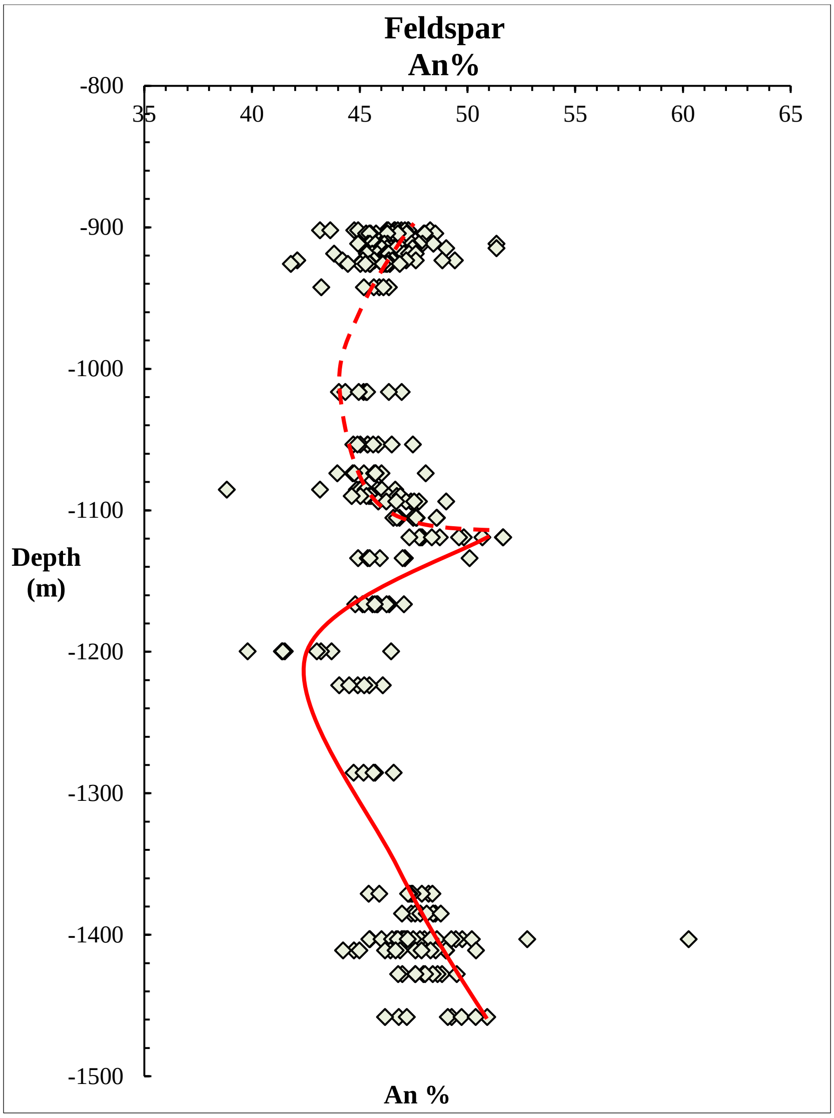

Figure 38. **Scatter plot illustrating the An% fluctuations throughout Cycle V (solid line) and Cycle VI (dashed line). Red lines inserted to illustrate possible trends within the data.**

The data for Cycle V (blue diamond symbols) and Cycle VI (yellow triangle symbols) have been re-plotted in Figure 39, along with data from Tegner *et al.* (2006) and the position of the magnetitite layers, as recorded by Tegner *et al.* (2006).

Cycle V starts at a depth of 1458.12 m with An% varying between 46-50. The An% decreases to values as low as 40% at a depth of 1199.75 m. From 1166.52 m, the An% begins to gradually increase until a depth of 1119.3 m where values as high as 52 An% were recorded and the average plagioclase composition were found to be 49 An%. From 1105.5 m the An% begins to decrease again.

According to the data from Tegner *et al.* (2006), the upper boundary of Cycle V is located between 1190.1 m and 1158.6 m depth. Using the unpublished data from Professor

R.K.W. Merkle of the University of Pretoria, the upper boundary of Cycle V was estimated around ~1100 m. Based on the data collected and the observed decrease in the An% at 1105.5 m depth, the upper boundary of Cycle V most likely lies at ~1119.3 m depth.

From the top of Cycle V (i.e. the base of Cycle VI), the average An% decreases gradually from around 48. The lowest values were recorded at depths of 1016.5 m and 942.4 m where the average compositions are at 45 An%. The sample taken at 990.09 m was found to be altered after microscopic examination and therefore no clear points could be found for a reliable analysis. After the analyses at 942.4 m, the An% begins to increase again although the overall plagioclase compositions showed a greater deal of variation compared to the previous trend. Despite this, the average An% increases from 45 An% at 942.4 m to 47 An% at 914.99 m. Plagioclase compositions showed a small decrease in the An% of 46.5% at 911.66 m to 46% at the top of the sample set at 902.3 m. Thus, Cycle VI is much shorter with an overall height of approximately 200 m compared to Cycle V at approximately 350 m.

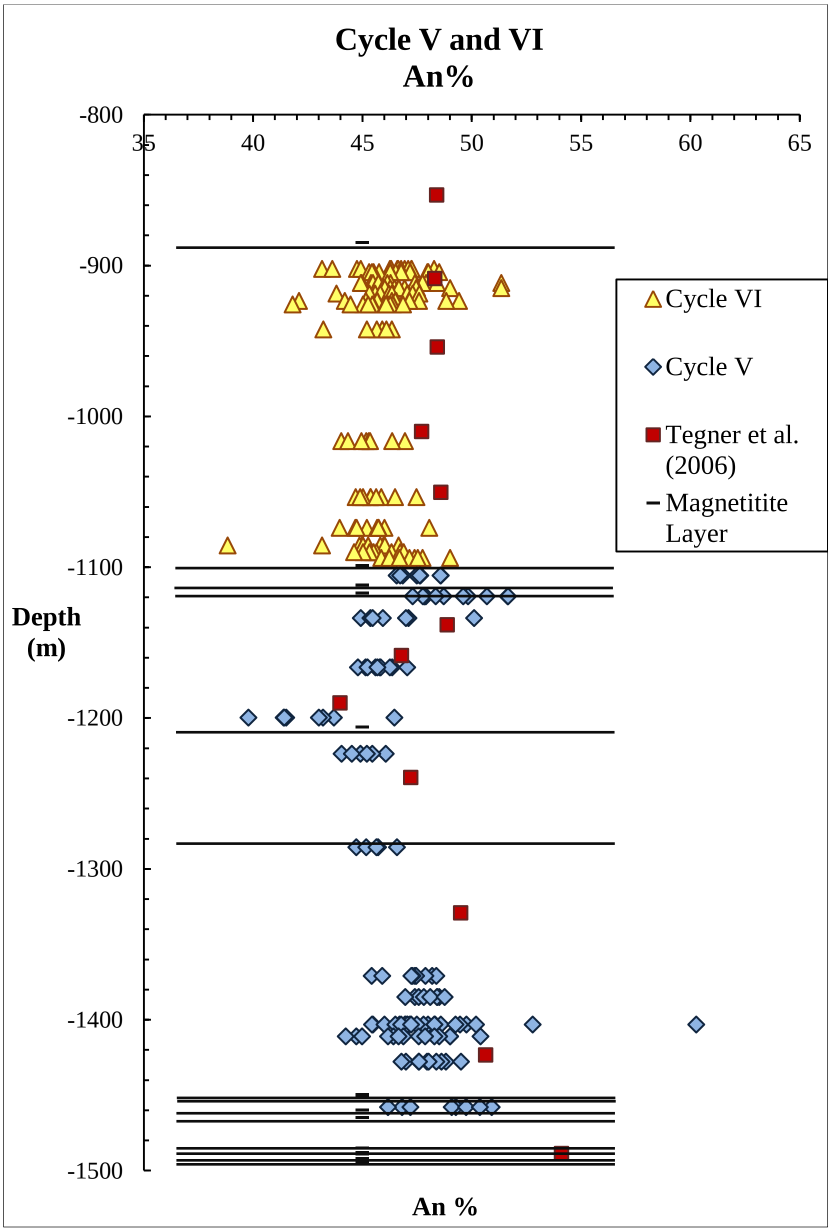

Figure 39. **Scatter plot illustrating the An% fluctuations throughout Cycle V (blue diamonds) and Cycle VI (yellow triangles). Included data from Tegner *et al.* (2006) is plotted as squares for the silicates and black lines for the magnetitite layers.**

From the data from Tegner *et al.* (2006), three observations can be made. The lower cycle (V) is very much in agreement with the previously published data, with the An% reported by Tegner *et al.* (2006) slightly higher than the current data. The upper cycle (VI) deviates greatly from the trend noted by Tegner *et al.* (2006), and a large amount of variation is present in the An content of the plagioclases. The third observation is that there is a spike in the An% between 1138.2 m and 1050.5 m, which was not detected by Tegner *et al.* (2006).

The magnetitite layers appear to be located at the top and bottom of each of the cycles. Cycle V shows a package of magnetitite layers at the bottom with two layers located above the magnetite-rich rock sampled at 1458.12 m. Another magnetitite layer is located almost below the gabbro sample taken at 1199.75 m where low proportions of magnetite were observed. The next package of magnetitite layers is located between Cycle V and Cycle VI. A single layer was recorded at 1099 m, between two gabbro samples with proportions of ~20% magnetite. These proportions are considered low for rocks overlying and underlying a magnetitite layer.

Olivine

The olivine compositions from Cycle V are shown in Figure 40. The olivine is predominantly fayalite with a wide spread in the values between 60 and 90%. The majority of the analyses plot between 75 and 85% fayalite, with a small group around 70% fayalite. Two points plot at ~60% fayalite, both originating from a magnetite-rich gabbro at a depth 1458.12 m.

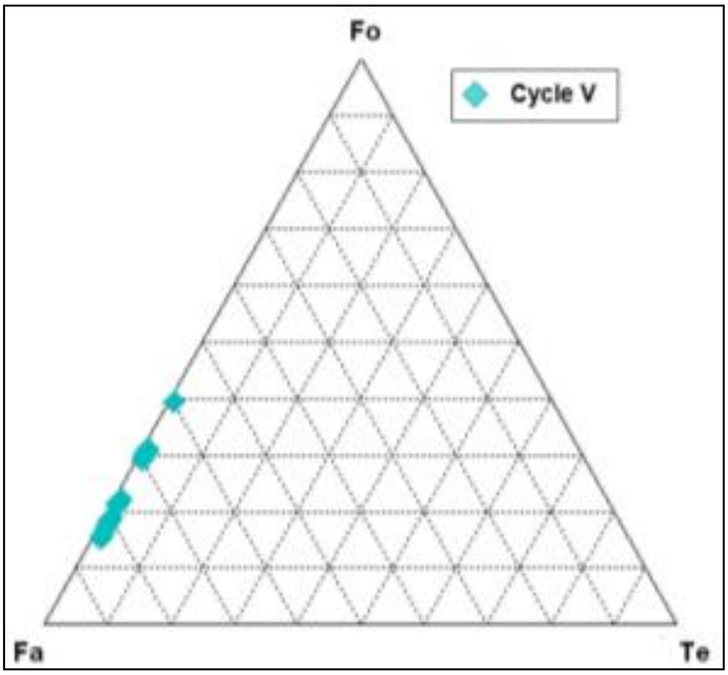

Figure 40. Ternary plot illustrating the compositions of the olivine analysed in Cycle V.

The olivine compositions from Cycle VI (Figure 41) appear to be more closely grouped compared to Cycle V. All the analyses plot as fayalite with all the data plotting between 70% and 90% fayalite. The number of olivine analyses is fewer due to the overall lower proportions of olivine throughout Cycle VI.

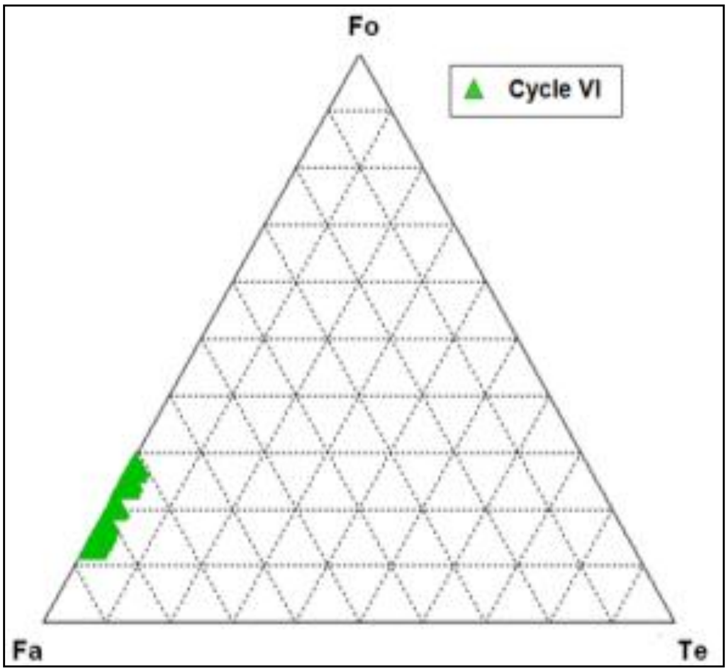

Figure 41. Ternary plot illustrating the compositions of the olivines analysed in Cycle VI.

The fluctuation in the Mg# of olivine with depth in Cycle V and Cycle VI is shown in Figure 42. The boundary between the two cycles is based on the study by Tegner *et al.* (2006) and the unpublished data from Merkle. However, the actual boundary is debatable and not necessarily in the suggested location based on the An%.

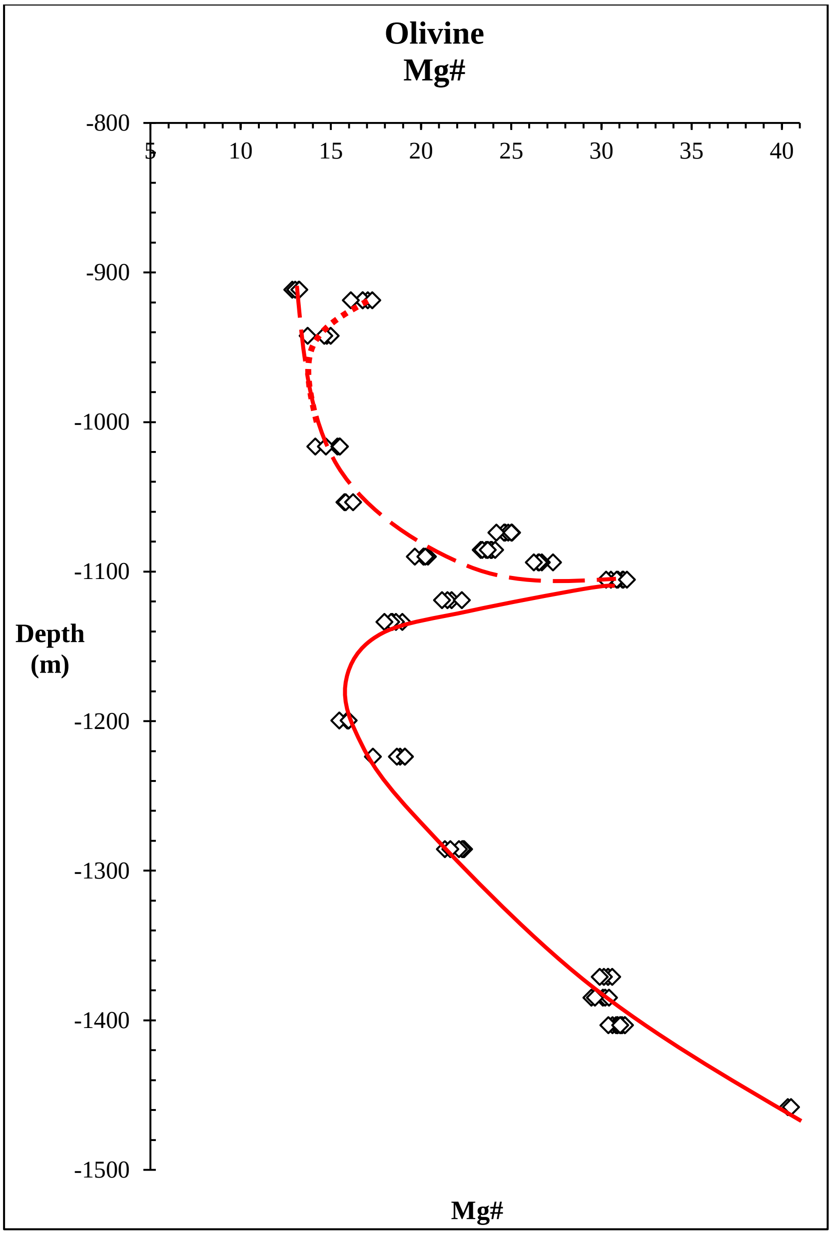

Figure 42. **Scatter plot illustrating the Mg# fluctuations of the olivines throughout Cycle V (solid line) and Cycle VI (dashed and dotted line). Red lines inserted to illustrate possible trends within the data.**

The data for Cycles V (blue diamond symbols) and Cycle VI (yellow triangle symbols) have been re-plotted in Figure 43, along with data from Tegner *et al.* (2006) and the position of the magnetitite layers, as recorded by Tegner *et al.* (2006).

The trend observed throughout Cycle V shows a Mg# of ~40 at the bottom of the cycle. Olivine compositions become increasingly fayalitic as depth decreases, and reach the lowest values of 16 at a depth of 1199.75 m. From here, the Mg# begins to increase once again where a maximum of 31 is reached at a depth of 1105.5 m.

The olivine analyses from 1105.5 m depth does not show the same trend that was observed in the An% plot. At this depth, the Mg# continues to increase rather than decrease as the data continues into Cycle VI.

Following the peak in the Mg# at 1105.5 m depth, the Mg# then begins to decrease again to Mg# of 20 at a depth of 942.4 m. The trend of the data towards the top of Cycle VI is somewhat ambiguous (indicated by the two dashed lines at the top of Cycle VI). The Mg# may continue to decrease after 911.66 m or begin to increase from 918.69 m. An increased density of analytical points higher up in the stratigraphy is required to clarify the trend.

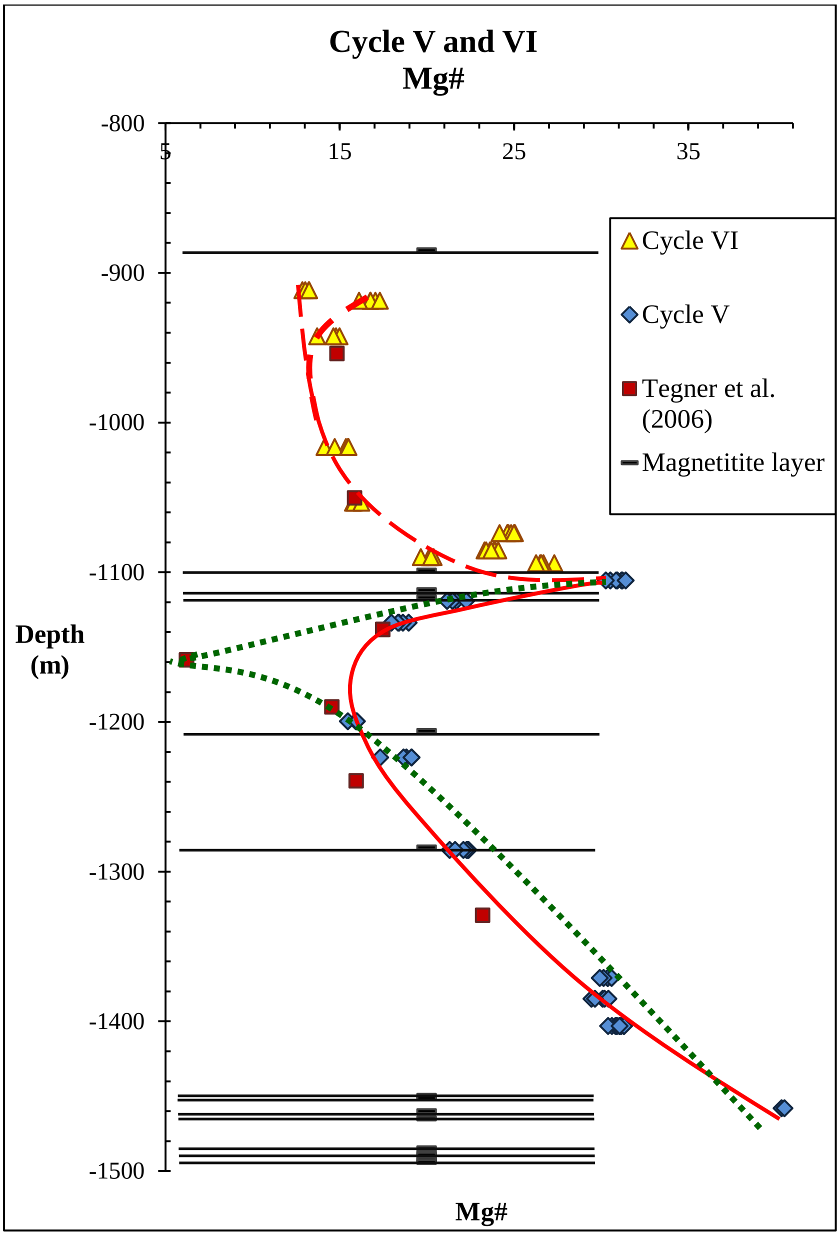

Figure 43. The Mg# variation of the olivine for Cycle V (blue diamond) and Cycle VI (yellow triangle). Included is data from Tegner *et al.* (2006) - squares for the silicates and black lines for the magnetitite layers. Red lines inserted to illustrate possible trends within the data.

The data from Tegner *et al.* (2006) appears to be following an almost identical trend to the current data. However, an absence of sampling between 1130 m and 1050 m depth means that the peak in the Mg# values observed by between the previously defined Cycle V and Cycle VI was not recorded. Data from Tegner *et al.* (2006) is limited for Cycle VI therefore no concrete correlation could be made between the two datasets.

Pyroxene

The pyroxene data from Cycle V is presented in Figure 44. The data shows a great deal of variation, with the bulk of the data plotting between diopside and hedenbergite. A few analyses plotted as augite, one as pigeonite and two as ferrosilite. The pigeonite analysis originated from a depth of 1105.5 m as did one of the ferrosilite analyses. The other ferrosilite analysis originated from the bottom of Cycle V at a depth of 1427.95 m.

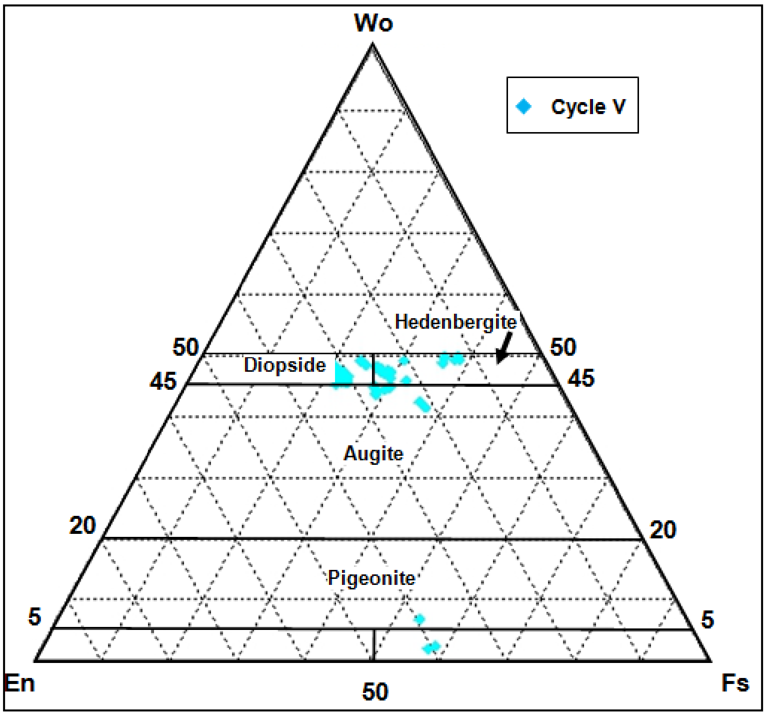

Figure 44. **Ternary plot illustrating the compositions of the pyroxenes analysed in Cycle V.**

The ferrosilite analysis from 1427.95 m was taken from the grain shown in Figure 45a (grain 2). The second ferrosilite analysis taken at a depth of 1105.5 m originated from a core-rim analysis of a partially overgrown pyroxene. The grain is visible in Figure 45b and is labelled as 1 and 2 in the image. Both the ferrosilite and pigeonite analyses originated from the core of the grains, whereas diopside was analysed at the rim of the grain.

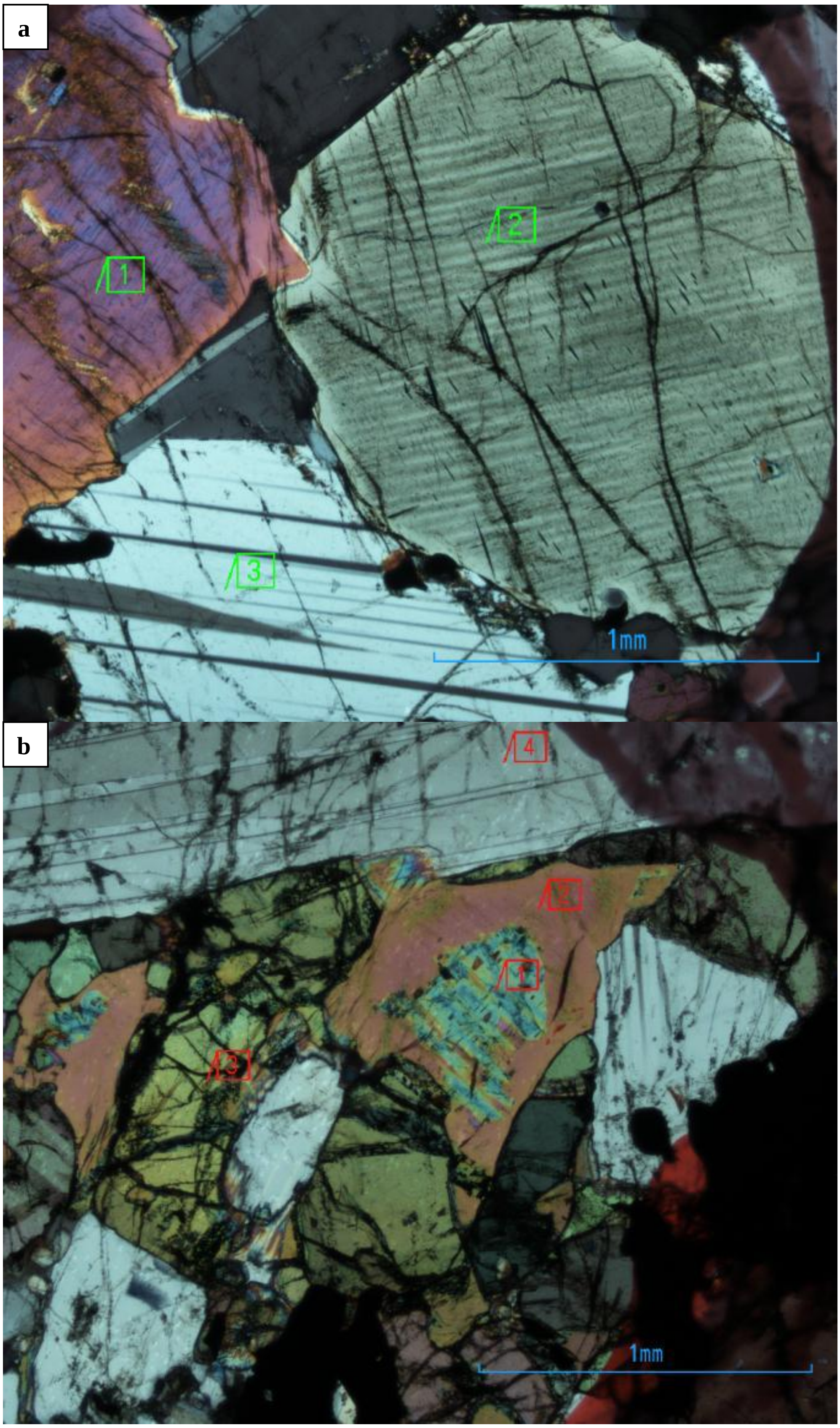

Figure 45. a. XPL image of the ferrosilite grain (labelled 2) analysed at 1105.5 m. b. XPL image of the partially overgrown pyroxene grain at 1105.5 m. The core (labelled 1) contained pigeonite, ferrosilite and diopside at the rim (labelled 2).

The data from the line analysis is presented in Figure 46 for the grain illustrated in Figure 45 (core 1 and rim 2). The centre of the grain (second order blue and green section) was made up of predominantly ferrosilite with smaller amounts of pigeonite. Surrounding the core is diopside (second order pink).

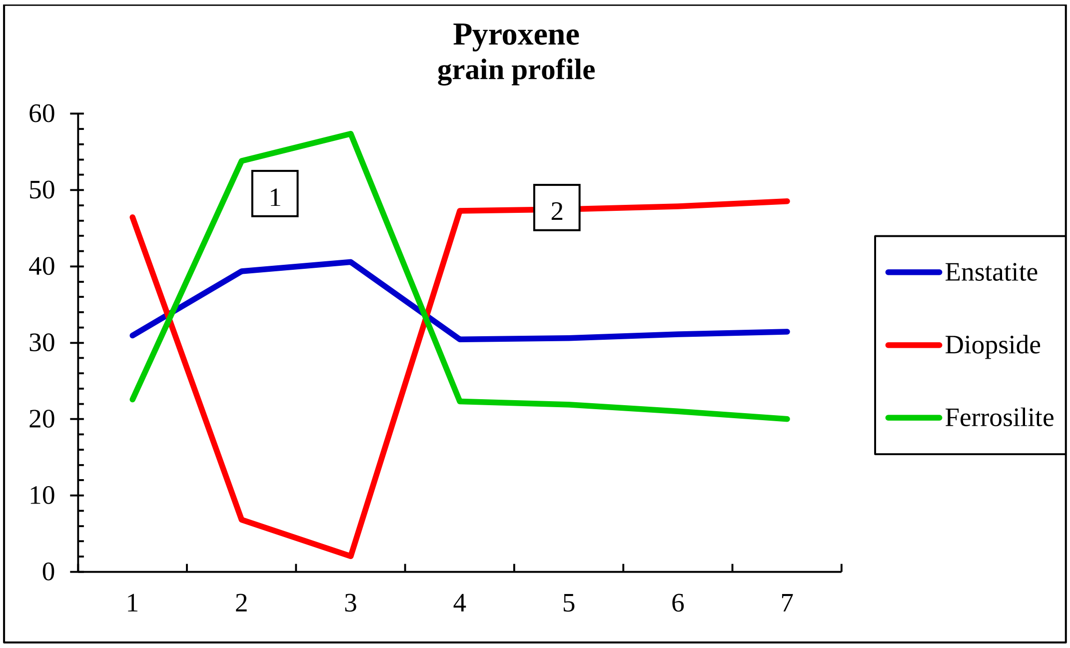

Figure 46. **Line analysis of overgrown pyroxene grain from a depth of 1105.5 m. The core (labelled 1) contains enstatite and ferrosilite. The rim (labelled 2) is diopside.**

The pyroxene analyses from Cycle VI show much less variation with the bulk of the data plotting as hedenbergite (Figure 47). The hedenbergite and augite analyses were taken from both gabbro and anorthosite samples. The remainder of the analyses plot as augite and two plot as ferrosilite. The ferrosilite analyses originated from a gabbro at a depth of 911.66 m.

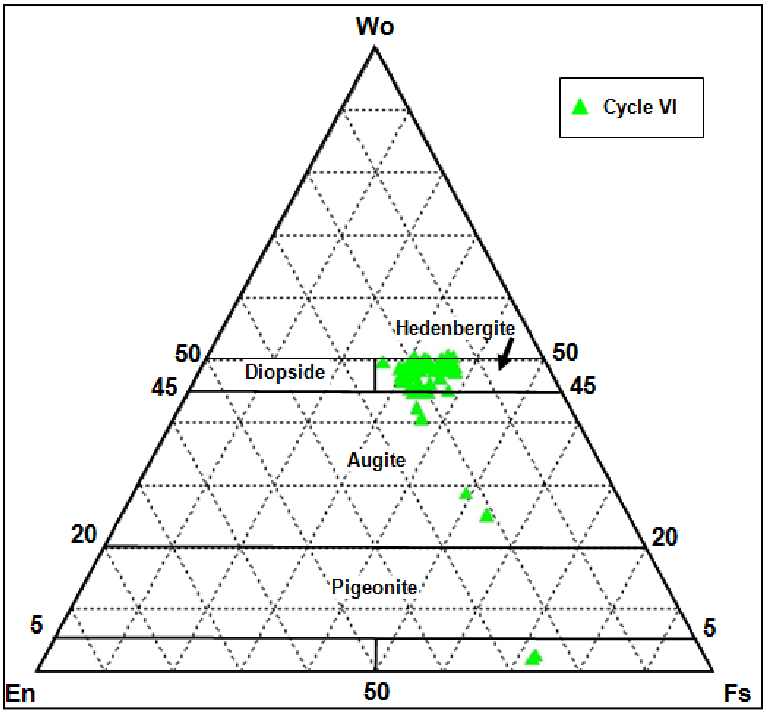

Figure 47. Ternary plot illustrating the compositions of the pyroxenes analysed in Cycle VI.

The two augite analyses originated at two different depths. In Figure 48a and b, the two augite grains are shown. No textural differences were identified between the two grains save for the difference in size.

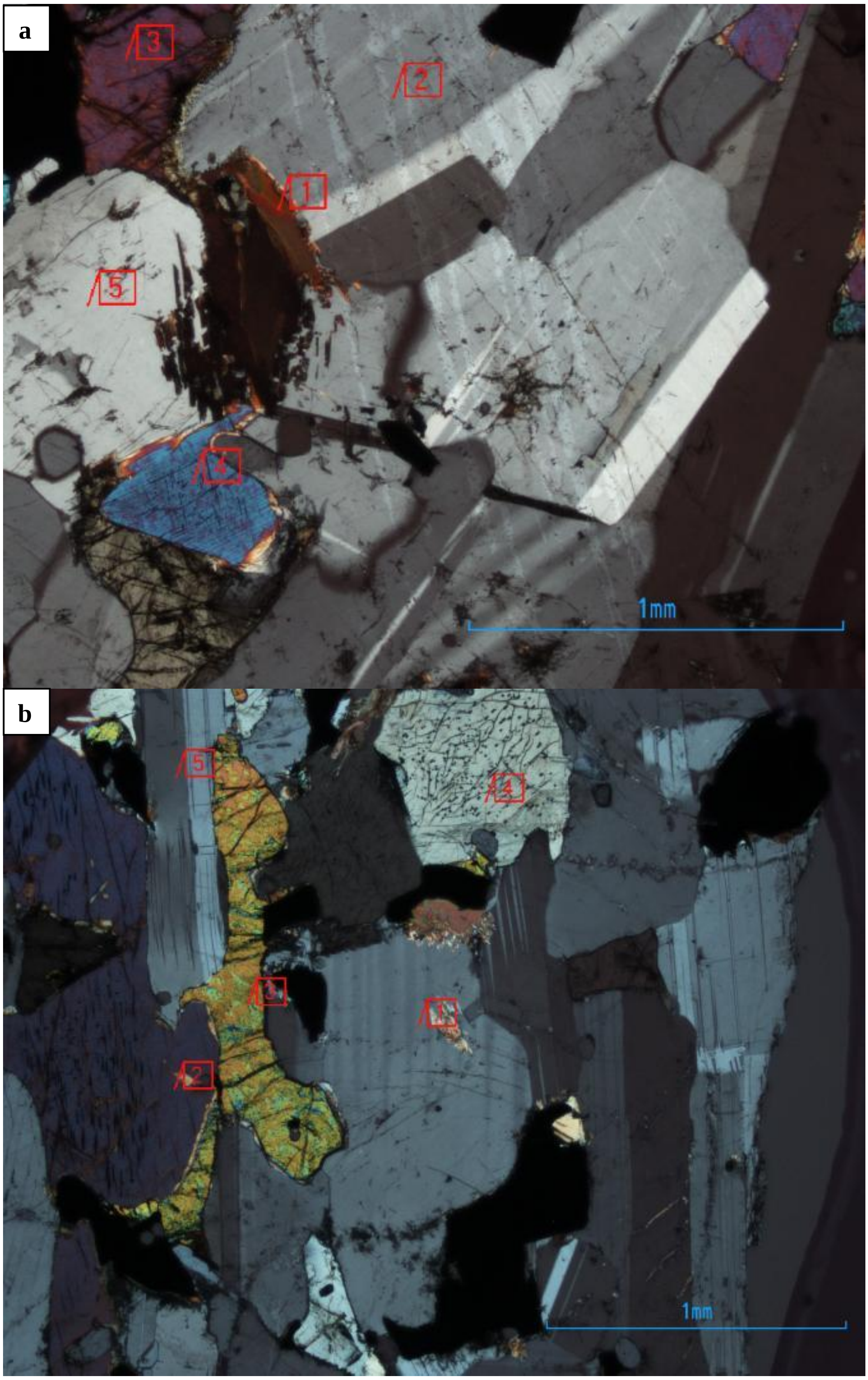

Figure 48. a. XPL image of the augite grain (labelled 4) analysed at 942.4 m. b. XPL image of the augite grain (labelled 2) analysed at 1016.5 m.

The fluctuation in the Mg# of the pyroxenes with depth is shown in Figure 49. The individual analyses showed a large amount of variation within a single sample. The trends observed throughout the pyroxene analyses are quite different from the previous minerals. The boundary between the two cycles is notably sharper than previously observed.

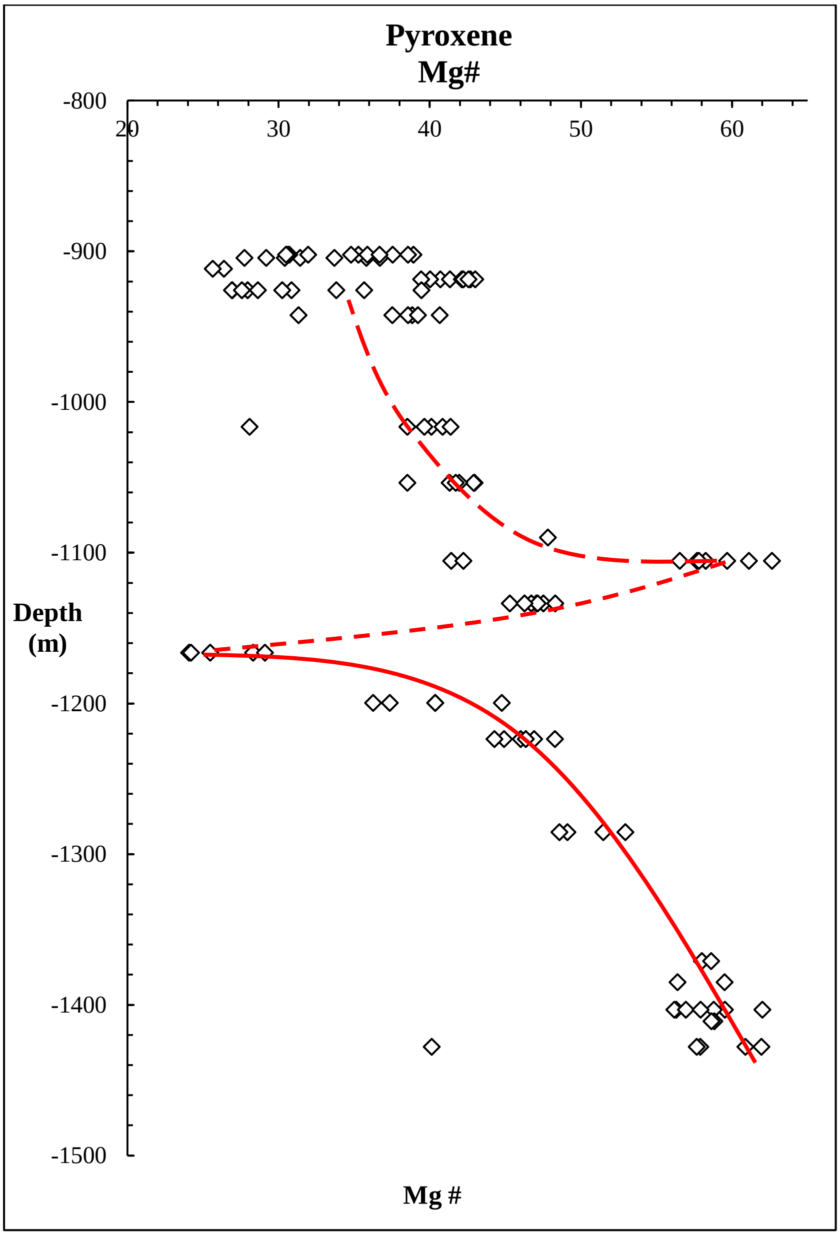

Figure 49. **The Mg# variation for the pyroxenes of Cycle V and Cycle VI. Red lines inserted to illustrate possible trends within the data.**

Cycle V and Cycle VI have been re-plotted in Figure 50 below. The highest Mg# was recorded at the base of Cycle V with values ranging in between 50 and 60. The Mg# begins to decrease towards minimum values as low as 24 at a depth of 1166.52 m. Above 1166.52 m, the Mg# begins to increase rapidly (short dashed line) to 47 and then 55 at a depth of 1105.5 m where another peak in the Mg# is reached. The low Mg# values at 1427.95 m and

1105.5 m correspond to the previously discussed augite and ferrosilite analyses. The highest Mg# was recorded in the magnetite-rich gabbros and the lowest values were recorded in the anorthosites.

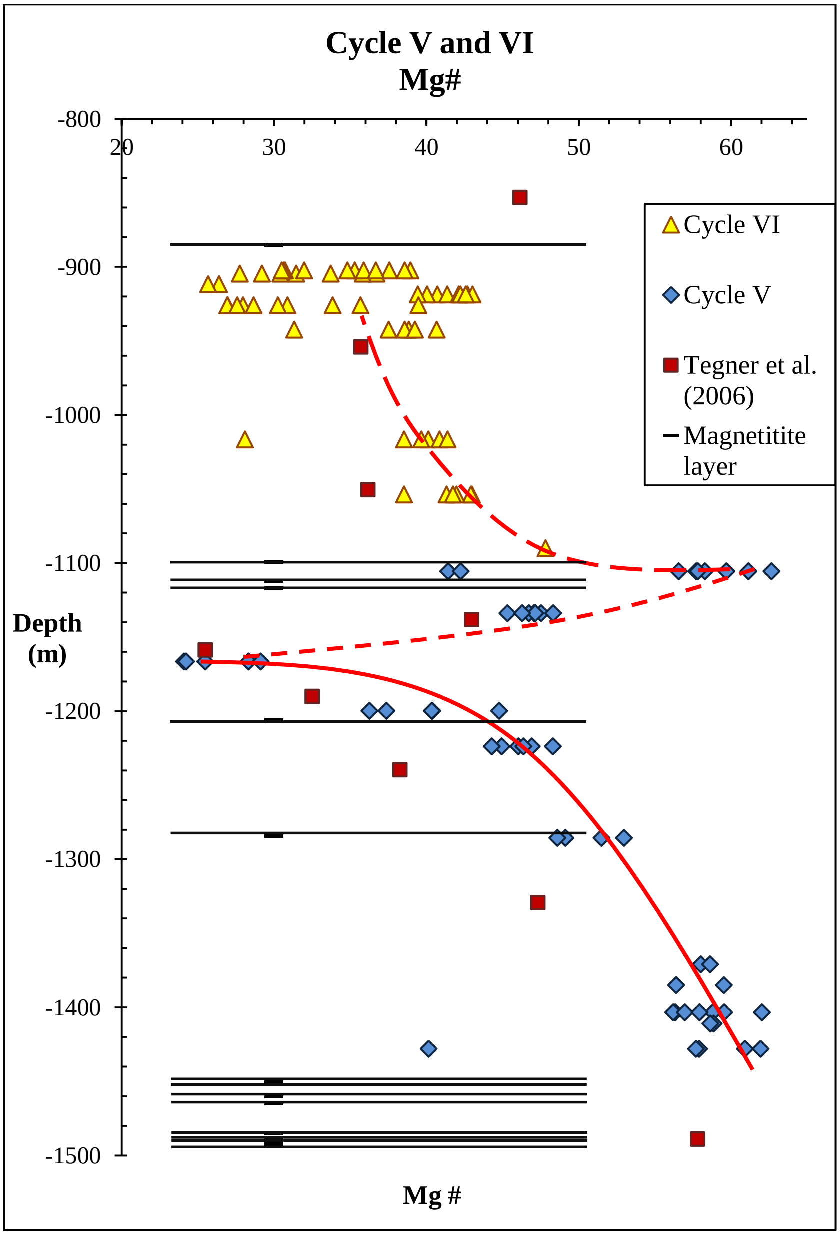

Figure 50. The Mg# variation in the pyroxenes in Cycle V (diamonds) and Cycle VI (triangles). Data from Tegner *et al.* (2006) is plotted as squares for the silicates and black lines for the magnetitite layers. Red lines inserted to illustrate possible trends within the data.

The trend observed for the Mg# of the pyroxenes of Cycle VI bears some resemblance to that of the Mg# of the olivines from Cycle VI. From the higher Mg# of Cycle V at 1105.5 m, the Mg# decreases from 48% to 42%. The pyroxene compositions are highly variable between the depths of 942.4 m and 902.3 m, with Mg# ranging between 43% and 26%. The presence of primary amphibole, which was recorded in the anorthosite samples between these depths, may be affecting the compositions of the pyroxenes.

Data from Tegner *et al.* (2006) has been included once again. The lower portion of this data appears to be following an identical trend to that of the current dataset. The upper portion of Tegner's data gives no additional insight into the composition of the current dataset. The spike in Mg# at 1105 m was not obvious in the Tegner *et al.* (2006) data.

Apatite

Cumulus apatite was analysed for Cycle V and Cycle VI from the gabbro samples only, as no apatite was identified in the anorthosites. The halogen concentrations of the apatites are shown in Figure 51a and b. All apatite analyses were corrected for oxygen before the analysis of the halogen concentrations.

The fluorine concentrations in the apatite from Cycle V showed large degrees of variation. No textural variations were observed between these apatites, so the chemical variations could possibly be attributed to the error when analysing for fluorine. However, the higher fluorine concentrations between 1427.95 m and 1403.32 m follow a generally decreasing trend towards 1105.5 m.

Cumulus apatite in Cycle VI was limited to the gabbros from 1094 m to 942.4 m. The F content varies between 2 wt% and 5 wt%, with the lower fluorine concentrations at the bottom of Cycle VI and the higher values towards the top.

The chlorine concentrations at the bottom of Cycle V show similar variations to those seen in the fluorine concentrations. A decrease in the chlorine concentrations is observed between 1371.05 m and 1199.75 m. The chlorine concentrations increase again at 1119.3 m and 1105.5 m.

Examining the chlorine concentrations of Cycle VI, the data is better grouped. The chlorine concentrations at the bottom of Cycle VI are slightly variable but there is a notable decrease of ~0.4 wt% at the bottom to ~0.3 wt% towards 1016.5 m. The values then increase again at towards ~ 0.5 wt% at 942.4 m.

The most abundant ion that could compensate for the decrease in the halogen concentration would be hydroxyl ion (OH^-). Cycle V shows a steady decrease in the fluorine and chlorine concentration from the base towards the top of the cycle that could then imply that the OH^- concentrations are increasing.

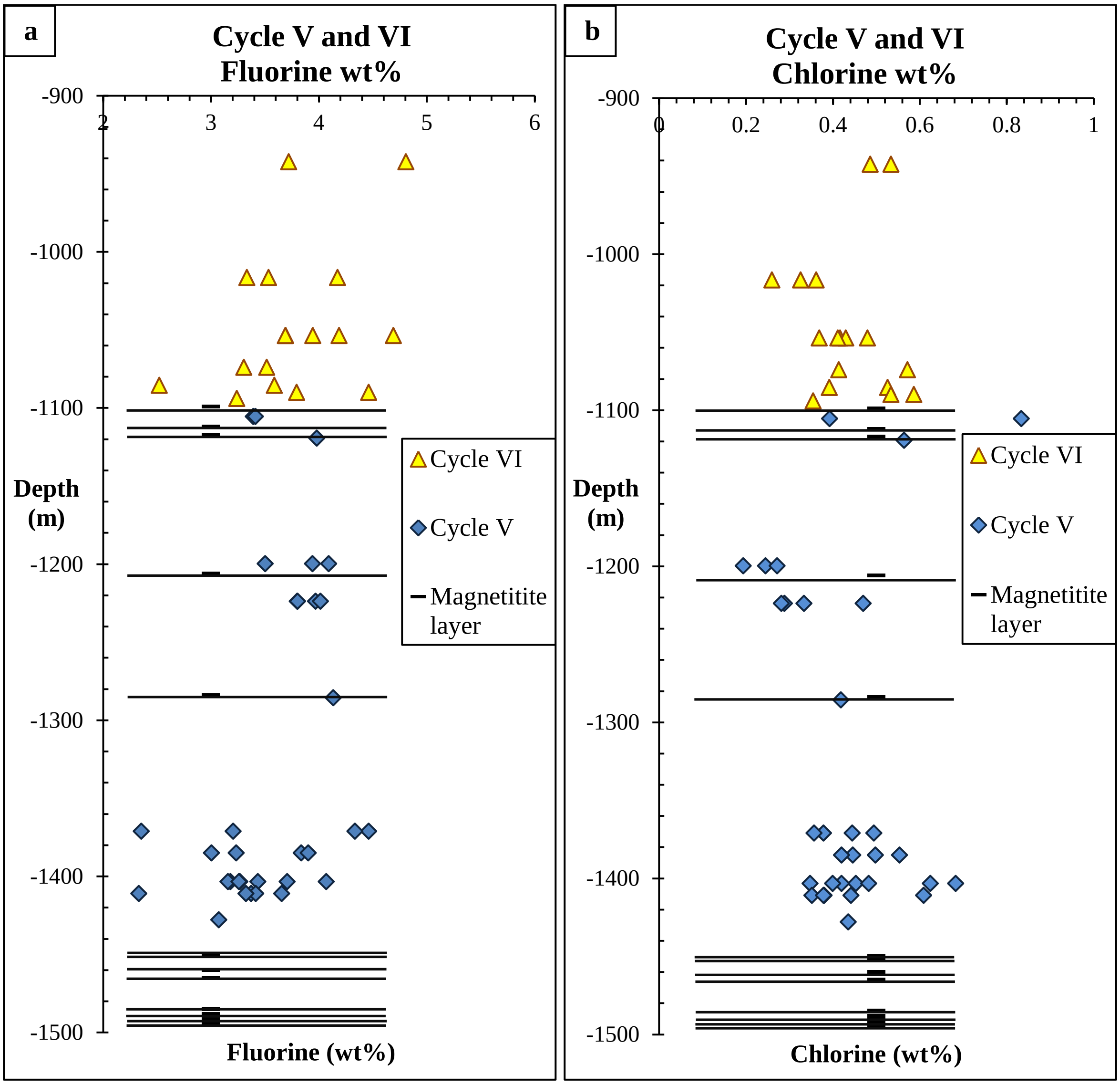

Figure 51. **a. Variation in the fluorine in apatites in Cycles V and VI. b. Variation in the chlorine in apatite in Cycles V and Cycle VI.**

Biotite

The variations in Mg# with depth in the biotite show noticeable trends in the two cycles (Figure 52), with a very different trend in each. The Mg# from Cycle V shows a decrease with a decrease in depth.

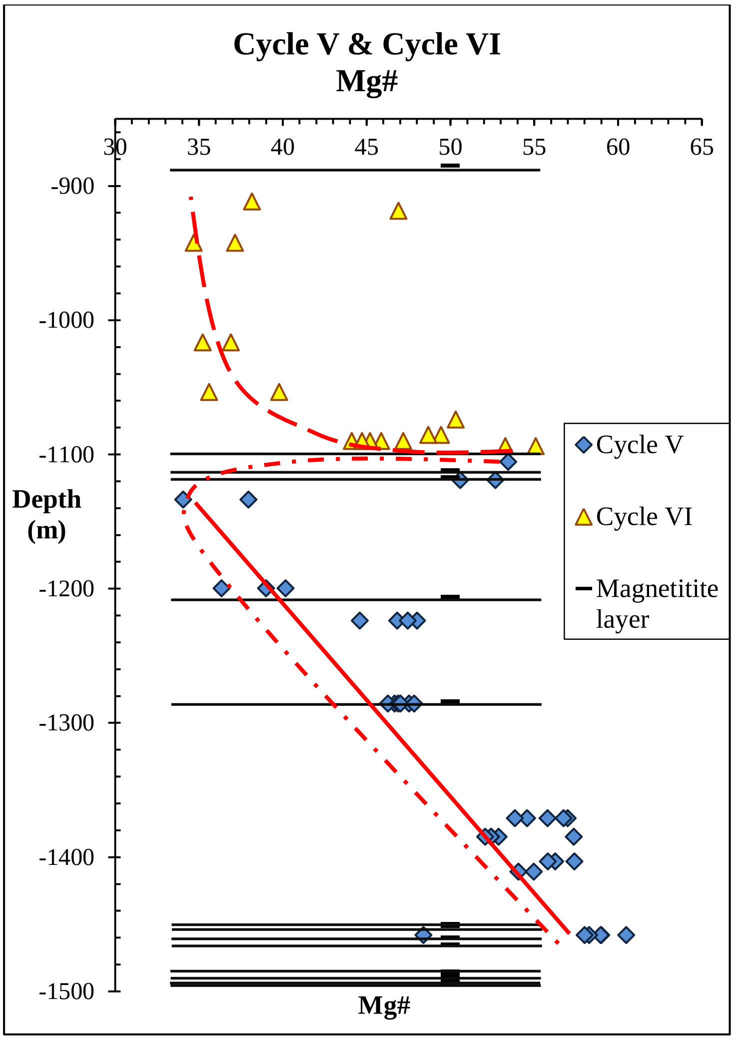

Figure 52. **The Mg# variation in the biotites in Cycle V (diamonds) and Cycle VI (triangles). Red lines inserted to illustrate possible trends within the data.**

A biotite analysis from a depth of 1458.12 m was found to be more Fe-rich. Beside the variations in size, no distinct petrological observations were made between other biotite grains analysed from the same depth. Grains “1”, “2” and “3” were all analysed with grain “1” being the Fe-rich grain in Figure 53 below.

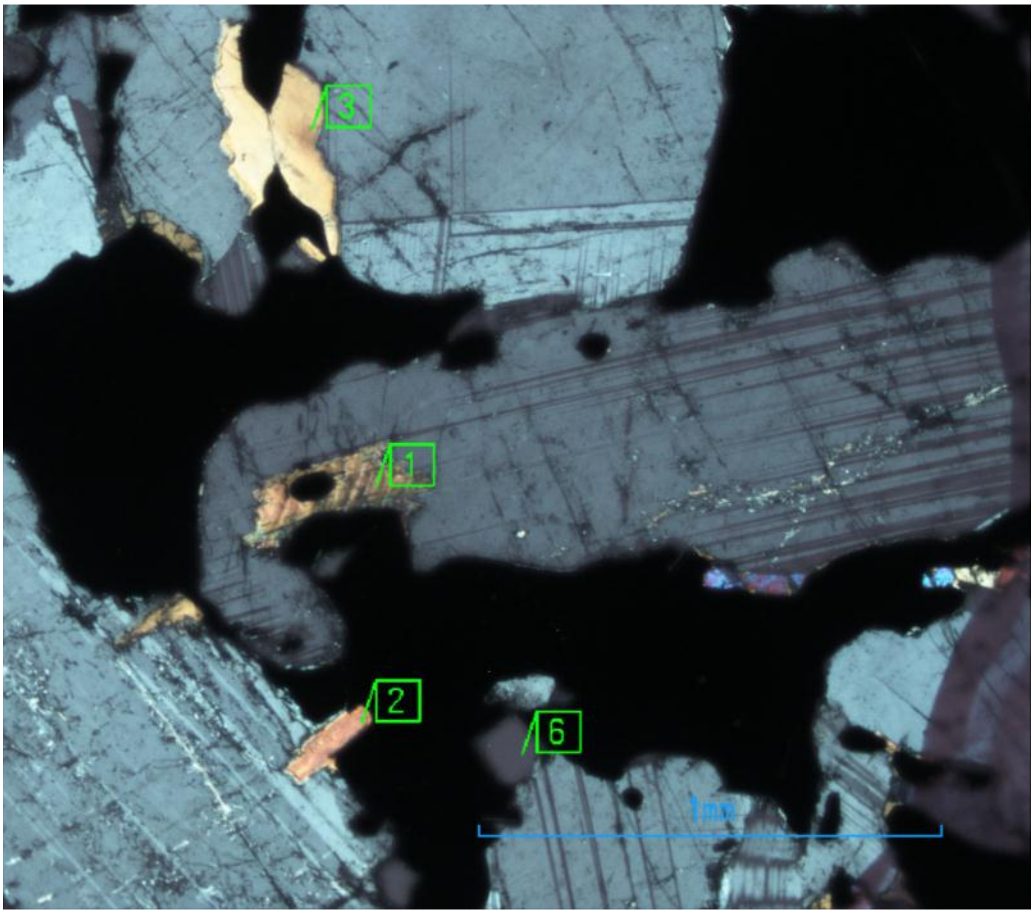

Figure 53. XPL image of the analysed biotite grains (labelled 1, 2 and 3) analysed at 1458.12 m.

A minimum in the Mg# of 34 is reached at a depth of 1133.85 m. The Mg# then shows a jump in the values to ~50 at a depth of 1119.3 m. The values remain high until the top of Cycle V. The nature of the trend of the biotite analyses from the top of Cycle V is arguable as the increase in the Mg# does coincide with a number of magnetitite layers.

The trend observed throughout Cycle VI is different to Cycle V. The values at the bottom of Cycle VI remain between 50 and 55, similar to the top of Cycle V. The Mg# then begins to decrease sharply with a decrease in depth. Between the depths of 1053.67 m and 942.4 m, the Mg# remains ~35. The top of Cycle VI becomes variable with values ranging from 18 through to 41.

Amphibole

Reliable amphibole analyses were collected from Cycle VI where large, isolated grains were identified. The identification of amphibole in Cycle V was limited to small grains of what appeared to be alteration surrounding magnetite and clinopyroxene in some thin sections. Due to the altered or un-equilibrated nature (Figure 32b from Chapter 4) of some of the grains, a number of the analyses were unreliable. No reliable analyses were collected from Cycle V. The anorthosites from Cycle VI yielded the most reliable analyses.

The Mg# of the amphiboles from Cycle VI (Figure 54) shows a general increase in Mg content with a decrease in depth. The lowest Mg# of 3.64 is recorded in an anorthosite at 923.61 m depth. The anorthosite at this depth contained a number of amphiboles with variable amounts of Mg ranging between ~3.5 and ~8. The Mg# of the amphibole in the anorthosite from 914.99 m depth was recorded at 6.65. The highest Mg# of 10.67 was recorded at the top of the cycle in the anorthosite at 904.5m depth.

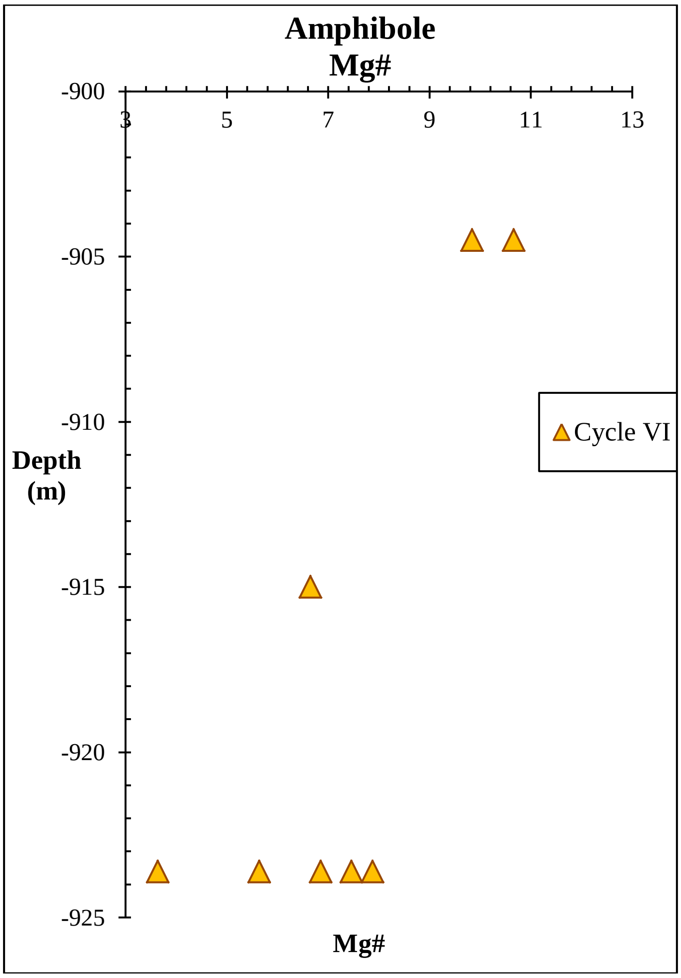

Figure 54. **Scatter plots illustrating the various trends within the geochemistry of the analysed amphiboles.**

Summary

The gabbros from Cycle V and Cycle VI contain various proportions of plagioclase, magnetite, olivine and pyroxene. Apatite and biotite are minor phases with apatite not always present in many of the gabbro samples towards the top of Cycle V and Cycle VI. In Cycle V, amphibole is present in small quantities in a number of samples: both gabbro and anorthosite. Where present, amphibole is commonly found as alteration surrounding grains such as magnetite or clinopyroxene. In Cycle VI, amphibole is present in much larger quantities in the anorthosites towards the top of the cycle.

The variations in the proportions between the two cycles show some similarities. Moving up the cycle towards anorthosite shows increases in the plagioclase content and decrease in the amount of magnetite. Apatite is present in both cycles with the higher amounts found at the base of the cycles. The amounts of apatite are higher in Cycle VI than in Cycle V. Larger proportions of olivine and pyroxene are observed in the gabbros from Cycle VI. Two anorthosite samples from Cycle VI contained large quantities of interstitial amphibole. Cycle V, on the other hand, contains significantly lower proportions of amphibole, which is present as rims around grains (Figure 31a and b from Chapter 4) and veins and thin layers running through the rock (Figure 31c and d from Chapter 4).

The grain sizes of the plagioclase and olivine in Cycle V is generally larger compared to Cycle VI. The grain sizes of pyroxene in Cycle VI are generally larger than Cycle V. The grain sizes of apatite in Cycle V show little variation. The apatite grain sizes, which are limited to the bottom of the cycle, show a steady decrease in the grain size with a decrease in depth.

The general paragenetic sequence of the gabbros varies with depth but a few features remain consistent. Magnetite is always present in two forms: 1. small rounded grains included in plagioclase, olivine and pyroxene, 2. interstitial magnetite that overgrows the majority of the mineralogy. When present, apatite is the first mineral to crystallise, followed by the smaller grains of magnetite and then biotite. The paragenetic sequence between plagioclase, olivine and pyroxene varies from sample to sample as was highlighted throughout Chapter 4.

The two magnetite-rich gabbros, while both containing high proportions of magnetite, were texturally and mineralogically different. The magnetite at the base of Cycle V contained plagioclase, magnetite, olivine, pyroxene, apatite and biotite. The magnetite-rich gabbro at the top of Cycle V contains no orthopyroxene or apatite but did contain symplectite textures between the plagioclase and olivine (Figure 14b from Chapter 4).

The paragenetic sequence of the anorthosites for Cycle V and Cycle VI remains relatively consistent. The single anorthosite from Cycle V contained large grains of plagioclase with interstitial orthopyroxene and minor clinopyroxene and magnetite. Amphibole was found as alteration around clinopyroxene and magnetite (Figure 31 from Chapter 4). Three out of the five anorthosites from Cycle VI were similar to the anorthosite in Cycle V. Two anorthosites from 923.61 m and 914.99 m depth contained large proportions of interstitial amphibole (Figure 32b from Chapter 4). Interstitial silica is found in all of the anorthosites except for the two anorthosites at 925.91 m and 914.99 m depth.

The variations in the An% of Cycle V and Cycle VI show different trends with a decrease in depth. Cycle V shows a gradual decrease in the An% until a minimum is reached at 1199.75 m depth. From 1166.52 m depth the An% begins to increase more rapidly. At 1119.3 m depth, the An% reaches a maximum followed by a decrease in the An% again at 1105.5 m depth. The An% trend observed in Cycle VI is more symmetrical with a decrease in depth. High An% are recorded at the bottom and top of the cycle with the lowest values being recorded in the central portion of Cycle VI. The highest An% are recorded at the top of Cycle VI, similar to that seen in Cycle V.

The trends in the Mg# of the olivine analyses between Cycle V and Cycle VI vary significantly. Cycle V shows similar trends to the An% with a gradual decrease in the Mg# until 1199.75 m depth. Observing the data from Tegner *et al.* (2006), a gap in the sampling between 1199.75 m and 1133.85 m resulted in the inability to analyse potentially lower Mg# in olivine. The Mg# begins to increase rapidly from 1133.85 m depth until 1105.5 m depth where a maximum is reached. This is unlike the An% with a maximum being reached at 1119.3 m depth. Cycle VI shows a significantly different trend in the Mg# compared to the An% trend in Cycle VI. The Mg# decreases more rapidly towards the top of the cycle. Above 942.4 m depth the trend becomes ambiguous as either one of two scenarios could occur with improved sampling densities. The Mg# at 918.69 m depth begins to increase which could produce a trend similar to that seen in the An%. Alternatively, the Mg# at 911.66 m depth continues to decrease without indication of what the trend may result in.

The trends observed in the Mg# from the pyroxene analyses from Cycle V and Cycle VI show a great deal of variation compared to the An% trends and the Mg# trends from the olivines. The Mg# decreases steadily from 1458.12 m until 1166.52 m depth. Above 1166.52 m, the Mg# begins to increase more rapidly compared to the Mg# of the olivines. A maximum is reached at 1105.5 m, the same situation as the An% trend. The Mg# of the pyroxenes from Cycle VI is uncertain due to the large amount of scattered observed at the top of the cycle. Generally, the Mg# shows a decrease from 1090.0 m to 1016.5 m. Above this depth, the Mg# varies significantly. The Mg# between 942.4m and 902.3m depth varies between 41 and 30 with apparent trend. The variable values coincide with the presence of significant proportions of amphibole.

Chapter 6 – Discussion

The Upper Zone is characterised by a number of thick magnetitite and anorthosite layers, and cyclic geochemical variations within the silicate mineralogy. The current study set out to investigate two of the Upper Zone cycles that contain magnetitite layers, anorthosite layers as well as the most pronounced cyclic variations in plagioclase, olivine and pyroxene.

The study involved the detailed investigation of Cycle V and Cycle VI using an increased sampling density. Petrological data and EMPA data was collected from fourteen samples from Cycle V and fifteen samples from Cycle VI. The higher sampling density has revealed a number of newly discovered features, which becomes apparent when the data is compared to that of Tegner *et al*. (2006). Additionally, the current dataset can now be applied to previously published models of the Upper Zone evolution, to see if they still remain valid with new and additional data.

Comparison of Cycle V and Cycle VI to Tegner *et al.* (2006)

In the study by Tegner *et al*. (2006), a relatively detailed study of the Upper Zone mineralogy was carried out. The study led to the identification of nine cycles (I-IX) within the Upper Zone. Twelve samples were collected over Cycle V and Cycle VI, which led to the general outline of the geochemical variations within each of these two cycles. This study has provided not only additional EMPA data but also detailed petrological data.

The results obtained throughout these works can be summarised briefly as follows:

1. The lithologies of the two cycles are similar; however, there are a few notable differences. Both cycles are made up of gabbro and anorthosite but Cycle V contained two magnetite-rich gabbros, whereas Cycle VI contained no magnetite-rich gabbros. Cycle VI included five anorthosites that are found towards the top of the cycle but Cycle V only included one anorthosite. This single anorthosite from Cycle V was identical to three of anorthosites from Cycle VI in terms of the interstitial pyroxene as opposed to interstitial amphibole in the remaining two anorthosites. The remaining two contained little to no pyroxene but did include high proportions of interstitial amphibole. Cycle V contained only small proportions of amphibole that was present in the form of veins and small layers and as alteration rims around silicates and oxides.

2. The previously defined boundary between Cycles V and VI by Tegner *et al*. (2006) needs to be re-considered, as the additional data collected in this study provides better

discrimination. Based on the petrology and the An% data, the boundary is more likely to be situated between 1130 m and 1120m as opposed to ~1180m.

3. Cyclic behaviour in mineral chemistry is present in both cycles. Figure 55 shows the variations in the An% and the Mg# throughout Cycle V and Cycle VI. In Tegner *et al*. (2006), Cycle VI appeared to show identical variations to Cycle V although the An% and Mg# were generally lower in Cycle VI.

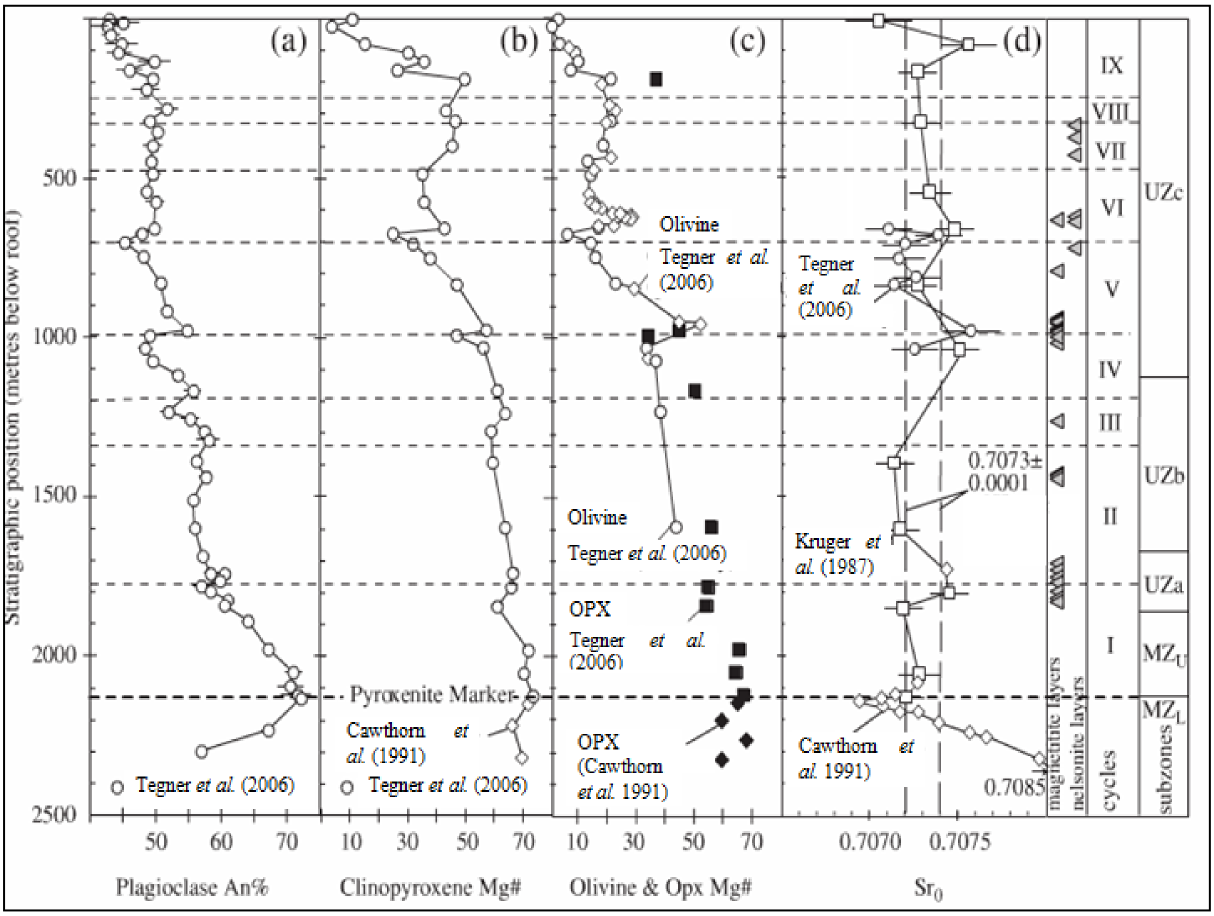

Figure 55. The variations in An% and the Mg# of olivine and pyroxene from Cycle V and Cycle VI from Tegner *et al.* (2006). Initial ^{87}Sr/^{86}Sr data from Kruger *et al.* (1987) showing near-homogenous isotopic ratios.

A comparison of the current data to that of Tegner *et al*. (2006) (Figure 56) shows a number of features. Firstly, Cycle V and Cycle VI are not as similar to one another as previously thought. Secondly, although the data from Tegner *et al*. (2006) shows some similarities compared to the current data, there are a number of notable differences.

a) The peak in the An% and the Mg# is much higher at the boundary between Cycle V and Cycle VI than originally recognised.

b) Using the An% and the presence of the second magnetite-rich gabbro, the boundary between Cycle V and Cycle VI is situated above 1119.3m but below 1105.5m depth.

c) The An% in Cycle VI shows greater variation compared to Tegner *et al*. (2006).

d) Data from Cycle VI from Tegner *et al*. (2006) was limited, therefore the variable Mg# of the olivines (Figure 56) and pyroxenes (Figure 50 from Chapter 5) at the top of Cycle VI were not recognised.

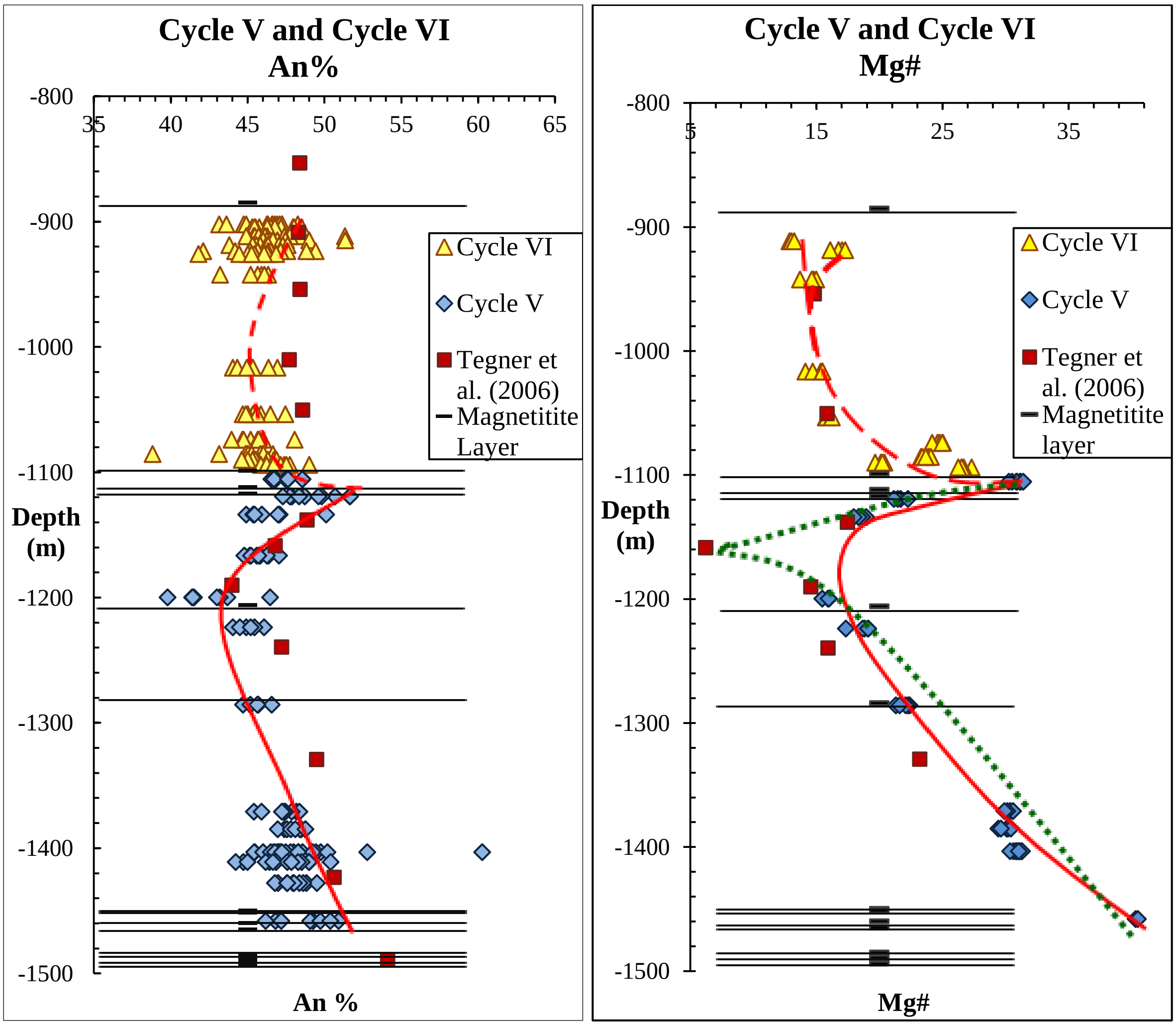

Figure 56. Geochemical trends observed in Cycles V and VI. a. An% from the plagioclase analysis, and b. Mg# from the olivine analysis. Positions of some magnetitite layers from Tegner *et al.* (2006) have been included. Red and green lines inserted to illustrate possible trends within the data.

The fluctuations of An% in plagioclase and Mg# in clinopyroxene with stratigraphic height depth is one of the main criteria for defining Cycle V and Cycle VI within the succession. However, Figure 38 shows the An% plotted against the Mg#, and shows that the inter-relationship of these two parameters is more complex than previously appreciated. Only the Mg# from the pyroxenes has been plotted, as olivine is not found in anorthosite. The triangular symbols represent Cycle V and the circular symbols represent Cycle VI.

In Figure 57a, the An% in the gabbros generally decreases as the Mg# decreases, as might be expected in a fractionally crystallising system. However, there is a clear division between the anorthosites and gabbros, with the anorthosites showing more primitive An% than would be expected from the Mg# of the clinopyroxenes present. Since the anorthosites form part of the gabbroic succession and are unlikely to represent unique new additions of magma, this would imply that either the clinopyroxenes in the anorthosites have lost Mg, or the plagioclases have gained Ca. In either case, the implication is that the anorthosites in Cycle V have been altered during their formation.

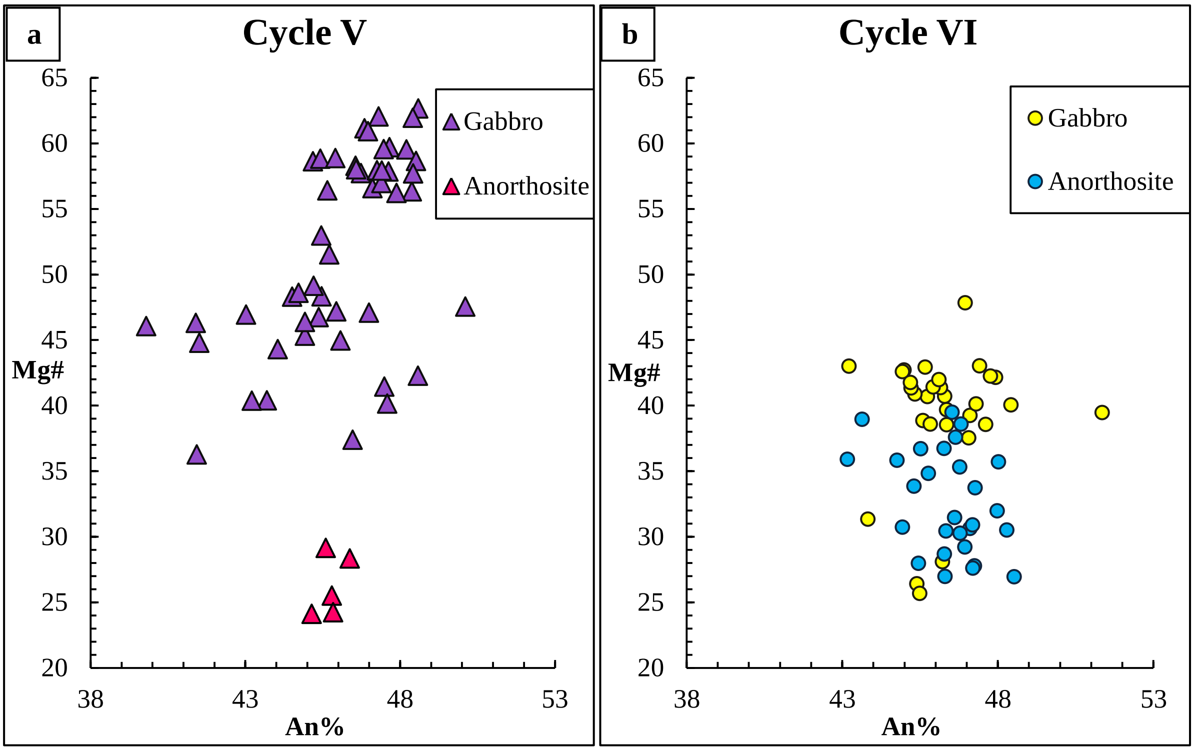

Figure 57. **An% versus Mg# from gabbros and anorthosites for a. Cycle V and b. Cycle VI.**

In Figure 57b, no clear trend is evident. All the rock types appear to have similar An% but variable Mg#. The majority of the gabbros have higher Mg# than the anorthosites except for a small group of gabbros that have particularly low Mg# Although no discernible trend can be identified within each group, one aspect is clear; the conditions operating during the crystallisation of each cycle is different for Cycle V and Cycle VI.

Possible mechanisms for the evolution of Cycles V & Cycle VI

The majority of models proposed for the Upper Zone assume the entire succession to have crystallised from a single batch of magma. Kruger *et al.* (1987) provided isotopic data from the Pyroxenite Marker to the top of the Upper Zone (Figure 55), which revealed homogenous ratios of 0.7073 ± 0.0001. These data were interpreted as strong evidence for the crystallisation of the Upper Zone from a single magma.

A number of studies have proposed models regarding the formation of the Upper Zone magnetitite layers and/or anorthosite layers. Many of these models incorporate the formation of these layers through the crystallisation of the whole Upper Zone magma. Therefore, the formation of the magnetitite and anorthosite layers overlap with the formation of the cyclic mineralogy and geochemistry. Using the data from Cycle V and Cycle VI, the proposed models can be put to the test as any one of these models, if the model is correct, should be able to reproduce the mineralogical, petrological and geochemical results collected in this study. Should none of the models fit perhaps the additional insight may give some evidence as to what mechanisms could have resulted in the formation of Cycle V and Cycle VI and by extension the whole Upper Zone.

a) Crystal fractionation, crystal settling and pressure fluctuations

Fractional crystallisation within the Rustenburg Layered Suite is said to occur up through the succession towards the top of the complex. Observing the An% and the Mg# shown in Figure 2 in Chapter 2, the compositions move from ultramafic to mafic compositions in the Lower Zone to more evolved compositions in the Upper Zone (Eales & Cawthorn, 1996). Wager & Brown (1968) posited that the crystallisation and fractionation of minerals by differential settling could result in the formation of graded modal layers. This theory, applied under extreme circumstances, could lead to the formation of pure anorthosite or magnetitite layers (Cawthorn & Ashwal, 2009).

Cawthorn & Ashwal (2009) discussed the theoretical application of Wager & Brown (1968) to the formation of magnetitite and anorthosite layers. The formation of the anorthosite layers would require fractional crystallisation until plagioclase is the sole crystallising phase. Plagioclase would then accumulate at the top of the modally graded lithology to form the anorthosite layers. The formation of magnetitite layers, according to Cawthorn & Ashwal (2009), would form through crystallisation of a magma saturated in magnetite, pyroxene and plagioclase. Based on the density, magnetite would accumulate first followed by pyroxene and then plagioclase. However, Cawthorn & Ashwal (2009) noted a discrepancy in the Upper Zone lithology as little cumulus pyroxene was observed overlying the magnetitite layers. Although fractional crystallisation does take place to a certain degree within the Upper Zone, is such an extreme would need to be the cause for the formation of these monomineralic layers.

The re-examined model of Cawthorn & Ashwal (2009) suggested the formation of the anorthosite and magnetitite layers by pulsed yet rhythmic crystallisation. Fluctuations in pressure resulted in rhythmic crystallisation that was induced by fluctuations in pressure, and associated crystal settling. Evidence supporting this model was based on the lack of reversals in An% over a number of anorthosite layers. The gradational upper contact of some of the magnetitite layers was also said to represent crystal settling. The An% was found to fluctuate above and below a number of the magnetitite layers and was subsequently interpreted as support for a mechanism controlled by fluctuations in pressure.

The formation of monomineralic layers could also form through fluctuations in pressure. Naslund and McBirney (1996) proposed the crystallisation of a single mineral phase due to changes in pressure. Laterally extensive and continuous layers could form due to a large-scale change in pressure. An increase in pressure would crystallise magnetitite layers and a reduction in pressure could crystallise anorthosite layers.

According to the current data, the geochemical reversals are more exaggerated than previously recorded. Using changes in pressure proposed by Cawthorn & Ashwal (2009), a number of observations would need to be explained. Firstly, the sharper boundary observed between Cycle V and Cycle VI. Due to the steep gradients before and after the boundary, the pressure change would have to be fast-acting and not to mention effective over an extremely large area based on the lateral continuity between the Eastern and Western Limbs (Eales & Cawthorn, 1996).

Observing the mineralogical proportions of Cycle V and Cycle VI, the plagioclase increases moving upwards in a cycle while magnetite decreases. The plagioclase grains also show some form of preferred alignment throughout the majority of the samples. These observations support fractional crystallisation. However, the periodic appearance and disappearance of olivine and cumulus apatite between Cycle V and Cycle VI challenges the validity of pressure being the only controlling variable on the formation of the Upper Zone cycles. The effect of pressure would control the proportions of plagioclase and magnetite crystallising but the disappearance of a mineral phase from Cycle V and reappearance in Cycle VI cannot simply be caused by changes in pressure.

By comparing Cycle V and Cycle VI, it is clear that the conditions affecting Cycle V are not the same as the conditions affecting Cycle VI. The An% for Cycle VI showed a more symmetrical trend whereas Cycle V showed gradual decreases in the An% followed by more rapidly increasing An%. Should the pressure conditions for two initially “identical” cycles be different, what then are the pressure conditions for the whole of the Upper Zone?

An additional point to consider is the cause of the pressure changes. According to Naslund & McBirney (1996) and Cawthorn & Walraven (1998), pressure changes could be brought about by an eruption. Cawthorn & Walraven (1998) noted the absence of a cumulus silica phase towards the top of the Upper Zone lithology. An erupted volume of 40% was calculated to have erupted from the Upper Zone. Although an eruption is plausible, a volume as much as 40% is somewhat excessive considering the overall mafic nature of the Upper Zone magma.

The eruptive mechanism would encompass multiple eruptions due to the presence of several anorthosite layers. Considering the number of layers, the mechanism responsible for triggering each eruption would need to be repetitive. A mechanism capable of inducing an eruption repeatedly would most likely be multiple injections of magma.

b) Double diffusive convection

A double diffusive convection system develops when two or more components have opposing effects on density and different molecular diffusivities. How double diffusive convection forms within a magma remains a field in need of additional research. According to Huppert and Sparks (1984), silicate melts are ideal fluids in which double diffusive convection can take place due to the differences in the diffusivity between heat and the molecular components making up the system.

In Figure 58, the variable “T” represents temperature and is depicted as the solid line whereas “S” represents the chemical components and is represented as the dashed line. The four graphs below illustrate the stable and unstable configurations between these two variables. In Figure 58, four temperature-composition settings are illustrated. Graph 58(a) represents the most stable condition where temperature increases upwards and density increases downwards. Graph 58(b) illustrates an unstable situation where temperature decreases upwards and the density increases upwards. Graph 58(c) and (d) illustrate the two instances where double diffusive convection would most likely develop.

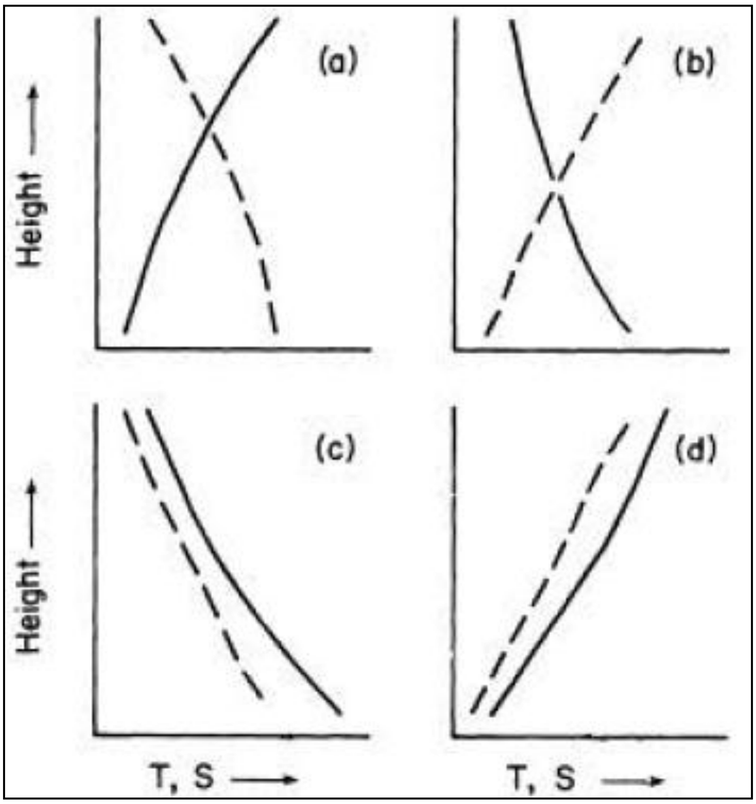

Figure 58. Graphical illustration of the four possible scenarios between two varying components within a magma. Temperature (T) is represented as the solid line. Composition (S) is represented as the dashed line (Huppert and Sparks, 1984).

Tegner *et al.* (2006) proposed a mechanism whereby stratification of the magma and subsequent cyclic mineralogy was achieved through double diffusive convection (DDC). The application of DDC to the formation of layers within an intrusion is discussed in detail by a number of authors but especially in the study by Irvine *et al.* (1983) and more recently by Tegner *et al.* (2006).

To maintain the single magma theory proposed by Kruger *et al.* (1987) and to explain the periodic appearance of olivine and apatite, Tegner *et al.* (2006) proposed the stratification of the Upper Zone magma by crystallisation and mixing between the underlying crystallising layer and the overlying Fe-rich magma. The model proposed included bottom crystallisation of a gabbronoritic rock type that led to the increased densification of the magma due to the increased iron content of the liquid. The higher density of the liquid would result in the magma pooling at the base of the magma chamber above the crystallised material. The difference in the diffusivities between the major elements and the heat within the magma would result in the separation of the magma body into separate double diffusive convection cells.

Once magnetite begins to crystallise the density of the overlying magma becomes increasingly lower. Eventually the density of the residual liquid becomes equivalent to that of the overlying magma layer, which in turn allows the mixing between a more evolved liquid and a less evolved liquid. A reversal in the Mg# as well as the An% would result. A simplified illustration of this setting is provided in Figure 59 below.

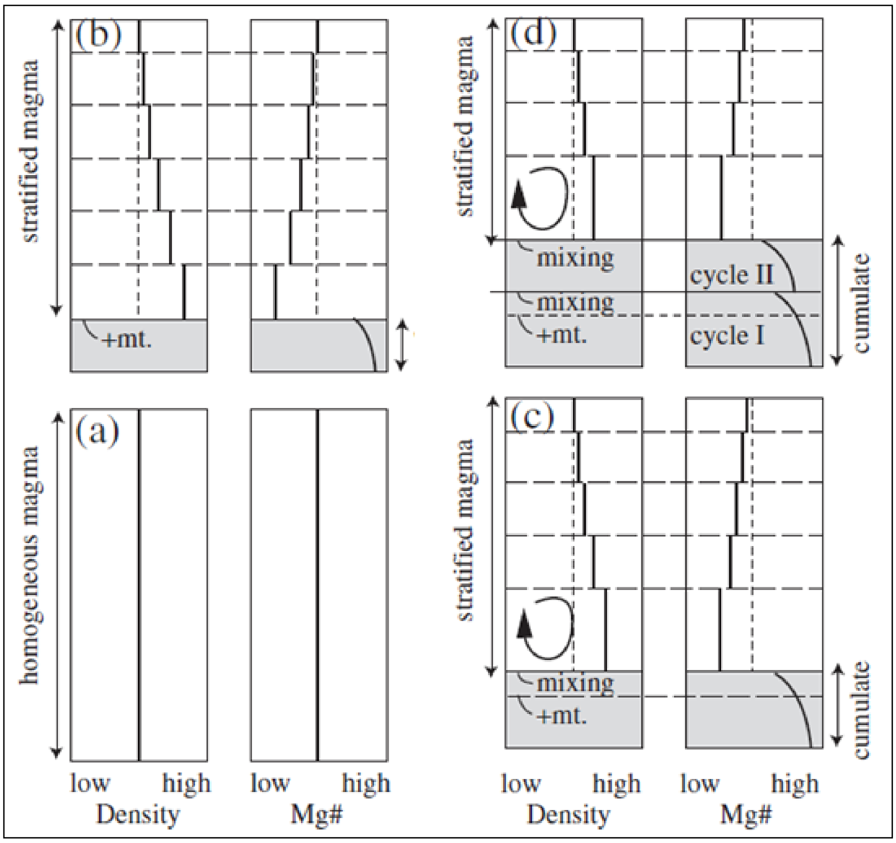

Figure 59. Schematic representation of Tegner's double diffusive convection to the formation of the upper Main Zone and the Upper Zone (Tegner *et al.* (2006).

The conditions resulting in the stratification of the whole Upper Zone magma resulted in the formation of at least nine convection cells or layers. The variables responsible for the formation of these layers are responsible for the separation of significantly iron-rich layers overlying one another including layer 21 that is situated in UZ_c.

According to Tegner *et al.* (2006), only small amounts of diffusion of the major elements would take place between cells. Referring to Figure 56 and Figure 57, the geochemical shifts in the An% and Mg# vary from cycle to cycle which leads to question the conditions affecting diffusion and the amount of diffusion. Although stratification of the magma chamber is achieved through DDC, other processes besides (or in addition to) fractional crystallisation appears to have occurred for Cycle VI.

The model proposed by Tegner *et al.* (2006) acknowledges the disappearance of both olivine and apatite from the cycles in UZ_c. After density-controlled mixing, fractional crystallisation continues until olivine crystallises once again. Although the crystallisation of olivine could easily be explained, the issue of the periodic appearance of apatite remains ambiguous.

In the study by Tegner *et al.* (2006), the periodic crystallisation of apatite is attributed to the mixing of the residual magma with an apatite-undersaturated magma. These particular magma-mixing events were subsequently used in Tegner *et al.* (2006) to place the cycle boundaries. This study has shown that the cycle boundary just between Cycle V and Cycle VI clearly needs to be relocated. In light of this, the theory of *in situ* magma mixing from Tegner *et al.* (2006) becomes questionable.

At this point, it is necessary to re-evaluate the fundamental data supporting the closed nature of the Upper Zone. The initial strontium (Sr/Sr_0) data from Kruger *et al.* (1987) and Tegner *et al.* (2006) are provided in Figure 60 plotted alongside the plagioclase data from this study. The Sr/Sr_0 data is only available for Cycle V as no data for Cycle VI could be found. Regardless, the trends between the two sets of data in Cycle V cannot be ignored.

In Figure 60, the An% and the initial strontium data in Cycle V show somewhat similar trends. The Sr/Sr_0 data shows a steady decrease until ~1200m depth. Above this, the ratios begin to increase until a maximum is reached at 1158.6m depth after which the ratio begins to decrease again. The An% also decreases until ~1200m depth and increases until 1105.5m depth. The turning point between these two may differ but the correlation between the two sets of data indisputable. This data shows two things- firstly, the Sr/Sr_0 ratio for the Upper Zone is NOT homogeneous, and the isotopic ratios show distinct cyclic behaviour in the same manner as the plagioclase chemistry. This in turn brings into question the basic assumption that a single magma created the Upper Zone.

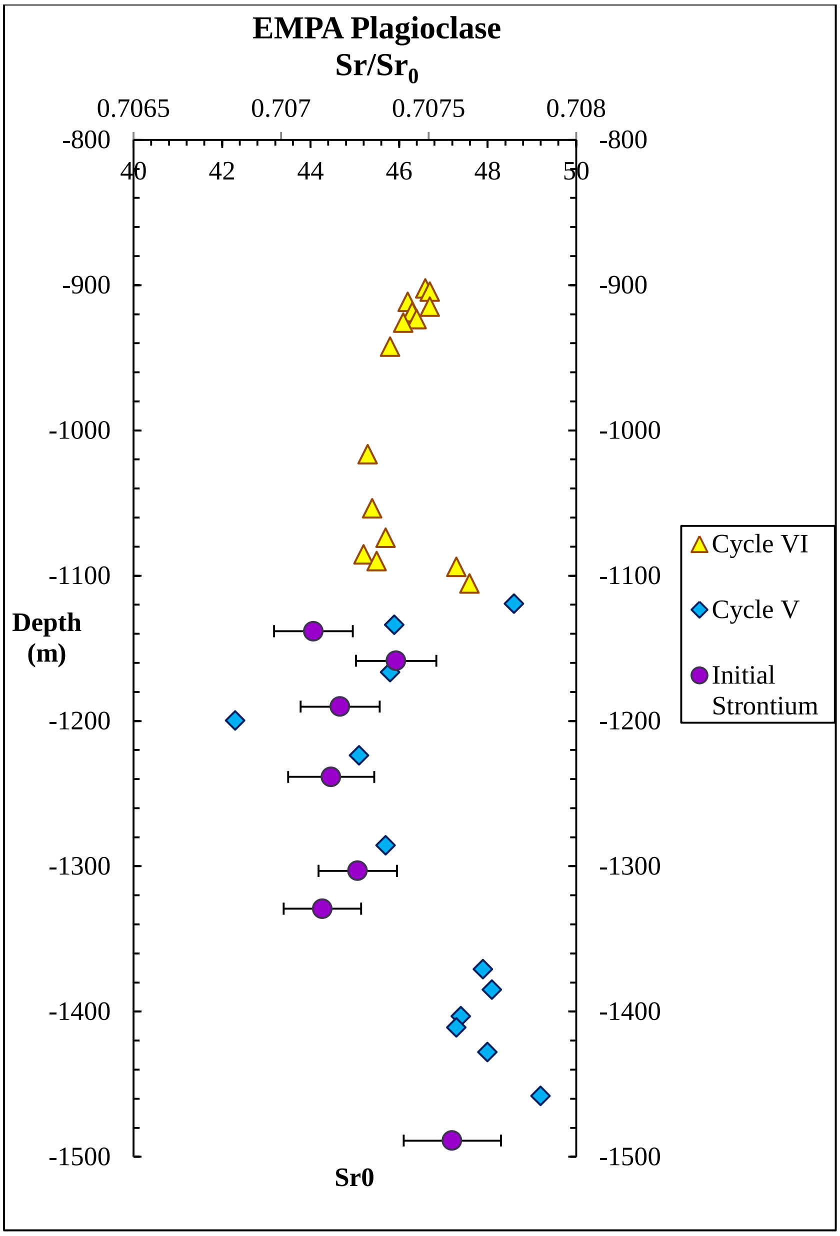

Figure 60. **Similarities in the median of the An% trend and the initial strontium data trend and the initial strontium data from Kruger *et al.* (1987) and Tegner *et al.* (2006).**

c) Multiple injections of magma

Magma mixing is one of the other processes next to fractional crystallisation that is responsible for the change in composition of a magma. Although a number of intrusions, especially layered intrusions, have proven to form from multiple magma recharge events, the Upper Zone is commonly accepted to have crystallised from a single magma (Kruger *et al.*, 1987). Important indicators of magma mixing include changes in isotopic ratios, sharp lithological breaks as well as geochemical breaks.

Although the concept is not favoured, the formation of the Upper Zone by multiple injections of magma has been recently argued. Scoon & Mitchell (2012) provide an alternative interpretation of field observations and previously published data. According to the authors, the formation of macro-layering and the geochemical reversals cannot be formed through closed system fractional crystallisation. Similar interpretations are discussed by Ashwal *et al.* (2005) based on similar results in a study of Bellevue core from the Upper Zone in the Northern Limb.

Kruger *et al.* (1987) acknowledged the possibility of the Upper Zone forming from multiple magma pulses but considered it improbable as the incoming magma would have to have an isotopic ratio similar to that of the mixed magma (the residual Main Zone magma and the incoming Upper Zone magma). Therefore, according to Scoon & Mitchell (2012), the relatively homogenous Sr^{87}/Sr^{86} data was achieved by sourcing the additional magma from a fractionally crystallising felsic tholeiite.

According to Scoon & Mitchell (2012), the magnetitite and anorthosite layers could also be formed through additional injections of magma into the Upper Zone. Mitchell & Manthree (2002) discussed a model whereby a new magma pulse injected into a crystal mush would result in disequilibrium partial melting of cumulates at the boundary between the Critical and the Main Zone. According to Naslund (1986), the first author to describe disequilibrium partial melting, plagioclase would survive as a refractory material while the mafic phases would undergo partial melting. Scoon and Mitchell (2012) suggested a two-stage process. Firstly, the crystallisation of plagioclase within the resident melt was followed by the additional enrichment through the removal of pyroxene from anorthosite-rich layers by means of disequilibrium partial melting. Scoon and Mitchell (2012) proposed that magnetitite layers could also form through multiple magma pulses, a theory based on the study by Zhang *et al.* (2012) on the Baima layered intrusion in SW China.

The study by Mitchell & Manthree (2002) presented the data in Figure 61 as evidence for disequilibrium partial melting. The data collected in this study, as discussed in Chapter 5, shows noticeably different trends. By comparing Critical and Main Zone data to the current Upper Zone data, it is evident that the Upper Zone anorthosites were unlikely to have formed by disequilibrium partial melting. In addition to this, no textural evidence was found in the anorthosite samples that would suggest the rocks had been subjected to any sorts of heat-induced disequilibrium.

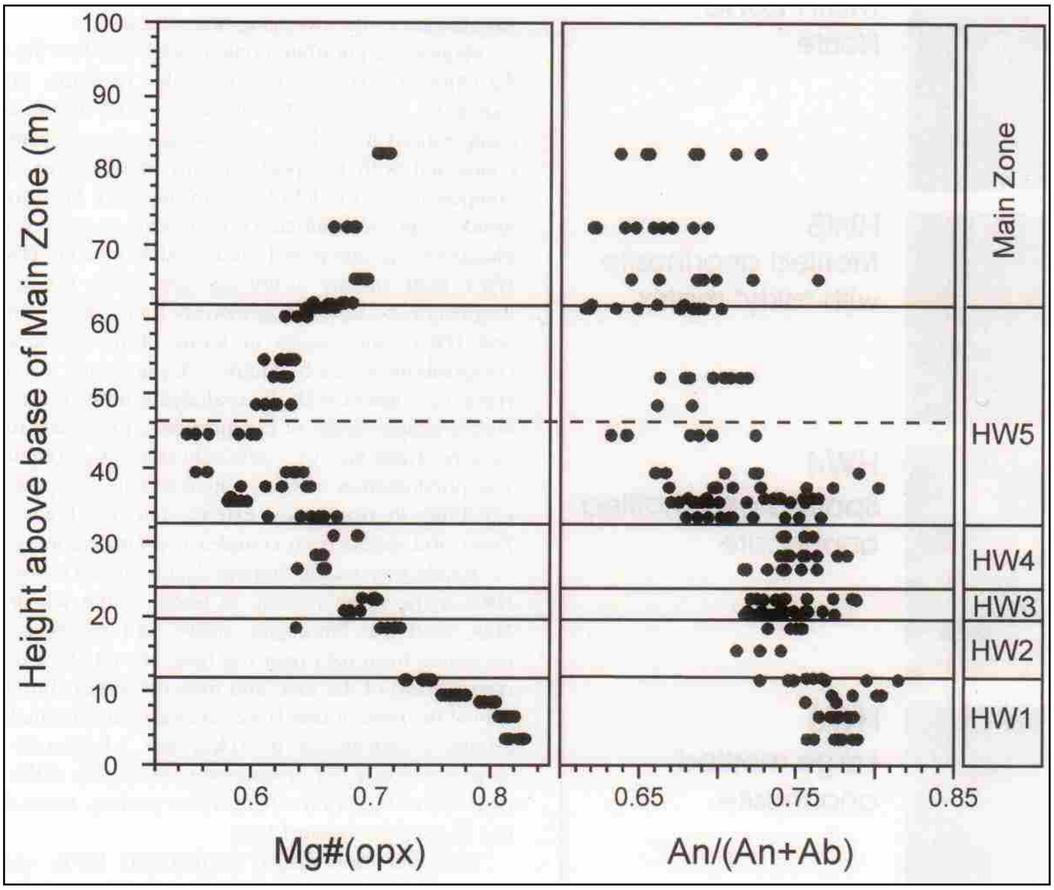

Figure 61. **EMPA data from a study of the Critical Zone by Mitchell & Manthree (2002) showing the variations in the Mg# of the orthopyroxene and the variations in the An% of the plagioclase from the Bastard Unit overlying the Main Zone.**

The formation of magnetitite layers through the extensive silicate mineral fractionation of a magma chamber at depth, and closed to oxygen, could produce a highly enriched Fe-Ti melt. The migration of the melt to shallower depths would result in magnetite crystallising as an early liquidus phase and based on the extent of the Fe-Ti enrichment could lead to thick successions of magnetite i.e. magnetitite layers (Zhang *et al.*, 2012). Reversals in the An% were interpreted as magma recharge events which were caused by the incoming Fe-Ti rich melt. Figure 62 is a figure from Zhang *et al.* (2012) that has been enhanced for clarity.

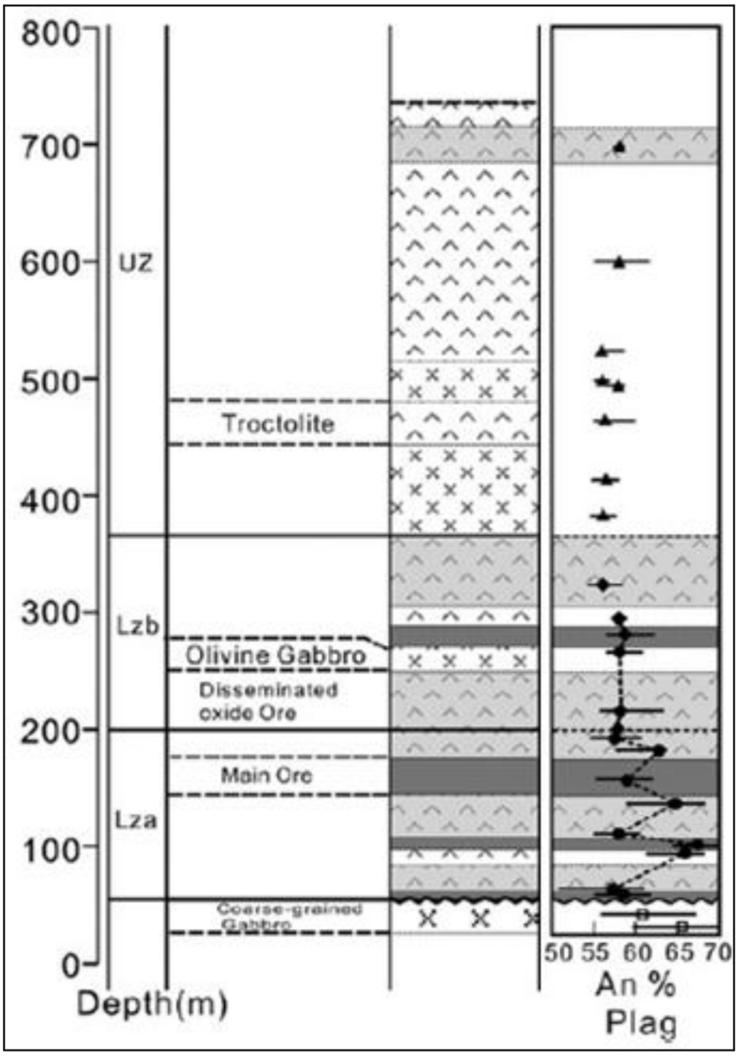

Figure 62. **Edited figure from Zhang *et al.* (2012) showing the lithology and geochemistry of the Baima layered intrusion in SW China.**

Comparing the current data to that of Zhang *et al*. (2012), the An% from Cycle V shows similar reversals. The boundary between Cycle V and Cycle VI, the An% reaches as maximum which coincides with a package of magnetitite layers. The data presented by Zhang *et al*. (2012) appears to show some similarity to the current data but additional research would be required to confirm the validity of these interpretations.

Vantongeren and Mathez (2013) discussed the formation of the Pyroxenite Marker by multiple injections of magma. Each successive pulse was introduced at a slow enough rate to allow for homogenisation between the residual melt and the incoming magma. A sufficient amount of cooling and crystallisation took place prior to the next injection of magma. The data from this study is provided in Figure 63.

The trend of the data is of particular interest to the current Upper Zone data. Highlighted in the red block is the geochemical data from just below the Pyroxenite Marker. Here the trends for Mg# from the pyroxenes has been plotted in addition to the An% from the plagioclase analyses. These trends show some form of resemblance to the current An% and Mg# data from Cycle V.

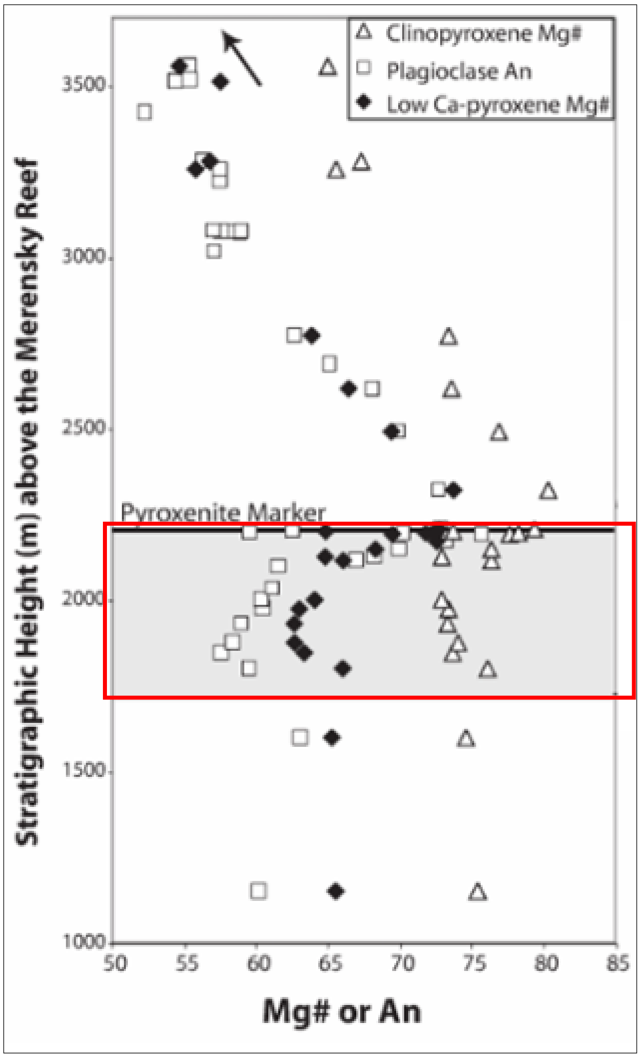

Figure 63. Data from Vantongeren and Mathez (2013) illustrating the trends observed within the An% and Mg# throughout the upper Main Zone and Upper Zone. Red block inset illustrating the observable similarities between the current dataset and data from Vantongeren and Mathez (2013).

The consecutive pulses of hotter and more mafic magma would allow the crystallisation of magnetite and olivine once again as well as reintroduce apatite to the liquidus once again. The data presented in this study bears some resemblance to the data from Vantongeren and Mathez (2013) regarding the sharp contacts between anorthosite and magnetitite layers and the geochemical breaks in the modal mineralogy (Figure 56).

Implications for the rest of the Upper Zone

The Upper Zone represents the most evolved state of magma compositions for the Rustenburg Layered Suite. Previously, the magma from which the Upper Zone crystallised was believed to be the last stage of magma recharge of the layered intrusion. The data presented for Cycle V and Cycle VI has shown that the conditions responsible for their evolution are not as simple as previously throughout.

Cycle V shows a fractional crystallisation trend followed by a sudden increase in the An% either attributed to small scale diffusion from the overlying, less evolved magma layer (Tegner *et al.*, 2006) or from an injection of a less evolved magma (Scoon & Mitchell, 2012). In contrast, Cycle VI shows different results. The An% shows a symmetrical trend with a decrease in the An% followed by an increase in the An%. The trends observed within the Mg# from the olivine pyroxene analysis are inconclusive. The Mg# from the pyroxene analysis shows a great deal of variation with no discernible trend visible. As mentioned previous chapters, the variable analysis of pyroxene does coincide with the appearance of large proportions of amphibole. Considering the hydrous nature of amphibole, a considerable percentage of fluid is present within Cycle VI.

The results presented in this study have provided a great deal of insight regarding two of the cycles from the Upper Zone. Despite studies providing strong evidence for the Upper Zone crystallising from a single pulse of magma, the unusually cyclic repetition of the modal mineralogy has posed complex set of circumstances that could possibly be explained by multiple injections of magma. Based on the dissimilarities between Cycle V and Cycle VI, if the Upper Zone did crystallise from a single magma, the model responsible for the evolution of the Upper Zone is still unknown. The assumption that a single model is responsible for the formation of each cycle is unrealistic. A more likely situation would involve a combination of particular features from each model that could result in the formation of the Upper Zone.

The small-scale study of the Upper Zone cycles revealed detailed information regarding the evolution of the Upper Zone and has shown that the model responsible for the formation of the Upper Zone has not been resolved. Further similar work on the remaining cycles of the Upper Zone needs to be done in order to determine whether the changes observed between Cycles V and VI are replicated elsewhere, and whether there is a progressive change in the nature of the cycles through the sequence in the UZ. An additional point to consider, although initially considered improbable, is the possibility of the Upper

Zone forming from multiple additions of magma. Should this theory hold some truth, the implications of on the theories regarding the Upper Zone eruption need to be reassessed?

Chapter 7 – Summary and Conclusions

The purpose of this study set to evaluate the mineralogical and geochemical changes that took place throughout Cycle V and VI of the Upper Zone. The collected petrological data and electron microprobe data has been presented and discussed. The relevance of these results has been presented through the comparison with existing models. Examination and the comparison of the collected data have provided new insights into the nature of two cycles within the Upper Zone.

The Upper Zone, popularly accepted as having crystallised from a single pulse of magma, consists of gabbronorite, gabbro and ferrodiorite. Throughout the stratigraphy, a number of anorthosite and magnetitite layers are present. Data presented by Tegner, *et al.* (2006) showed the mineralogy of the Upper Zone to be cyclic. Nine cycles were identified by electron microprobe analysis of samples taken from the upper Main Zone all through the Upper Zone. Although a model involving double diffusive convection was proposed for the formation of the Upper Zone, this model leaves many questions unanswered.

The cyclic nature of the Upper Zone has led to a complex set of questions regarding the evolution of the Upper Zone. The large sampling density of two particularly distinct cycles forms the basis of this study. Thirty samples were collected over the six hundred metres represented by Cycles V and VI, from a borehole through the $UZ_{c,}$ the BK1 borehole. Examination of the samples included petrography, which included modal mineralogy identification, modal mineralogy proportions and grain size variations within each modal mineral phase. The modal mineralogy was analysed using EMPA. The data collected from these samples could help in uncovering the controlling factors behind the mineralogical and geochemical cyclicity of the Upper Zone.

The lithology of Cycles V and Cycle VI include magnetite-rich gabbro, gabbro, plagioclase-rich gabbro and anorthosite. The modal mineralogy included plagioclase, olivine, pyroxene and magnetite. Other minerals included cumulus apatite, biotite amphibole and minor proportions of silica. The proportions were calculated and the grain sizes were measured for each of the mineral phases. Using electron microprobe analysis, the geochemistry for plagioclase, olivine, pyroxene, apatite, biotite and amphibole were collected. The minerals important for this study are plagioclase, olivine, pyroxene and apatite.

The proportions of each mineral phase, whether primary of secondary, were calculated using spectral identification Adobe Photoshop. The largest proportions consisted of plagioclase, which was predominantly present as larger, tabular shaped grains. Smaller, rounded grains were identified in between grain boundaries of larger plagioclase grains. The gabbro samples consisted of varying proportions of magnetite, olivine and sometimes pyroxene and apatite. Pyroxene and plagioclase dominated the anorthosite samples.

The electron microprobe analysis was conducted on plagioclase, olivine, pyroxene, apatite, biotite and amphibole. The minerals of particular interest were plagioclase, olivine, pyroxene and apatite. The An% from the plagioclase and the Mg# number from the olivine and pyroxene provided the most beneficial insight into the trends of Cycles V and VI geochemistry.

The trends in the An% between Cycles V and VI are similar. Both cycles show increases in An% at the bottom at top of the cycles and lower An% values in the middle of the cycles. Cycle V exhibits an obvious decrease in the An% whereas Cycle VI is not as pronounced perhaps due to a sampling gap. The included data from Tegner *et al.* (2006) displayed similar trends although limited sampling resulted in the oversight of a much higher shift in the An% between Cycles V and VI.

The trends in the Mg# of olivines and pyroxenes between Cycle V and Cycle VI exhibit a greater amount of variation. The Mg# of olivine and pyroxene show similar trends of high Mg# at the base of the cycle and reach a minimum just before the top of the cycle. The steadily declining Mg# shows a rapid increase in Mg# towards the boundary between Cycles V and VI.

The Mg# of olivine and pyroxene from Cycle VI is notable different to Cycle V. After the spike in the Mg# of Cycle V, the values begin to decrease once again and far more rapidly compared to the base of Cycle V. The olivine Mg# showed much less variation compared to the Mg# from the pyroxene analyses.

The models regarding the formation of magnetitite or anorthosite layers or the cyclic mineralogy of the Upper Zone were discussed and assessed based on the current dataset. The validity of a number of models is questionable while others are promising, but additional research is required.

The study by Kruger, *et al.* (1987) provided strong evidence for the crystallisation of the Upper Zone from a single magma injected at the Pyroxenite Marker. The residual magma from the crystallising Main Zone homogenised with the newly injected magma from which the Upper Zone crystallised. Although this model is most commonly accepted, new studies have argued that multiple injection of a isotopically homogenous magma formed the Upper Zone. However, the majority of the models attempt to explain the formation of the Upper Zone through the crystallisation of a single pulse of magma.

Cawthorn & Ashwal (2009) discussed mechanisms resulting in the formation of anorthosite and magnetitite layers. Changes in pressure were accompanied pulsed crystallisation followed by crystal settling. The model would require repetitive changes in pressure in order to form the number of layers present. Despite the possibilities of the model proposed by Cawthorn & Ashwal (2009), the periodic disappearance of olivine and apatite from the liquidus rules this model as unlikely especially if pressure changes are considered in isolation.

Tegner *et al.* (2006) realised this discrepancy and subsequently proposed that the evolution of the Upper Zone involved stratification of the magma closely followed by crystallisation of an iron-rich magma. Crystallisation and density controlled mixing subsequently resulted in the resetting of the fractional crystallisation sequence in each successive layer. According to Tegner *et al*. (2006), stratification of the magma explained the periodic appearance of phases such as olivine and apatite.

Although stratification could be achieved through double diffusive convection, the effectiveness of density in DDC is questionable especially when considering crystallisation of extremely thick and iron-rich layers much higher in the Upper Zone stratigraphy. A layer of magma with enough iron to crystallise the 7m thick magnetitite layer, aka Layer 21,

The assessment of two popular models involving the evolution of the Upper Zone in a system closed to additional pulses of magma has provided some possible explanation to what is observed through the Upper Zone. However, the data collected has resulted in more questions regarding these models rather than affirmation.

The study by Scoon & Mitchell (2012) reassessed the formation of the Upper Zone and concluded that the Upper Zone more likely formed from multiple magma pulses. The anorthosite layers were attributed to disequilibrium partial melting (Mitchell & Manthree,

2002) and the magnetitite layers to crystallisation of a Fe-Ti rich magma due to a reduction in pressure through the migration of the melt to shallower depths (Zhang *et al.*, 2012). The cyclic trends observed in the An% and the Mg# throughout the Upper Zone are easily explained by the addition of slightly more primitive magmas from a fractional crystallising staging chamber.

The formation of the anorthosite layers by disequilibrium partial melting was ruled out due to the lack of textural evidence and the dissimilarities between the data provided in Mitchell & Manthree (2002) and the current dataset. The application of Zhang *et al.* (2012) remains possible and the newly discovered trends in the An% and Mg# may support multiple magma injections.

A model discussed by Vantongeren and Mathez (2013) involved the formation the Pyroxenite Marker. However, such a model could be proposed for the formation of the Upper Zone. Such a model could easily explain the sharp increase in both the An% and Mg# between Cycles V and VI. The appearance and disappearance of apatite could also be explained using this model in addition to creating a homogenous isotopic ratio throughout the Upper Zone.

Vantongeren and Mathez (2013) proposed the addition of multiple pulses of magma that were injected at specific intervals and at slow enough rates. Addition of magma in such a manner would allow for the homogenisation of the magma, after which cooling would then take place. The formation of a crystal mush before the next injection of magma would allow for a sufficient volume of melt to remain and then mix with the next injection of melt. The result would be an isotopically homogenous lithology.

The evolution of the Upper Zone by multiple injections of magma appears to be a model worth revisiting. Although the near homogenous isotopic data has served as the strongest support for a system closed to multiple injections of magma, the near-identical fluctuations between the initial strontium data and the An% cannot be ignored.

In conclusion, the data collected throughout this study has provided important insight into two of the cycles from the Upper Zone. The data collected included petrological data in the form of minerals present, modal proportions and variations in grain sizes. Additional electron microprobe data was also collected for the modal mineralogy. The applicability of previously existing models was examined. Based on the additional data, support for a model encompassing multiple additions of magma is favoured. However, the application of such a model to the entire Upper Zone is yet to be explored.

Future research

In light of the data presented in this project, the genesis of the Upper Zone is just one avenue where research will continue. Additionally, a number of interesting features are mentioned but unfortunately, did not fall within the scope of the project. In future, studies of the remaining Upper Zone cycles will take place; secondly, documenting the state of the silica polymorph throughout the Upper Zone using RAMAN analysis; and lastly, recording of the distribution and mineral associated minerals of the symplectites and implication these features hold for the Upper Zone.

The increased sampling density simply between two cycles revealed detail behind the cyclic nature of the Upper Zone. If a thorough understanding of the Upper Zone mineralogy and cyclicity is to be achieved, more of the cycles will need to be studied. The cycles both above and below Cycle V and Cycle VI, have the potential to answer some of the questions brought up throughout this study.

Future research will include larger sampling densities throughout Cycles I-IV and from Cycles VII-IX. Petrography and microprobe analysis will form part of the database; however, incorporation of Selfrag analysis will allow for the improved accuracy of both mineral proportions estimations and grain size distributions. Petrography will include detailed studies of the microstructures throughout the Upper Zone.

The ambiguous nature of the silica component in the anorthosites remains an unanswered. The use of RAMAN analysis will provide crystallographic information regarding the two silica polymorphs. Perhaps the state of the silica could provide insight into the pressure fluctuations throughout the crystallisation of the Upper Zone.

Notable observations of symplectites in one magnetite-rich gabbro represent an interesting problem. Firstly, additional studies will include investigations into what formed the symplectites and why this magnetite-rich sample differs from the remaining samples. Secondly, do these symplectites occur elsewhere in the Upper Zone, and if so, why?

References

Ashwal, L.D., Webb, S.J., Knoper, M.W. 2005. Magmatic stratigraphy in the Bushveld Northern Lobe: continuous geophysical and mineralogical data from the 2950 m Bellevue drill core. South African Journal of Geology 108, 199-232.

Bédard, J., Marsh, B., Hersum, T., Naslund, H., Mukasa, S. 2007. Large-scale Mechanical Redistribution of Orthopyroxene and Plagioclase in the Basement Sill, Ferrar Dolerites, McMurdo Dry Valleys, Antarctica: Petrological, Mineral-chemical and Field Evidence for Channelized Movement of Crystals and Melt. Journal of Petrology, 48, 2289–2326.

Buchanan, P.C., Reimold, W.U. 1998. Studies of the Rooiberg Group, Bushveld Complex, South Africa: no evidence for an impact origin. Earth and Planetary Science Letters 155, 149–165.

Buick, I., Maas, R., Gibson, R. 2001. Precise U-Pb titanite age constraints on the emplacement of the Bushveld Complex, South Africa. Journal of the Geological Society 158, 36.

Cameron, E. 1980. Evolution of the Lower Critical Zone, central sector, eastern Bushveld Complex, and its chromite deposits. Economic Geology 75, 845-871.

Cawthorn, R. G. & Ashwal, L. 2009. Origin of Anorthosite and Magnetitite Layers in the Bushveld Complex, Constrained by Major Element Compositions of Plagioclase. Journal of Petrology 50, 1607-1637.

Cawthorn, R. G. & McCarthy, T. S. 1980. Variations in Cr content of magnetite from the Upper Zone of the Bushveld Complex—evidence for heterogeneity and convection currents in magma chambers. Earth and Planetary Science Letters 46, 335-343.

Cawthorn, R. G. & Walraven, F. 1998. Emplacement and Crystallization Time for the Bushveld Complex. Journal of Petrology 39, 1669-1687.

Cawthorn, R. G. & Webb, S. 2001. Connectivity between the western and s of the Bushveld Complex. Tectonophysics 330, 195-209.

Cawthorn, R. G. 1999*a*. Platinum-group element mineralization of the Bushveld Complex, a critical reassessment of geochemical models. South African Journal of Geology 102, 268-281.

Cawthorn, R. G. 1999*b*. The platinum and palladium resources of the Bushveld Complex. South African Journal of Science 95, 481-489.

Cawthorn, R. G., Meyer, P. S., & Kruger, F. J. 1991. Major addition of magma at the Pyroxenite Marker in the western Bushveld Complex, South Africa. Journal of Petrology 32, 739-763.

Cawthorn, R., Walraven, F. 1998. Emplacement and Crystallization Time for the Bushveld Complex. Journal of Petrology 39, 1669-1687.

Cawthorn, R.G., Walsh, K.L. 1988. The use of phosphorus contents in yielding estimates of the proportion of trapped liquid in cumulates of the Upper Zone of the Bushveld Complex. Mineralogical Magazine 52, 81–89.

Crisp, J. A. 1984. Rates of magma emplacement and volcanic output. Journal of Volcanology and Geothermal Research, 20, 177-211.

Eales, H. V. & Cawthorn, R. G. 1996. The Bushveld Complex. Developments in Petrology, 15, 181-229.

Eales, H. V., Klerk, D. W., Butcher, A. R. & Kruger, F. J. 1990. The cyclic unit beneath the UG1 chromitite (UG1FW unit) at RPM union section platinum mine—Rosetta stone of the Bushveld upper critical zone. Mineralogical Magazine, 54, 23-43.

Gain, S. B. & Mostert, A. B. 1982. The geological setting of the planetoid and base metal sulphide mineralisation in the Platreef of the Bushveld Complex in Drenthe, north of Potgietersrus. Economic Geology, 77, 1395-1404.

Harney, D., Gruenewaldt, G., Merkle, R. 1996. The use of plagioclase composition as an indicator of magmatic processes in the Upper Zone of the Bushveld Complex. Mineralogy and Petrology 56, 91-103.

Harney, D., Merkle, R. & Gruenewaldt, G. 1990. Platinum-Group Element Behaviour in the Lower Part of the Upper Zone, Eastern Bushveld Complex-Implications for the Formation of the Main Magnetitite Layer. Economic Geology, 85, 1777-1789.

Hatton, C. J., Schweitzer, J. K. 1995. Evidence for synchronous extrusive and intrusive Bushveld magmatism. Journal of African Earth Sciences 21, 579-594.

Hatton, C. J., Schweitzer, J. K. 1995. Mantle plume origin for the Bushveld and . Ventersdorp magmatic provinces. Journal of African Earth Sciences 21, 571-577.

Irvine, T. N. 1977*a*. Origin of chromitite layers in the Muskox intrusion and other layered intrusions: a new interpretation. Geology 5, 273-277.

Irvine, T. N., Keith, D. W., Todd, S. G. 1983. The J-M Platinum-Palladium Reef of the Stillwater Complex, Montana: II. Origin by Double Diffusive Convective Magma Mixing and Implications for the Bushveld Complex. Economic Geology, 78, 1287-1334.

Kinnaird, J., Hutchinson, D., Schurmann, L., Nex, P., Lange, R. 2005. Petrology and mineralisation of the southern Platreef: northern limb of the Bushveld Complex, South Africa. Mineralium Deposita 40, 576–597.

Klemm, D., Henckel, J., Dehm, R., Gruenewaldt, G. 1985. The geochemistry of titanomagnetite in magnetite layers and their host rocks of the eastern Bushveld Complex. Economic Geology 80, 1075-1088.

Kruger, F. J., Cawthorn, R. G., Walsh, K. L. 1987. Strontium isotopic evidence against magma addition in the Upper Zone of the Bushveld Complex.Earth and Planetary Science Letters, 84(1), 51-58.

Lenhardt, N., Eriksson, P. 2012. Volcanism of the Palaeoproterozoic Bushveld Large Igneous Province: The Rooiberg Group, Kaapvaal Craton, South Africa. Precambrian Research 214-215, 82-94.

Maaloe, S. 1978. The origin of rhythmic layering. Mineralogical Magazine, 42, 337-345.

McCarthy, T., Cawthorn, R., Wright, C., McIver, J. 1985. Mineral layering in the Bushveld Complex; implications of Cr abundances in magnetite from closely spaced magnetitite and intervening silicate-rich layers. Economic Geology 80, 1062-1074.

Merkle, R. K., & von Gruenewaldt, G. 1986. Compositional variation of Co-rich pentlandite; relation to the evolution of the upper zone of the western Bushveld Complex, South Africa. The Canadian Mineralogist, 24(3), 529-546.

Mitchell, A.A., Manthree, R. 2002. The Giant Mottled Anorthosite: a transitional sequence at the top of the Upper Critical Zone of the Bushveld Complex. South African Journal of Geology 105, 15-24.

Molyneux, T. G. 1974. A geological investigation of the Bushveld Complex in Sekhukhuneland and part of the Steelpoort valley. Transactions of the Geological Society of South Africa 77, 329-338.

Mondal, S. & Mathez, E., 2006. Origin of the UG2 chromitite layer, Bushveld Complex. Journal of Petrology 48, 495–510.

Morse, S. A. 1979*a*. Kiglapait geochemistry I: Systematics, sampling and density (Abstract). Journal of Petrology, 20, 555-590.

Morse, S. A. 1979*b*. Kiglapait geochemistry II: Petrography (Abstract). Journal of Petrology, 20, 591-624.

Naldrett, A. J., Wilson, A. H., Kinnaird, J. & Chunnett, G. 2009. PGE tenor and metal ratios across, within, and below the Merensky Reef, Bushveld Complex: implications for its genesis. Journal of Petrology 50, 625-659.

Naslund, H. R. & McBirney, A. R. 1996. Mechanisms of formation of igneous layering. In: Cawthorn, R. G. (ed.) Layered Intrusions. Amsterdam: Elsevier, 1-44.

Naslund, H.R. 1986. Disequilibrium partial melting and rheomorphic layer formation in the contact zone of the Basistoppen sill, East Greenland. Contributions to Mineralogy and Petrology 93, 359-367.

Nex, P.A., Kinnaird, J.A., Ingle, L.J., Van, B.A. 1998. A new stratigraphy for the Main Zone of the Bushveld Complex, in the Rustenburg area. South African Journal of Geology, 101, 215-223.

Reynolds, I. 1985*a*. Contrasted mineralogy and textural relationships in the uppermost titaniferous magnetite layers of the Bushveld Complex in the Bierkraal area north of Rustenburg. Economic Geology 80, 1027-1048.

Reynolds, I. 1985*b*. The nature and origin of titaniferous magnetite-rich layers in the Upper Zone of the Bushveld Complex: a review and synthesis. Economic Geology 80, 1089-1108.

Rhodes, R.C. 1975. New evidence for impact origin of the Bushveld Complex, South Africa. Geology 3, 549-554.

SACS -- South African Committee for Stratigraphy. 1980. Stratigraphy of South Africa. Part 1 (Comp. L.E. Kent). Lithostratigraphy of the Republic of South Africa, South West Africa/Namibia and the Republics of Bophuthatswana, Transkei and Venda. Handbook Geological Survey South 580 Africa 8, 690.

Scoon, R.N., & Mitchell, A.A., 2012. The Upper Zone of the Bushveld Complex at Roossenekal, South Africa: Geochemical Stratigraphy and Evidence of multiple episodes of magma replenishment. South African Journal of Geology 115, 515-534.

Tegner, C., Cawthorn, R., Kruger, F., 2006. Cyclicity in the Main and Upper Zones of the Bushveld Complex, South Africa: Crystallization from a Zoned Magma Sheet. Journal of Petrology 47, 2257-2279.

Vantongeren, J. A., Mathez, E. A., & Kelemen, P.B. 2010. A felsic end to Bushveld differentiation. Journal of Petrology 51(9), 1891-1912.

Vantongeren, J. A., Mathez, E. A. 2013. Incoming Magma Composition and Style of Recharge below the Pyroxenite Marker, Eastern Bushveld Complex, South Africa. Journal of Petrology 54, 1585-1605.

Von Gruenewaldt, G. 1973. The Main and Upper zones of the Bushveld Complex in the Roossenekal area, Eastern Transvaal Transactions of the Geological Society of South Africa 76, 207-227.

Von Gruenewaldt, G. 1970. On the phase change orthopyroxene-pigeonite and the resulting textures in the Main and Upper Zones of the Bushveld Complex in the Eastern Transvaal. In: Visser, D.J.L. & von Gruenewaldt, G. (eds) Symposium on the Bushveld Igneous Complex and other layered intrusions. Johannesburg: Geological Society of South Africa, 67-73.

Von Gruenewaldt, G. 1993. Ilmenite-apatite enrichments in the Upper Zone of the Bushveld Complex: A major titanium-rock phosphate resource. International Geology Review 35, 987-1000.

Wager, L. R. & & Brown, G. M. 1968. Layered Igneous Rocks. Oliver and Boyd, Edinburgh.

Walraven, F., & Wolmarans, L. G. 1979. Stratigraphy of the upper part of the Rustenburg Layered Suite, Bushveld Complex, in western Transvaal. Annals of the Geological Survey of South Africa 13, 109-114.

Webb, S., Ashwal, L., Cawthorn, R. 2010. Continuity between eastern and western Bushveld Complex, South Africa, confirmed by xenoliths from kimberlite. Contributions to Mineralogy and Petrology 162, 101-107.

Webb. S. J., Nguuri. T., Cawthorn. R. G., James, D. 2004. Gravity modelling of Bushveld Complex connectivity supported by southern African seismic experiment results. South African Journal of Geology 107, 207-218.

White, S. M., Crisp, J. A., & Spera, F. J. 2006. Long-term volumetric eruption rates and magma budgets. Geochemistry, Geophysics, Geosystems 7(3).

Willemse, J. 1969*a*. The geology of the Bushveld Igneous Complex, the largest repository of magmatic ore deposits in the world. Economic Geology Monograph 4, 1-22.

Willemse, J. 1969*b*. The vanadiferous magnetic iron ore of the Bushveld Igneous Complex. Economic Geology Monograph 4, 187-208.

Willmore, C.C., Boudreau, A.E., Kruger, F.J., 2000. The halogen geochemistry of the Bushveld Complex, Republic of South Africa: implications for chalcophile element distribution in the lower and critical zones. Journal of Petrology 41, 1517-1539.

Zhang, X-Q., Song, X-Y., Chen, L-M., Xie, W., Yu, S-Y., Zheng, W-Q., Deng, Y-F., Zhang, J-F., Gui, S-G. 2012. Fractional crystallization and the formation of thick Fe-Ti-V oxide layers in the Baima layered intrusion, SW China. Ore Geology Reviews 49, 96-108.

Zeh, A., Ovtcharova, M., Wilson, A., Schaltegger, U. 2015. The Bushveld Complex was emplaced and cooled in less than one million years – results of zirconology, and geotectonic implications. Earth and Planetary Science Letters 418, 103-114.